EXPLORATION GEOPHYSICS
https://doi.org/10.1080/08123985.2020.1726176

The magnetic gradient tensor of a triaxial ellipsoid, its derivation and its application to the determination of magnetisation direction

K. Blair McKenzie[a,b]

[a]Department of Earth and Environmental Sciences, Macquarie University, North Ryde, Australia; [b]Tensor Research Pty Ltd, Greenwich, Australia

ABSTRACT

This paper presents a theory for the anomalous magnetic gradient tensor due to a uniformly magnetised general triaxial ellipsoid. Expressions for the magnetic field vector and its gradient tensor are derived from expressions for the gravitational field or the gravity gradient tensor via an application of Poisson's theorem. This theory provides increased capability in forward modelling, inversion and equivalent source applications in both magnetic and gravimetric exploration. It provides an accurate and computationally efficient means of modelling the magnetic gradient tensor of ellipsoidal bodies which may possess isotropic or anisotropic magnetic susceptibility, remanent magnetisation and, in the case of highly magnetic ellipsoids, may be subject to the effect of self-demagnetisation. This paper presents a novel method based on the eigenvector decomposition of the magnetic gradient tensor to provide estimates of the magnetisation direction over an ellipsoidal source. This includes an investigation of the influence of shape detail, observation height and inclination of magnetisation on the positioning of global maxima in normalised source strength and how this affects the problem of estimating magnetisation direction. This study confirms that magnetisation directions may be accurately estimated for extremely elongated ellipsoidal bodies where the ratio of smallest observation height to maximum elongation (in plan view) is greater than 1.

ARTICLE HISTORY
Received 6 May 2019
Accepted 30 December 2019

KEYWORDS
Ellipsoid; magnetic gradient tensor; magnetisation; self-demagnetisation; eigenvector; normalised source strength

Introduction

The general triaxial ellipsoidal model in gravity and magnetic modelling is an extremely versatile one with several advantages over other simple body types. First, the ellipsoidal model can provide a useful representation of a variety of discrete gravitational and magnetic sources. These include equidimensional or spheroidal sources, elongate or pencil-like sources (the prolate ellipsoid) or flattened, sheet-like sources (the oblate ellipsoid). Geologically, the equidimensional model may approximate a spheroidal cavity in gravity modelling or a dipole source in magnetic modelling. The prolate ellipsoid may be used to model elongated sources such as lava tunnels in gravity investigations or pipes and quasi-symmetric intrusive bodies in both gravity and magnetic investigations. The oblate ellipsoid may be used to model lenticular, flattened or sheet-like bodies such as sills, lopoliths and some stratabound ore-bodies including banded iron formation deposits. Second, the magnetic ellipsoidal model which includes the general triaxial ellipsoid, the prolate and oblate ellipsoids of revolution, the sphere, and the infinite horizontal elliptic and circular cylinder body classes (see Emerson, Clark and Saul 1985; Clark, Saul, and Emerson 1986; Takahashi and Oliviera 2017) are the only body types that can account for the phenomenon of self-demagnetisation in uniformly magnetised sources. Self-demagnetisation is particularly important in bodies which possess very high magnetic susceptibility, namely, corrections are advisable when the magnetic volume susceptibility k is above 0.1 SI units (Clark 2014). The Tennant Creek Field of the Northern Territory, Australia can be considered a type example of the utility of ellipsoid modelling in a highly magnetic environment where self-demagnetisation is important. Farrar (1979), Clark and Tonkin (1987), Hoschke (1991) and Clark (2000) show examples of ellipsoid modelling of magnetite-rich ironstone bodies that host Cu–Au mineralisation in this area.

Why the magnetic gradient tensor?

Several authors including Pedersen and Rasmussen (1990), Schmidt and Clark (2006), Foss (2006) and Clark (2012) have reported that the magnetic gradient tensor has several theoretical advantages over the conventional measurement of the total magnetic field intensity (TMI). In particular, the gradient tensor contains more information on magnetic sources than both the magnetic field vector and the TMI. Importantly, the gradient tensor carries information on the curvature of the

CONTACT K. Blair McKenzie keith.mckenzie@students.mq.edu.au, blair.mckenzie@tensor-research.com.au Department of Earth and Environmental Sciences, Macquarie University, North Ryde, NSW 2109, Australia; Tensor Research Pty Ltd, P.O. Box 5189, Greenwich, NSW 2065, Australia

magnetic potential which is important in inversion (Reid and Thurston 2014). The magnetic gradient tensor is superior to the TMI at low magnetic field inclinations and in areas of rugged topography (Clark 2012). Furthermore, tensor gradient measurements are less affected by background interference and time-varying geomagnetic fields which are commonplace in magnetic field survey data. The gradient tensor and its eigenvalues and eigenvectors facilitate determination of the direction of magnetisation and the centre of magnetisation either by inversion or by magnetic moment analysis (Phillips et al. 2007; Beiki et al. 2012; Clark 2012, 2014). The gradient tensor may also provide estimates of magnetisation direction in regions where there is an anomalous peak in the normalised source strength (NSS) over a variety of compact dipole-like magnetic sources (Beiki et al. 2012; Clark 2012).

The importance of knowledge about magnetisation intensity and direction

The correct determination of magnetisation direction is fundamental to the interpretation of magnetic field and gradient tensor data (Austin et al. 2014; Clark 2012, 2014; Foss 2017; Takahashi and Oliviera 2017). It is essential to the successful modelling and inversion of magnetic targets which may carry anisotropy of magnetic susceptibility, remanence and self-demagnetisation. All of these phenomena can rotate the magnetisation of magnetic bodies away from the direction of the inducing geomagnetic field. Incorrect magnetisation directions can lead to erroneous determinations of the location and dip of magnetic bodies. Knowledge of the magnetisation intensity and Koenigsberger or Q ratios may contain important information on the nature of magnetic carriers in rocks while knowledge of the magnetisation direction may be utilised in age determinations for remanently magnetised bodies. Most importantly, knowledge of the magnetisation direction is often essential to the successful application of the general phase transformation to magnetic survey data (Blakely 1995).

Theory

The expressions for the gravity and magnetic fields due to a general triaxial ellipsoid with uniform density ρ, uniform magnetisation $\mathbf{M}$ and semiaxes $a \geq b \geq c$ were derived in an earlier paper by Clark, Saul, and Emerson (1986). I refer to this paper quite extensively but with a slight change in nomenclature, namely, that the major, intermediate and minor semiaxes are now referred to as $a_1 \geq a_2 \geq a_3$ respectively replacing the a, b, c nomenclature in Clark, Saul and Emerson (1986). Hence the equation of the surface for a general triaxial ellipsoid centred at the origin is now (Stratton 1941; Clark, Saul and Emerson 1986)

$$\frac{x_1^2}{a_1^2} + \frac{x_2^2}{a_2^2} + \frac{x_3^2}{a_3^2} = 1, \tag{1}$$

where x_1, x_2, x_3 are the Cartesian coordinates with respect to its principal axes, i.e. the body axis coordinates $\mathbf{r}_b$. The expression for a family of ellipsoidal surfaces centred at the origin and containing any internal ($\lambda < 0$) or external ($\lambda > 0$) observation point $P(x_1, x_2, x_3)$ is

$$\frac{x_1^2}{(a_1^2+\lambda)} + \frac{x_2^2}{(a_2^2+\lambda)} + \frac{x_3^2}{(a_3^2+\lambda)} = 1, \tag{2}$$

where λ is its principal ellipsoidal coordinate (see Appendix A1). Furthermore, the $A(\lambda)$, $B(\lambda)$ and $C(\lambda)$ Green's functions in Equations (11)–(18) of Clark, Saul and Emerson (1986) which describe the external gravitational potential U_{ext} of an ellipsoid are now replaced by $A_1(\lambda)$, $A_2(\lambda)$ and $A_3(\lambda)$ respectively. The theory presented here and by Clark, Saul and Emerson (1986) is in the body or principal axis coordinate system of the ellipsoid (see Figure 1). The survey axis coordinate system $\mathbf{r}_s$ adopted here uses the convention for the International Geomagnetic Reference Field (IGRF), i.e. x is North, y is East and z is vertically down. Expressions for transforming vectors and gradient tensors between the survey axis and body axis coordinate systems are given in Appendix A3.

An expression for the gravitational scalar potential U_{ext} of a general triaxial ellipsoid with uniform density ρ is given by Kellogg (1929) and Clark, Saul and Emerson (1986). For an external observation point $P(\mathbf{r}_b)$ in the body axis coordinate system of the ellipsoid, i.e. $\mathbf{r}_b = (x_1, x_2, x_3)^T$, the gravitational potential $U_{ext}(\mathbf{r}_b)$ is given by the following integral (Clark, Saul and Emerson 1986, Equation (11)):

$$U_{ext}(\mathbf{r}_b) = \pi G \rho a_1 a_2 a_3 \int_\lambda^\infty \left\{1 - \sum_{i=1}^{3} \frac{x_i^2}{(a_i^2+u)}\right\} \times \frac{1}{R(u)} du \quad \text{for } \lambda > 0, \tag{3}$$

while for an internal point $P(\mathbf{r}_b)$, the gravitational potential $U_{int}(\mathbf{r}_b)$ is (Clark, Saul and Emerson 1986, Equation (13)):

$$U_{int}(\mathbf{r}_b) = \pi G \rho a_1 a_2 a_3 \int_0^\infty \left\{1 - \sum_{i=1}^{3} \frac{x_i^2}{(a_i^2+u)}\right\} \times \frac{1}{R(u)} du \quad \text{for } \lambda = 0, \tag{4}$$

where

$$R(u) = \sqrt{(a_1^2+u)(a_2^2+u)(a_3^2+u)}, \tag{5}$$

and G is the universal gravitational constant.

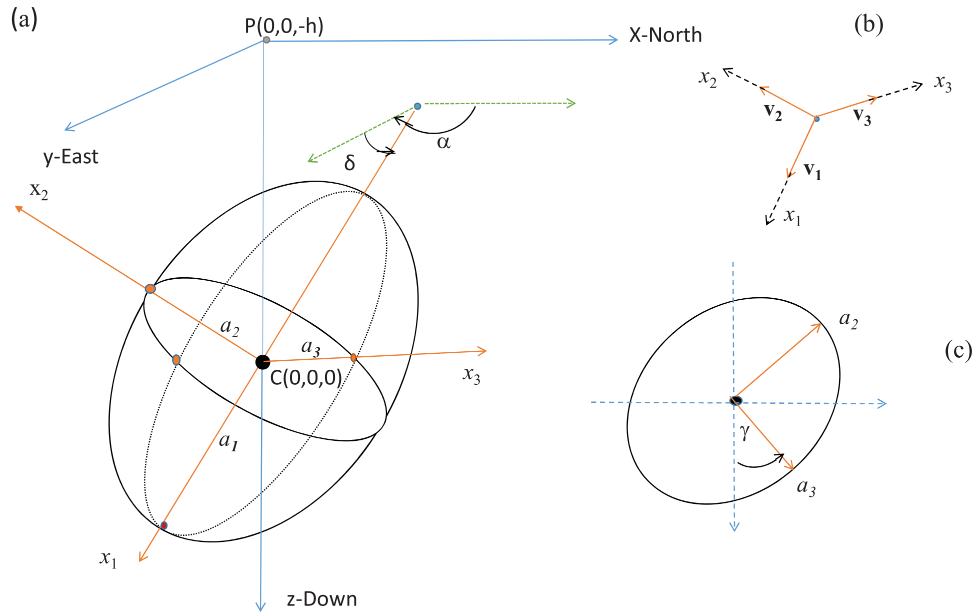

Figure 1. The body axis coordinate system $\mathbf{r}_b = (x_1, x_2, x_3)^T$ for a general triaxial ellipsoid centred at the origin with semiaxes $a_1 > a_2 > a_3$. The orientation of the ellipsoid is defined by three direction cosine vectors $\hat{\mathbf{v}}_1, \hat{\mathbf{v}}_2, \hat{\mathbf{v}}_3$ along the a_1, a_2, a_3 semiaxes or x_1, x_2, x_3 body axes (see Figure 1(a,b)). The direction cosine vectors are uniquely specified via three ellipsoidal angles α, δ, γ, i.e. α is the azimuth of the downward pointing major semiaxis, δ is its plunge, and γ is the rotation of the ellipsoid about its downward pointing major axis as shown in Figure 1(c). Figure 1(c) shows an inclined section through the ellipsoid which contains the a_2 and a_3 semiaxes. The view is looking down the major axis with anticlockwise rotations defined as negative. The vertical dotted line in Figure 1(c) is the trace of the vertical plane containing the major axis.

The expression for the external gravitational potential may be rewritten as (see Clark, Saul, and Emerson 1986, Equations (14)–(18)),

$$U_{ext}(\mathbf{r}_b) = \pi G\rho a_1 a_2 a_3 \left[D(\lambda) - \sum_{i=1}^{3} A_i(\lambda) x_i^2 \right], \quad (6)$$

where

$$D(\lambda) = \int_{\lambda}^{\infty} \frac{1}{R(u)} du, \quad (7)$$

and

$$A_i(\lambda) = \int_{\lambda}^{\infty} \frac{1}{(a_i^2 + u)R(u)} du, \quad \text{for } i = 1,2,3, \quad (8)$$

and where λ is the principal ellipsoidal coordinate of the observation point P with respect to the centre of the ellipsoid (see Clark, Saul, and Emerson 1986, Equations (2)–(9)).

The expressions for the body axis components g_1, g_2, g_3 respectively of the anomalous gravitational field $g(\mathbf{r}_b)$ due to a general uniform triaxial ellipsoid at an external point $P(\mathbf{r}_b)$ where $\mathbf{r}_b = (x_1, x_2, x_3)^T$ are obtained by taking the gradient of the scalar potential $U_{ext}(\mathbf{r}_b)$ in Equation (3):

$$g(\mathbf{r}_b) = \nabla U_{ext}(\mathbf{r}_b) = \left\{ \left(\frac{\partial U_{ext}}{\partial x_1}\right) \hat{\mathbf{u}}_1 + \left(\frac{\partial U_{ext}}{\partial x_2}\right) \hat{\mathbf{u}}_2 + \left(\frac{\partial U_{ext}}{\partial x_3}\right) \hat{\mathbf{u}}_3 \right\}, \quad (9)$$

where $\hat{\mathbf{u}}_1$, $\hat{\mathbf{u}}_2$, $\hat{\mathbf{u}}_3$ are the direction cosines along the x_1, x_2, x_3 body axes, respectively.

Hence, by the chain rule of partial differentiation in Equation (6), the ith component of the anomalous gravitational field due to the triaxial ellipsoid is (see also Clark, Saul, and Emerson 1986, Equations (21)–(23)):

$$g_i(\mathbf{r}_b) = \frac{\partial U_{ext}}{\partial x_i} = \left(\frac{\partial U_{ext}}{\partial \lambda}\right)\left(\frac{\partial \lambda}{\partial x_i}\right) = -2\pi G\rho a_1 a_2 a_3 x_i A_i(\lambda), \quad \text{for } i = 1,2,3. \quad (10)$$

Closed form expressions for the Green's functions $A_1(\lambda)$, $A_2(\lambda)$ and $A_3(\lambda)$ in Equations (8) and (10) are given in Appendix A1 and a derivation of Equation (10) is given in Appendix A2.

Poisson's relation and the magnetic scalar potential

From the second Maxwell equation, when there are no electric currents present within a region of investigation, the magnetic induction b is irrotational, i.e. $\nabla \times \mathbf{b} = 0$, and according to the Helmholtz theorem, there exists a scalar potential V within that region such that $\mathbf{b} = -\nabla V$. The magnetic scalar potential $V_{ext}(\mathbf{r}_b)$ due to a uniformly magnetised ellipsoid with magnetisation $\mathbf{M} = (M_1, M_2, M_3)^T$ may be derived from Equation (10) via Poisson's relation (see Grant and West 1965, 213; Clark, Saul, and Emerson 1986, 191, Equations (24)–(25), Blakely 1995, 92):

$$V_{\text{ext}}(\mathbf{r}_{\text{b}}) = -\left(\frac{C_m}{G\rho}\right)\nabla U_{\text{ext}} \cdot \mathbf{M} = -\left(\frac{C_m}{G\rho}\right)\text{g}^{\text{T}} \cdot \mathbf{M}$$
$$= 2\pi C_m a_1 a_2 a_3 \sum_{i=1}^{3} x_i A_i(\lambda) M_i, \quad (11)$$

where C_m is a constant which depends on the system of electromagnetic units used (see Blakely 1995, 67–68). In the International Standard (SI) system of units used here, C_m has a value of 100 nH/m or 100 nTm/A for magnetic fields expressed in nanotesla (nT) and magnetisations expressed in ampere per metre (A/m). The magnetic scalar potential is expressed in nWb/m or nTm.

The body axis components of the anomalous magnetic field $\mathbf{b}(\mathbf{r}_\text{b}) = (b_1, b_2, b_3)^\text{T}$ due to a uniformly magnetised general triaxial ellipsoid at an external point $P(\mathbf{r}_\text{b})$ where $\mathbf{r}_\text{b} = (x_1, x_2, x_3)^\text{T}$ are obtained by taking the gradient of the magnetic scalar potential $V_{\text{ext}}(\mathbf{r}_\text{b})$ (see Clark, Saul, and Emerson 1986, Equations (26)–(28)).

$$\mathbf{b}(\mathbf{r}_\text{b}) = -\nabla V_{\text{ext}}(\mathbf{r}_\text{b})$$
$$= -\left\{\left(\frac{\partial V_{\text{ext}}}{\partial x_1}\right)\hat{\mathbf{u}}_1 + \left(\frac{\partial V_{\text{ext}}}{\partial x_2}\right)\hat{\mathbf{u}}_2 + \left(\frac{\partial V_{\text{ext}}}{\partial x_3}\right)\hat{\mathbf{u}}_3\right\}. \quad (12)$$

The negative sign in Equation (12) follows the convention in Kellogg (1929) for electrostatic fields (see Blakely 1995, 7, Chapter 1). Thus from Equations (11) and (12), the external magnetic field components $b_i(\mathbf{r}_\text{b})$ are

$$b_i(\mathbf{r}_\text{b}) = -\left(\frac{\partial V_{\text{ext}}}{\partial \lambda}\right)\left(\frac{\partial \lambda}{\partial x_i}\right) = -2\pi C_m a_1 a_2 a_3$$
$$\times \left\{A_i(\lambda) M_i + \left[\sum_{j=1}^{3} x_j A'_j(\lambda) M_j\right]\left(\frac{\partial \lambda}{\partial x_i}\right)\right\}, \quad (13.1)$$

where

$$A'_i(\lambda) = \frac{\partial A_i(\lambda)}{\partial \lambda} = -\left[\frac{1}{(a_i^2 + \lambda) R(\lambda)}\right] \quad i = 1,2,3, \quad (13.2)$$

$$R(\lambda) = \sqrt{(a_1^2 + \lambda)(a_2^2 + \lambda)(a_3^2 + \lambda)}, \quad (13.3)$$

and

$$\frac{\partial \lambda}{\partial x_i} = \left[\frac{2x_i}{(a_i^2 + \lambda)\, S(\lambda)}\right]; \quad S(\lambda) = \sum_{j=1}^{3}\left[\frac{x_j}{(a_j^2 + \lambda)}\right]^2. \quad (13.3)$$

The expressions for the body components of the anomalous magnetic field of a triaxial ellipsoid agree with those of Clark, Saul, and Emerson (1986, Equations (26)–(28)).

The gravity gradient tensor of the triaxial ellipsoid

From Equations (11) and (12), it may be deduced that the external magnetic field vector may also be expressed in terms of the gravity gradient tensor $\boldsymbol{\Gamma}$ which is defined as the gradient of the gravity field vector, i.e. $\boldsymbol{\Gamma}(\mathbf{r}_\text{b}) = \nabla \mathbf{g}(\mathbf{r}_\text{b})$, or in tensor notation, $\boldsymbol{\Gamma}(\mathbf{r}_\text{b}) = \partial g_i(\mathbf{r}_\text{P})/\partial x_j$ for $i, j = 1, 2, 3$,

$$\mathbf{b}(\mathbf{r}_\text{b}) = -\nabla V(\mathbf{r}_\text{b}) = \left(\frac{C_m}{G\rho}\right)\nabla \mathbf{g}^\text{T} \cdot \mathbf{M}$$
$$= \left(\frac{C_m}{G\rho}\right)\boldsymbol{\Gamma}^\text{T}(\mathbf{r}_\text{b}) \cdot \mathbf{M} = C_m \mathbf{T}^\text{T}(\mathbf{r}_\text{b}) \cdot \mathbf{M}, \quad (14)$$

where $\mathbf{T}^\text{T}$ denotes the transpose of $\mathbf{T}$. The 3×3 matrix $\mathbf{T} = T_{ij}; i,j = 1,2,3$ is a second-order symmetric tensor of Green's functions, i.e.

$$T_{ij}(\mathbf{r}_\text{b}) = \left(\frac{1}{G\rho}\right)\Gamma_{ij}(\mathbf{r}_\text{b}) = \left(\frac{1}{G\rho}\right)\frac{\partial g_i(\mathbf{r}_\text{b})}{\partial x_j}$$
$$= -2\pi a_1 a_2 a_3 \left\{A_i(\lambda)\delta_{ij} + x_i \text{A}'_i(\lambda)\left(\frac{\partial \lambda}{\partial x_j}\right)\right\}, \quad (15)$$

where δ_{ij} is Kronecker delta.

Hence from Equation (15), the expression for the anomalous gravity gradient tensor at a point $P(\mathbf{r}_\text{b})$ external to a uniform triaxial ellipsoid is

$$\Gamma_{ij}(\mathbf{r}_\text{b}) = \frac{\partial g_i(\mathbf{r}_\text{b})}{\partial x_j} = -2\pi G\rho a_1 a_2 a_3$$
$$\times \left\{A_i(\lambda)\delta_{ij} + x_i A'_i(\lambda)\left(\frac{\partial \lambda}{\partial x_j}\right)\right\} \text{ (for } i,j = 1,2,3). \quad (16)$$

Expressions for $A'_i(\lambda)$ and $\left(\frac{\partial \lambda}{\partial x_j}\right)$ are given by Equations (13.2) and (13.3) while those for the Green's functions $A_i(\lambda), i = 1,2,3$ are given in Appendix A1. Inspection of Equation (16) shows that the gravity gradient tensor is symmetric, i.e. $\Gamma_{ij} = \Gamma_{ji}$ for $i \neq j = 1,2,3$. Furthermore, it may be shown that the gravity gradient tensor of a triaxial ellipsoid at an external observation point is also traceless, i.e. $\text{Tr}\{\boldsymbol{\Gamma}\} = \boldsymbol{\Gamma}_{11} + \boldsymbol{\Gamma}_{22} + \boldsymbol{\Gamma}_{33} = 0$. This is easily deduced from the following identity

$$\sum_{\text{i}=1}^{3} A_i(\lambda) = -\sum_{\text{i}=1}^{3} x_i A'_i(\lambda)\left(\frac{\partial \lambda}{\partial x_j}\right) = \frac{2}{R(\lambda)}.$$

The magnetic gradient tensor

The magnetic gradient tensor $\mathbf{B}(\mathbf{r}_\text{b})$ is defined as the gradient of the magnetic field vector, i.e. $\mathbf{B}(\mathbf{r}_\text{b}) = \nabla \mathbf{b}(\mathbf{r}_\text{b})$, or in tensor notation, $\mathbf{B}(\mathbf{r}_\text{b}) = \partial b_i(\mathbf{r}_\text{b})/\partial x_j$ for $i,j = 1,2,3$. Expressions for the tensor elements at a point $P(\mathbf{r}_\text{b})$ external to a uniformly magnetised general triaxial ellipsoid where $\mathbf{r}_\text{b} = (x_1, x_2, x_3)^\text{T}$ are obtained by differentiation of Equation (13.1) with respect to x_j for $j = 1, 2, 3$. Then,

$$B_{ij}(\mathbf{r}_b) = \left(\frac{\partial b_i}{\partial x_j}\right) = -2\pi C_m a_1 a_2 a_3 \frac{\partial}{\partial x_j} \times \left\{ A_i(\lambda)M_i + \left[\sum_{j=1}^{3} x_j A_j'(\lambda)M_j\right]\left(\frac{\partial \lambda}{\partial x_i}\right)\right\}. \tag{17}$$

Hence for the six off-diagonal $B_{ij}(\mathbf{r}_b)$ tensor elements where $i \neq j$ and $i, j = 1, 2, 3$

$$\begin{aligned} B_{ij}(\mathbf{r}_b) &= -2\pi C_m a_1 a_2 a_3 \\ &\times \left\{ \begin{aligned} & A_i'(\lambda)M_i\left(\tfrac{\partial\lambda}{\partial x_j}\right) + A'_j(\lambda)M_j\left(\tfrac{\partial\lambda}{\partial x_i}\right) \\ & + \left[\sum_{k=1}^{3} x_k A_k'(\lambda)M_k\right]\left(\tfrac{\partial^2\lambda}{\partial x_i \partial x_j}\right) \\ & + \left[\sum_{k=1}^{3} x_k A_k''(\lambda)M_k\right]\left(\tfrac{\partial\lambda}{\partial x_i}\right)\left(\tfrac{\partial\lambda}{\partial x_j}\right) \end{aligned} \right\}, \\ &= B_{ji}(\mathbf{r}_b). \end{aligned} \tag{18.1}$$

and for the three diagonal $B_{ij}(\mathbf{r}_b)$ tensor elements where $i = j = 1,2,3$,

$$\begin{aligned} B_{ii}(\mathbf{r}_b) &= -2\pi C_m a_1 a_2 a_3 \\ &\times \left\{ \begin{aligned} & 2A_i'(\lambda)M_i\left(\tfrac{\partial\lambda}{\partial x_i}\right) + \left[\sum_{k=1}^{3} x_k A_k'(\lambda)M_k\right] \\ & \times\left(\tfrac{\partial^2\lambda}{\partial x_i^2}\right) + \left[\sum_{k=1}^{3} x_k A_k''(\lambda)M_k\right]\left(\tfrac{\partial\lambda}{\partial x_i}\right)^2 \end{aligned} \right\}, \end{aligned} \tag{18.2}$$

where

$$\begin{aligned} \frac{\partial^2\lambda}{\partial x_i \partial x_j} &= \frac{\partial}{\partial x_j}\left[\frac{2x_i}{(a_i^2+\lambda)S(\lambda)}\right] \quad \text{for } i, j = 1, 2, 3 \\ &= \frac{2}{(a_i^2+\lambda)S(\lambda)}\delta_{ij} \\ &\quad - \left[\frac{1}{(a_i^2+\lambda)}\left(\frac{\partial\lambda}{\partial x_j}\right) + \frac{1}{S(\lambda)}\left(\frac{\partial S(\lambda)}{\partial x_j}\right)\right]\left(\frac{\partial\lambda}{\partial x_i}\right), \end{aligned} \tag{19}$$

and

$$\begin{aligned} S(\lambda) &= \sum_{i=1}^{3}\left[\frac{x_i}{(a_i^2+\lambda)}\right]^2; \\ \frac{\partial S(\lambda)}{\partial x_i} &= 2\left\{\frac{x_i}{(a_i^2+\lambda)^2} - \left[\sum_{j=1}^{3}\frac{x_j^2}{(a_j^2+\lambda)^3}\right]\left(\frac{\partial\lambda}{\partial x_i}\right)\right\}, \end{aligned} \tag{20}$$

and

$$A_i''(\lambda) = \frac{\partial^2 A_i(\lambda)}{\partial\lambda^2} = \frac{\partial A_i'(\lambda)}{\partial\lambda} = \frac{\partial}{\partial\lambda}\left[\frac{-1}{(a_i^2+\lambda)R(\lambda)}\right], \tag{21.1}$$

and

$$\frac{\partial A_i'(\lambda)}{\partial x_i} = \left(\frac{\partial A_i'(\lambda)}{\partial\lambda}\right)\left(\frac{\partial\lambda}{\partial x_i}\right) = A_i''(\lambda)\left(\frac{\partial\lambda}{\partial x_i}\right). \tag{21.2}$$

The expressions for $A_1''(\lambda)$, $A_2''(\lambda)$ and $A_3''(\lambda)$ are derived by differentiating the expression for $A_i'(\lambda)$ in Equation (21.1), namely,

$$\begin{aligned} A_1''(\lambda) &= \frac{\partial^2 A_1(\lambda)}{\partial\lambda^2} \\ &= \frac{1}{2R(\lambda)}\left\{\frac{3}{(a_1^2+\lambda)^2} + \frac{(a_2^2+\lambda)+(a_3^2+\lambda)}{R^2(\lambda)}\right\}, \end{aligned} \tag{22.1}$$

$$\begin{aligned} A_2''(\lambda) &= \frac{\partial^2 A_2(\lambda)}{\partial\lambda^2} \\ &= \frac{1}{2R(\lambda)}\left\{\frac{3}{(a_2^2+\lambda)^2} + \frac{(a_1^2+\lambda)+(a_3^2+\lambda)}{R^2(\lambda)}\right\}, \end{aligned} \tag{22.2}$$

$$\begin{aligned} A_3''(\lambda) &= \frac{\partial^2 A_3(\lambda)}{\partial\lambda^2} \\ &= \frac{1}{2R(\lambda)}\left\{\frac{3}{(a_3^2+\lambda)^2} + \frac{(a_1^2+\lambda)+(a_2^2+\lambda)}{R^2(\lambda)}\right\}. \end{aligned} \tag{22.3}$$

It is noted that equations (18.1)–(18.2), (19)–(21) and (22.1)–(22.3) completely define the magnetic gradient tensor due to a uniformly magnetised general triaxial ellipsoid. Importantly it may be shown that the magnetic gradient tensor at an external observation point is a harmonic potential function, i.e. it is symmetric, traceless (satisfying Laplace's equation). These properties follow directly from Maxwell's equations in the magnetostatic limit and in the absence of conduction currents so that $\nabla.\mathbf{b}(\mathbf{r}_b) = 0$. Furthermore, the generic nature of this formulation allows for the development of extremely efficient and compact source code for the computation of the magnetic field components and gradient tensor elements of a triaxial ellipsoid. Although not shown in this paper, the formulation presented here is easily applied to other ellipsoidal bodies including the prolate and oblate ellipsoids of revolution and the perfect sphere.

The internal gravitational and magnetic fields of a general triaxial ellipsoid

An expression for the internal gravitational potential $U_{int}(\mathbf{r}_b)$ of a homogeneous triaxial ellipsoid is obtained by integration of Equation (4), namely (see Clark, Saul, and Emerson 1986, Equation (19))

$$U_{\text{int}}(\mathbf{r}_b) = \pi G\rho a_1 a_2 a_3 \left[D(0) - \sum_{i=1}^{3} A_i(0) x_i^2 \right] \quad (\lambda = 0).$$

The body axis components of the internal gravitational field due to a uniform triaxial ellipsoid are derived by differentiation of Equation (4). Hence

$$g_{i(\text{int})}(\mathbf{r_b}) = \frac{\partial U_{\text{int}}}{\partial x_i} = -2\pi G\rho a_1 a_2 a_3 x_i A_i(0), \text{ for } i = 1,2,3, \tag{23.1}$$

where

$$A_i(0) = \int_0^\infty \frac{1}{(a_i^2 + \text{u})\sqrt{(a_1^2+u)(a_2^2+u)(a_3^2+u)}} du \quad \text{for } i = 1,2,3. \tag{23.2}$$

By inspection of Equation (23.1), the internal gravitational field of a triaxial ellipsoid with uniform density ρ is a linear function of its spatial coordinates. This is because the $A_i(0)$ Green's functions only depend on the dimensions of the ellipsoid (see Appendix A4). Whence the internal gravity gradient tensor for the triaxial ellipsoid $\Gamma_{ij}(\mathbf{r}_b)$ is

$$\Gamma_{ij}(\mathbf{r}_b) = \frac{\partial g_{i(\text{int})}(\mathbf{r_b})}{\partial x_j} = \frac{\partial}{\partial x_j}[-2\pi G\rho a_1 a_2 a_3 x_i A_i 0)]$$
$$= -2\pi G\rho a_1 a_2 a_3 A_i(0)\delta_{ij} \quad \text{for } i,j = 1,2,3. \tag{24}$$

Hence the off-diagonal elements of the gravity gradient tensor are zero while its trace, the sum of its three diagonal elements, is non-zero satisfying Poisson's equation, namely,

$$\nabla^2 U_{\text{int}}(\mathbf{r}_b) = \text{Tr}\{\Gamma(\mathbf{r}_b)\} = \Gamma_{11}(\mathbf{r}_b) + \Gamma_{22}(\mathbf{r}_b) + \Gamma_{33}(\mathbf{r}_b)$$
$$= -2\pi G\rho a_1 a_2 a_3 \sum_{i=1}^{3} A_i(0).$$

However, from Appendix A4, it may be shown that $\sum_{i=1}^{3} A_i(0) = 2/(a_1 a_2 a_3)$, therefore,

$$\nabla^2 U_{\text{int}}(\mathbf{r}_b) = \text{Tr}\{\Gamma(\mathbf{r}_b)\} = -2\pi G\rho a_1 a_2 a_3 (2/(a_1 a_2 a_3)$$
$$= -4\pi G\rho. \tag{25}$$

The body axis components of the internal magnetic field $\mathbf{H}_{\text{int}}$ due to a uniform triaxial ellipsoid are derived by differentiation of the expression for the internal scalar potential $V_{\text{int}}(\mathbf{r}_b)$ derived from Equation (23.1) via Poisson's relation, namely,

$$V_{\text{int}}(\mathbf{r}_b) = -\left(\frac{C_m}{G\rho}\right) \nabla U_{\text{int}} \cdot \mathbf{M} = -\left(\frac{C_m}{G\rho}\right) \text{g}_{\text{int}}^{\text{T}} \cdot \mathbf{M}$$
$$= 2\pi C_m a_1 a_2 a_3 \sum_{j}^{3} x_j A_j(0) M_j. \tag{26}$$

The internal demagnetising field of a triaxial ellipsoid $\mathbf{H}_{\text{int}}$ in the SI system of units is given by the following expression:

$$H_{j(\text{int})} = -\left(\frac{1}{4\pi}\right)\frac{\partial V_{\text{int}}}{\partial x_j} = -\frac{1}{2} a_1 a_2 a_3 A_j(0) M_j, \quad \text{for } j = 1,2,3, \tag{27}$$

where both the magnetic field intensity $\mathbf{H}_{\text{int}}$ and the magnetisation $\mathbf{M}$ are expressed in ampere/metre (A/m) units.

This internal magnetic field which arises from the magnetisation is known as the self-demagnetising field $\mathbf{H}_{\text{d}}$ (Clark, Saul, and Emerson 1986; Clark and Emersom, 1999). This field exists in all magnetically susceptible bodies which are subject to an external magnetic field. Its overall effect is to produce a back field $\mathbf{H}_{\text{d}}$ which reduces the external inducing magnetic field $\mathbf{H}_0$. Hence the resultant or effective internal magnetic field $\mathbf{H}_{\text{eff}}$ is

$$\mathbf{H}_{\text{eff}} = \mathbf{H}_0 + \mathbf{H}_{\text{d}} = \mathbf{H_0} - \mathbf{NM}, \tag{28}$$

where $\mathbf{N}$ is a demagnetising tensor and $\mathbf{M}$ is the intrinsic magnetisation of the body. For ellipsoidal bodies, the self-demagnetisation field is independent of x_1, x_2, x_3 and is therefore uniform. It is related to the principal demagnetising factors N_1, N_2, N_3 along the a_1, a_2, a_3 semiaxes of the ellipsoid by the relation

$$H_{j(\text{int})} = -N_j M_j \quad \text{for } j = 1,2,3. \tag{29.1}$$

In the SI system of units, the sum of the principal demagnetisation factors is identically 1, i.e. $\sum_{j=1}^{3} N_j = N_1 + N_2 + N_3 = 1$, while in the electromagnetic system (emu) of units it is 4π. By inspection of Equations (27) and (29.1), the demagnetising factors N_j for an ellipsoid in the SI system of units are related to the Green's functions $A_i(0)$ by the relation (Clark, Saul, and Emerson 1986; Takahashi and Oliviera 2017)

$$N_j = \frac{1}{2} a_1 a_2 a_3 \text{A}_i(0) \quad \text{for } j = 1,2,3. \tag{29.2}$$

Computational aspects

Computation of the magnetic fields and gradient tensors due to a general triaxial ellipsoid involve the following steps:

(1) calculate the orthogonal matrix $\mathbf{U}$ for transformations from the survey coordinate system $\mathbf{r}_s = (x,y,z)^{\text{T}}$ to the body axis coordinate system $\mathbf{r}_b = (x_1,x_2,x_3)^{\text{T}}$ of the triaxial ellipsoid
(2) determination of the components of magnetisation $\mathbf{M} = (M_1,M_2,M_3)^{\text{T}}$ in the body axis coordinate system of the triaxial ellipsoid
(3) transformation of each survey observation point $P(\mathbf{r}_s) = (x,y,z)^{\text{T}}$ to the body axis coordinate system $P(\mathbf{r}_b) = (x_1,x_2,x_3)^{\text{T}}$ of the triaxial ellipsoid
(4) calculate all magnetic field components $\mathbf{b}(\mathbf{r}_b) = (b_1,b_2,b_3)^{\text{T}}$ and gradient tensor elements $B_{ij}(\mathbf{r}_b)$; i,

$j = 1{,}2{,}3$ at each observation point $P(\mathbf{r}_b)$ in the body axis coordinate system of the triaxial ellipsoid.

(5) transformation of each computed magnetic field vector $\mathbf{b}(\mathbf{r}_b)$ and gradient tensor $\mathbf{B}(\mathbf{r}_b)$ from the body axis coordinate system $\mathbf{r}_b = (x_1, x_2, x_3)^T$ of the triaxial ellipsoid to the survey axis coordinate system $\mathbf{r}_s = (x, y, z)^T$ for each observation point $P(\mathbf{r}_s)$.

(6) eigenvector decomposition of the gradient tensor $\mathbf{B}(\mathbf{r}_s)$ to find three ordered eigenvalues $\lambda_1 > \lambda_2 > \lambda_3$ and three corresponding eigenvectors $\hat{\mathbf{e}}_1, \hat{\mathbf{e}}_2, \hat{\mathbf{e}}_3$ for each observation point $P(\mathbf{r}_s)$ of the tensor $\mathbf{B}(\mathbf{r}_s)$.

Expressions for the orthogonal transformation matrix $\mathbf{U}$ which defines the body axis coordinate system of a general triaxial ellipsoid are given in Appendix A3. The treatment of magnetisation in this paper is completely general, i.e. ellipsoidal bodies may possess isotropic or anisotropic magnetic susceptibility, remanent magnetisation and, in the case of highly magnetic ellipsoids, may be subject to the effect of self-demagnetisation. As noted previously, all survey coordinates and magnetisations require transformation from the survey coordinate system $\mathbf{r}_s = (x, y, z)^T$ to the body axis coordinate system $\mathbf{r}_b = (x_1, x_2, x_3)^T$ of the ellipsoid. All magnetic and gravity field components and their gradient tensors are calculated in the body axis coordinate system $\mathbf{r}_b = (x_1, x_2, x_3)^T$ of the ellipsoid which require transformation back to the survey coordinate system $\mathbf{r}_s = (x, y, z)^T$. These transformations are outlined in Appendix A3.

The expressions for the magnetic and gravitational fields due to a general triaxial ellipsoid involve the $A_1(\lambda)$, $A_2(\lambda)$, $A_3(\lambda)$ Green's functions (see Equation (10)). The closed form expressions for the three Green's functions contain incomplete elliptic integrals of the first $F(k, \beta)$ and second $E(k, \beta)$ kind (see Appendix A1). These elliptic integrals are computed in double precision using an algorithm based on Landen's transformation (Abramowitz and Stegun 1964; Press et al. 1992). Both elliptic integrals $F(k, \beta)$ and $E(k, \beta)$ have been successfully tested to eight significant figures respectively by comparison with tables in Abramowitz and Stegun (1964, Tables 17.5 and 17.6, respectively). The three eigenvalues and eigenvectors of the magnetic gradient tensor are calculated using a series of Jacobi orthogonal similarity transformations of a real symmetric matrix (see Press et al. 1992).

The effective or resultant magnetisation of a general triaxial ellipsoid

The magnetisation $\mathbf{M}$ within a triaxial ellipsoid is assumed to be homogeneous and quite general. It may possess a weak or strong induced magnetisation and/or it may possess a significant remanent component. Clark, Saul, and Emerson (1986) and also Emerson, Clark, and Saul (1985) show how to incorporate the effects of isotropic or anisotropic magnetic susceptibility, remanence and self-demagnetisation into the computation of the body axis components of the magnetisation vector $\mathbf{M}$ within a triaxial ellipsoid.

When an ellipsoid is weakly or moderately magnetic, the resultant magnetisation vector $\mathbf{M}$ is almost exactly equal to the total resultant magnetisation $\mathbf{M_{tot}}$ which is defined as the vector sum of its induced $\mathbf{M_{ind}}$ and remanent $\mathbf{M_{nrm}}$ magnetisation vectors, namely,

$$\mathbf{M_{tot}} = \mathbf{M_{ind}} + \mathbf{M_{nrm}} = \mathbf{KF} + \mathbf{M_{nrm}},$$

where $\mathbf{K}$ is the initial magnetic volume susceptibility tensor and $\mathbf{F}$ is the local geomagnetic field vector. Expressions for calculating the magnetic susceptibility tensor when anisotropy is present are given in Emerson, Clark, and Saul (1985). However in highly magnetic ellipsoids where demagnetisation effects are significant, i.e. where the bulk magnetic susceptibility k is high (i.e. in the range from 0.05 to 0.1 SI units), the resultant magnetisation vector $\mathbf{M_{res}}$ is no longer equal to the total resultant magnetisation $\mathbf{M_{tot}}$. A method for estimating the magnetisation vector $\mathbf{M_{res}}$ accounting for demagnetisation, remanence and anisotropy of susceptibility has been outlined by Emerson, Clark, and Saul (1985) and Clark, Saul, and Emerson (1986). This method is exact for triaxial ellipsoids and their degenerate forms including the prolate and oblate ellipsoids of revolution and the perfect sphere (Emerson, Clark, and Saul 1985; Clark, Saul, and Emerson 1986). The resultant or effective magnetisation corrected for self-demagnetisation is estimated using the following expression (Clark, Saul, and Emerson 1986, Equation (38))

$$\mathbf{M_{res}} = \mathbf{D}^{-1}\mathbf{M_{tot}} = (\mathbf{I} + \mathbf{KN})^{-1}(\mathbf{M_{ind}} + \mathbf{M_{nrm}}), \quad (30)$$

where $\mathbf{D}$ is the demagnetisation or depolarisation matrix, i.e.

$$D_{ij} = \delta_{ij} + k_{ij}N_j \quad (\text{for } i, j = 1{,}2{,}3),$$

where $\delta_{ij}; i, j = 1, 2, 3$ is the Kronecker delta function, $k_{ij}; i, j = 1, 2, 3$ is the initial magnetic volume susceptibility tensor, and $N_j; j = 1, 2, 3$ are the demagnetisation factors along the a_1, a_2, a_3 body axes respectively of the triaxial ellipsoid such that $N_1 + N_2 + N_3 = 1$.

A derivation of Equation (30) is supplied in Appendix A6.

An example: the magnetic gradient tensor for Magmod XV

To illustrate the theory presented and the importance of correctly accounting for the magnetisation properties of ellipsoidal bodies, I present images of the six magnetic gradient tensor elements $B_{xx}, B_{xy}, B_{xz}, B_{yy}, B_{yz}, B_{zz}$ due to a highly magnetic, general triaxial ellipsoid. For this example I have used the synthetic models Magmod XVA, XVB and XVC presented by Clark, Saul, and

Table 1. Body properties for the Magmod XV triaxial ellipsoid.

Ellipsoid property description	Ellipsoid body properties
The semiaxial lengths ($a_1 > a_2 > a_3$)	$a_1 = 250$ m, $a_2 = 150$ m, $a_3 = 100$ m
The centroid coordinates $C(x, y, z)$	$C_x = 0$ m, $C_y = 0$ m, $C_z = 300$ m
Volume $v = \frac{4\pi}{3} a_1 a_2 a_3$	$v = 1.57079632679 \times 10^7$ m^3
The ellipsoid orientation angles (α, δ, γ) forming a right-hand clockwise coordinate system	
Azimuth of the downward a_1 semiaxis	$\alpha = 320°$
Plunge of the downward a_1 semiaxis	$\delta = 45°$
Rotation of the downward a_3 semiaxis from the vertical	$\gamma = -45°$
Declination and inclination of the x_1, x_2, x_3 body axes:	
Body axis $\hat{\mathbf{u}}_1$ (along x_1 or a_1 semiaxis)	Dec $\hat{\mathbf{u}}_1 = 320.00°$, Inc $\hat{\mathbf{u}}_1 = 45.00°$
Body axis $\hat{\mathbf{u}}_2$ (along x_2 or a_2 semiaxis)	Dec $\hat{\mathbf{u}}_2 = 14.736°$, Inc $\hat{\mathbf{u}}_2 = -30.00°$
Body axis $\hat{\mathbf{u}}_3$ (along x_3 or a_3 semiaxis)	Dec $\hat{\mathbf{u}}_3 = 85.264°$, Inc $\hat{\mathbf{u}}_3 = 30.00°$
Demagnetisation factors along the a_1, a_2, a_3 axes (SI)	$N_1 = 0.1674, N_2 = 0.3240, N_3 = 0.5086$
The local geomagnetic field vector $\mathbf{b_0}$ (nT):	$\lvert\mathbf{b_0}\rvert = 60000$ nT Dec $\mathbf{b_0} = 10°$ Inc $\mathbf{b_0} = -65°$
Magnetic volume susceptibility (SI)	Magmod XVA1, Magmod XVB1
Intrinsic isotropic bulk susceptibility k_b	$k_b = 1.256637$ SI
Intrinsic anisotropy of magnetic volume susceptibility (SI)	Magmod XVC1
Major axis k_1, declination D_{k_1}, inclination I_{k_1}	$k_1 = 1.507964, D_{k_1} = 90°, I_{k_1} = 0°$
Major axis k_2, declination D_{k_2}, inclination I_{k_2}	$k_2 = 1.256637, D_{k_2} = 180°, I_{k_2} = 0°$
Minor axis k_3, declination D_{k_3}, inclination I_{k_3}	$k_3 = 1.005310, D_{k_3} = 0°, I_{k_3} = 90°$
Intrinsic bulk susceptibility $k_b = (k_1 + k_2 + k_3)/3$	$k_b = 1.256637$ SI
Anisotropy $P = k_1/k_3$	$P = k_1/k_3 = 1.500$
Lineation $L = k_1/k_2$	$L = k_1/k_2 = 1{,}200$
Foliation $F = k_2/k_3$	$F = k_2/k_3 = 1.250$

Note: The intrinsic susceptibilities k_1, k_2, k_3 are exactly 0.48, 0.40, 0.32 π SI units respectively.

Emerson (1986) in their seminal paper on the magnetic fields due to a triaxial ellipsoid. Magmod XVA incorporates isotropic magnetic volume susceptibility and remanence with no self-demagnetisation; Magmod XVB incorporates isotropic magnetic volume susceptibility and remanence with self-demagnetisation while Model XVC incorporates anisotropic magnetic volume susceptibility, remanence and self-demagnetisation. The body properties of the ellipsoid in Magmod XV are summarised in Table 1 and a three-dimensional perspective plot is shown in Figure 2. The intrinsic remanent magnetisation $\mathbf{M_{nrm}}$ in each of these models is 120 A/m with declination 0° and inclination 90°, i.e. at the north magnetic pole. To illustrate the effect of self-magnetisation with increasing magnetic susceptibility, I have calculated the effective induced magnetisation $\mathbf{M_{idm}}$, the effective remanent magnetisation $\mathbf{M_{rdm}}$, the intrinsic total resultant magnetisation $\mathbf{M_{tot}} = \mathbf{M_{ind}} + \mathbf{M_{nrm}}$ and the resultant or effective magnetisation $\mathbf{M_{res}} = \mathbf{M_{idm}} + \mathbf{M_{rdm}}$ corrected for self-demagnetisation for three increasing bulk susceptibilities, namely, 1.25, 1.90 and 2.77 SI units. The magnetisations for each of these models are shown in Table 2 and the computed images of the gradient magnetic tensor for Magmod XVB2 are shown in Figure 3 for an observation height of 300 m above the centre of the ellipsoid.

The bulk susceptibility in Model XVC1 is also 1.256637 SI units or 0.4π SI units exactly. However, its intrinsic magnetic susceptibility $k_{\text{ams}} = \lvert\mathbf{M_{ind}}/\lvert\mathbf{b_0}$ accounting for anisotropy but not self-demagnetisation (anisotropy $P = 1.50$) is approximately 1.056373 SI units, while its effective magnetic susceptibility $k_{\text{eff}} = \lvert\mathbf{M_{idm}}\rvert/\lvert\mathbf{b_0}\rvert$ accounting for both anisotropy and self-demagnetisation is 0.795751 SI (see Tables 1 and 2). The second susceptibility of 1.90 SI (Model XVA2) corresponds to where the intrinsic total resultant magnetisation is almost parallel to the direction of strike of the ellipsoid while the third susceptibility of 2.77 SI (Model XVA3) corresponds to where the intrinsic total resultant magnetisation is horizontal. Models XVA1, XVA2, XVA3 do not account for self-demagnetisation so that the intrinsic total resultant $\mathbf{M_{tot}}$ and resultant magnetisations $\mathbf{M_{res}}$ are identical. However models XVB1, XVB2, XVB3 do incorporate self-demagnetisation so that their resultant magnetisations $\mathbf{M_{res}} = \mathbf{M_{idm}} + \mathbf{M_{rdm}}$ are significantly lower in magnitude than their intrinsic total resultant magnetisations $\mathbf{M_{tot}} = \mathbf{M_{ind}} + \mathbf{M_{nrm}}$ and, most importantly, their directions are deflected by at least 7 degrees or more. This is also the case for both the effective induced magnetisation vector $\mathbf{M_{idm}}$ and the effective remanent magnetisation vector $\mathbf{M_{rdm}}$. Under the influence of self-demagnetisation, both these magnetisations have significantly lower magnitudes than their intrinsic counterparts, $\mathbf{M_{idm}}$ and $\mathbf{M_{idm}}$ (see Table 2). Furthermore, for models XVB1 to XVB3, the effective induced magnetisation is deflected from the inducing field direction by between 5° and 9° while the effective remanent magnetisation vector $\mathbf{M_{rdm}}$ is deflected from the intrinsic remanent magnetisation direction by between 6.9° and 11.1°. The effect of self-demagnetisation on the resultant magnetisation $\mathbf{M_{res}}$ and the effective induced magnetisation vector $\mathbf{M_{idm}}$ becomes more pronounced as the magnetic volume susceptibility increases (see Table 2). This also has the effect of slightly increasing the effective Koenigsberger ratio $Q_{\text{sdm}} = \lvert\mathbf{M_{rdm}}\rvert/\lvert\mathbf{M_{idm}}\rvert$ (Figure 2).

Parameters shown in Table 2 are as follows: k_{bulk} is the intrinsic bulk magnetic susceptibility and k_{eff} is the effective magnetic susceptibility accounting for

Table 2. Magnetisation parameters for ellipsoidal models Magmod XVA, XVB and XVC.

Parameter	XVA1	XVA2	XVA3	XVB1	XVB2	XVB3	XVC1
k_{bulk} (SI)	1.256637	1.900000	2.773091	1.256637	1.900000	2.773091	1.256637
k_{eff} (sdm) (SI)	1.256637	1.900000	2.773091	0.909282	1.210265	1.523574	0.795751
$\|\mathbf{M_{ind}}\|$ (A/m)	60.0000	90.7183	132.4054	60.0000	90.7183	132.4054	50.4381
$D_{\mathbf{ind}}$	10.000°	10.000°	10.000°	10.000°	10.000°	10.000°	11.947°
$I_{\mathbf{ind}}$	−65.000°	−65.000°	−65.000°	−65.000°	−65.000°	−65.000°	−59.5982°
$\|\mathbf{M_{nrm}}\|$ (A/m)	120.0000	120.0000	120.0000	120.0000	120.0000	120.0000	120.0000
D_{nrm}	0.000°	0.000°	0.000°	0.000°	0.000°	0.000°	0.000°
I_{nrm}	90.000°	90.000°	90.000°	90.000°	90.000°	90.000°	90.000°
Q_{nrm}	2.00000	1.32278	0.90631	2.00000	1.32278	0.90631	2.37915
$\|\mathbf{M_{tot}}\|$ (A/m)	70.3503	53.8268	55.9569	70.3503	53.8268	55.9569	80.6433
D_{tot}	10.000°	10.000°	10.000°	10.000°	10.000°	10.000°	11.947°
I_{tot}	68.8728°	44.5801°	0.0000°	68.8728°	44.5801°	0.0000°	71.5477°
$\|\mathbf{M_{res}}\|$ (A/m)	70.3503	53.8268	55.9569	53.8470	37.3103	31.2248	64.5243
D_{res}	10.000°	10.000°	10.000°	351.253°	357.218°	3.9061°	347.062°
I_{res}	68.8728°	44.5801°	0.0000°	66.6478°	44.6862°	3.8932°	69.7861°
$\|\mathbf{M_{idm}}\|$ (A/m)	60.0000	90.7183	132.4054	43.4150	57.7859	72.7453	37.9943
D_{idm}	10.000°	10.000°	10.000°	21.5936°	25.5419°	29.7604°	21.3230°
I_{idm}	−65.0000°	−65.0000°	−65.0000°	−66.3144°	−66.7914°	−67.2905°	−62.1733°
$\|\mathbf{M}_{rdm}\|$ (A/m)	120.0000	120.0000	120.0000	89.8487	80.3411	70.5461	94.9866
D_{rdm}	0.000°	0.000°	0.000°	296.788°	298.174°	299.552°	294.472°
I_{rdm}	90.0000°	90.0000°	90.0000°	83.0794°	80.9779°	78.8970°	82.3942°
Q_{sdm}	2.00000	1.32278	0.90631	2.06953	1.39032	0.96977	2.50002
$\angle\mathbf{b_0M_{ind}}$	0.0000°	0.0000°	0.0000°	0.0000°	0.0000°	0.0000°	5.4764°
$\angle\mathbf{b_0M_{idm}}$	0.0000°	0.0000°	0.0000°	4.9482°	6.5757°	8.2730°	5.7670°
$\angle\mathbf{M_{ind}M_{nrm}}$	155.0000°	155.0000°	155.0000°	155.0000°	155.0000°	155.0000°	149.5982°
$\angle\mathbf{M_{ind}M_{tot}}$	133.8728°	109.5801°	65.0000°	133.8728°	109.5801°	65.0000°	131.1459°
$\angle\mathbf{M_{ind}M_{res}}$	133.8728°	109.5801°	65.0000°	132.3329°	110.1399°	69.0395°	130.5984°
$\angle\mathbf{M_{ind}M_{idm}}$	0.0000°	0.0000°	0.0000°	4.9482°	6.5757°	8.2730°	5.2345°
$\angle\mathbf{M_{nrm}M_{rdm}}$	0.0000°	0.0000°	0.0000°	6.9206°	9.0221°	11.1030°	7.6058°
$\angle\mathbf{M_{nrm}M_{res}}$	21.1272°	45.4199°	90.0000°	23.1274°	45.3138°	86.1068°	20.2139°
$\angle\mathbf{M_{tot}M_{res}}$	0.0000°	0.0000°	0.0000°	7.4022°	9.0869°	7.2274°	8.3602°
Moment $\|\mathbf{m}\|$ GAm^2	1.10506	0.845509	0.878969	0.845827	0.586068	0.490479	1.01355

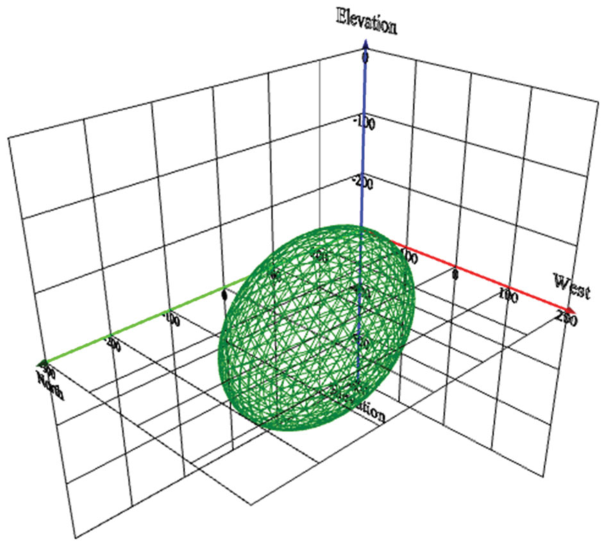

Figure 2. Three-dimensional perspective plot of the triaxial ellipsoid model Magmod XV.

self-demagnetisation and anisotropy; $\mathbf{M_{ind}}$ is the intrinsic induced magnetisation with declination D_{ind} and inclination I_{ind}; $\mathbf{M_{nrm}}$ is the intrinsic natural remanent magnetisation with declination D_{nrm} and inclination I_{nrm}; $Q_{nrm} = |\mathbf{M_{nrm}}|/|\mathbf{M_{ind}}|$ is the intrinsic Koenigsberger ratio; $\mathbf{M_{tot}} = \mathbf{M_{ind}} + \mathbf{M_{nrm}}$ is the intrinsic total magnetisation with declination D_{tot} and inclination I_{tot}; $\mathbf{M_{res}}$ is the resultant or effective magnetisation accounting for self-demagnetisation with declination D_{res} and inclination I_{res}; $\mathbf{M_{idm}}$ is the effective induced magnetisation accounting for self-demagnetisation with declination D_{idm} and inclination I_{idm};$\mathbf{M_{rdm}}$ is the effective natural remanent magnetisation accounting for self-demagnetisation with declination D_{rdm} and inclination I_{rdm}; $Q_{sdm} = |\mathbf{M}_{rdm}|/|\mathbf{M}_{idm}|$ is the effective Koenigsberger ratio accounting for self-demagnetisation; $\angle\mathbf{b_0M_{ind}}$ is the angle between the geomagnetic field and the intrinsic induced magnetisation; $\angle\mathbf{b_0M_{idm}}$ is the angle between the geomagnetic field and the effective induced magnetisation (accounting for self-demagnetisation); $\angle\mathbf{M_{ind}M_{nrm}}$ is the angle between the intrinsic induced and remanent magnetisations; $\angle\mathbf{M_{ind}M_{tot}}$ is the angle between the intrinsic induced and total magnetisations; $\angle\mathbf{M_{ind}M_{res}}$ is the angle between the intrinsic induced magnetisation and the resultant or effective magnetisation (accounting for self-demagnetisation); $\angle\mathbf{M_{nrm}M_{rdm}}$ is the angle between the intrinsic remanent and the effective remanent magnetisation; $\angle\mathbf{M_{nrm}}$ $\mathbf{M_{res}}$ is the angle between the intrinsic remanent magnetisation and the resultant magnetisation (accounting for self-demagnetisation); $\angle\mathbf{M_{tot}M_{res}}$ is the angle between the intrinsic total magnetisation and the resultant magnetisation (accounting for self-demagnetisation) and $|\mathbf{m}|$ is the magnetic moment intensity.

The eigenvector decomposition of the magnetic gradient tensor and a novel approach to determining the magnetisation direction

The NSS is a parameter that was introduced to applied geophysics by the CSIRO Magnetics Group (Beiki et al.

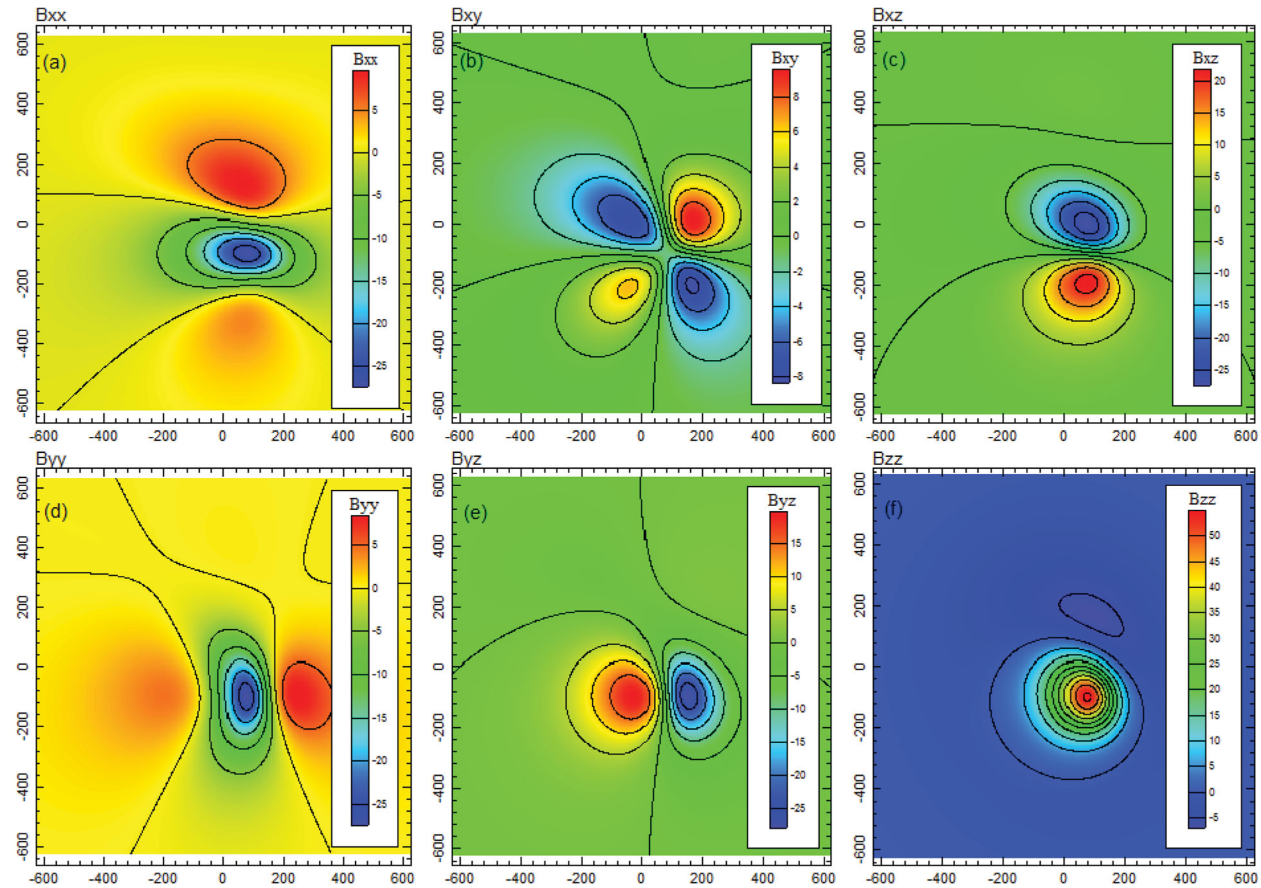

Figure 3. Images of the magnetic gradient tensor associated with model Magmod XVB2 which incorporates isotropic magnetic susceptibility, remanence and self-demagnetisation. Figure 3(a–c) (top row: left to right) show gridded images of tensor elements $B_{xx-NN}, B_{xy-NE}, B_{xz-ND}$ respectively while Figure 3(d–f) (bottom row: left to right) show tensor elements B_{yy-EE}, B_{yz-ED}, B_{zz-DD} respectively. The body properties for Magmod XVB are summarised in Table 1 and the magnetisations for Magmod XVB2 are shown in Table 2. The 1.25 × 1.25 km grids were generated by forward modelling using a spacing of 2.50 m at a height of 300 m above the centre of the ellipsoid.

2012; Clark 2012). Importantly, the NSS is a generalisation of the scaled magnetic moment of a dipole source. The scaled or normalised magnetic moment was originally defined by Wilson (1985) and later by Wynn (1999) in the context of tracking magnetic dipole sources. The NSS, as denoted by μ, is defined in terms of the eigenvalues of its magnetic gradient tensor, namely,

$$\mu = \sqrt{-\lambda_2^2 - \lambda_1\lambda_3} \quad \text{for } \lambda_1 \geq \lambda_2 \geq \lambda_3, \tag{31}$$

where $\lambda_1 > 0$ is the first eigenvalue which is always positive, λ_2 is the second or intermediate eigenvalue which has the smallest absolute value and $\lambda_3 < 0$ is always negative. The tracelessness property of the tensor, combined with the ordering of the eigenvalues, ensures that the quantity under the square root sign in Equation (31) is always positive unless there is no gradient, in which case all eigenvalues are zero and the NSS is also zero. Therefore the NSS is always real and positive definite whenever a magnetic field gradient is present, and this is irrespective of the nature of the magnetic sources.

The scaled moment vector $\boldsymbol{\mu}$ for a point dipole source of magnetic moment $\mathbf{m}$ is (Clark 2012)

$$\boldsymbol{\mu}(\mathbf{r}) = \frac{3C_m\mathbf{m}}{r^4} = \frac{3C_m m}{r^4}\hat{\mathbf{u}}_{\mathrm{m}} = \mu\hat{\mathbf{u}}_{\mathrm{m}}; \mu = \frac{3C_m m}{r^4}, \tag{32.1}$$

where $\hat{\mathbf{u}}_{\mathrm{m}}$ is the unit direction cosine vector for the magnetic moment $\mathbf{m}$. For a dipole source, the magnitude μ of the scaled moment is proportional to the magnitude of the dipole moment and inversely proportional to the fourth power of the distance from the source. It can be calculated directly from the eigenvalues of the gradient tensor, using Equation (31).

The external field of a uniformly magnetised sphere is identical to that of a point dipole with the same magnetic moment $\mathbf{m}$. located at the centre of the sphere. Hence for a uniformly magnetised sphere of radius a and intensity of magnetisation M, the magnitude μ of the scaled moment or NSS at an external point a distance r from the centre is

$$\mu(\mathbf{r}) = \frac{3C_m m}{r^4} = \frac{4\pi C_m M a^3}{r^4} \quad \left(\text{for } m = Mv = \frac{4\pi a^3 M}{3}\right). \tag{32.2}$$

Importantly for a horizontal observation plane, the NSS peaks directly above the centre of the sphere regardless of the orientation of the magnetic moment. This conclusion also holds approximately for any compact source with a reasonably coherent magnetisation direction, for which the external field is dominated by the dipole moment. Clark (2012) and Beiki et al. (2012) showed that the NSS, defined by Equation (31), peaks directly over the source for a number of useful elementary models and that it is completely independent of magnetisation direction for arbitrary 2D sources, as well as for spheres and axially magnetised narrow plunging pipes. The NSS is also only weakly dependent on magnetisation direction for a wide variety of 3D magnetic models.

These observations lead to a formulation for the magnetic gradient tensor in terms of the components of magnetisation of a magnetic sphere. In particular, for an observation point directly above a dipole or a uniformly magnetised sphere of radius a with magnetisation $\mathbf{M}$, it may be shown (see Appendix A5) that the magnetic gradient tensor $\mathbf{B}$ is given by

$$\mathbf{B}(0,0,z) = \frac{4\pi C_m a^3}{r^4}\begin{bmatrix} -M_z & 0 & -M_x \\ 0 & -M_z & -M_y \\ -M_x & -M_y & 2M_z \end{bmatrix} = f\begin{bmatrix} -M_z & 0 & -M_x \\ 0 & -M_z & -M_y \\ -M_x & -M_y & 2M_z \end{bmatrix}, \tag{33}$$

where $f = (4\pi C_m a^3)/z^4$ and $z < -a$ ($a = 0$ for a point dipole).

The three eigenvalues $\lambda_1, \lambda_2, \lambda_3$ are found by solving for the roots of the characteristic equation det ($\mathbf{B} - \lambda\mathbf{I}) = 0$. These eigenvalues are obtained by solving the depressed cubic equation in λ (see Appendix A5 for details).

The ordering of the three eigenvalues is determined by the sign of the vertical component of magnetisation M_z. For $M_z > 0$, the eigenvalues at an axial station in descending order $\lambda_1 > \lambda_2 > \lambda_3$ are given by the following expressions:

$$\lambda_1 = \frac{f}{2}\left[M_z + \sqrt{4(M_x^2 + M_y^2) + 9M_z^2}\right] = \frac{fM_z}{2}\left[1 + \sqrt{4\cot^2 I_M + 9}\right] = \frac{fM_z}{2}(1 + \Delta), \tag{34.1}$$

$$\lambda_2 = -fM_z, \tag{34.2}$$

$$\lambda_3 = \frac{f}{2}\left[M_z - \sqrt{4(M_x^2 + M_y^2) + 9M_z^2}\right] = \frac{fM_z}{2}\left[1 - \sqrt{4\cot^2 I_M + 9}\right] = \frac{fM_z}{2}(1 - \Delta), \tag{34.3}$$

where I_M is the inclination of the magnetisation vector $\mathbf{M}$,

$$I_M = \arctan\left[\frac{M_z}{\sqrt{(M_x^2 + M_y^2)}}\right] \text{or} I_M = \arctan\left(\frac{M_z}{M_h}\right), \tag{35}$$

and

$$\Delta = \sqrt{4(M_x^2 + M_y^2)/M_z^2 + 9} = \sqrt{4(M_h^2/M_z^2) + 9} = \sqrt{4\cot^2 I_M + 9}. \tag{36}$$

Importantly for magnetisations where M_z is positive (such as induced magnetisations in the northern magnetic hemisphere), the second eigenvalue λ_2 is always negative, whereas for magnetisations in the southern magnetic hemisphere where M_z is negative, the second eigenvalue λ_2 is always positive and the λ_1 and λ_3 eigenvalues are interchanged. The NSS $\mu(0,0,z)$ along the vertical axis through the centre of the sphere may now be derived from Equations (34.1) o (34.3), namely,

$$\mu(0,0,z) = \sqrt{-\lambda_2^2 - \lambda_1\lambda_3} = \sqrt{-f^2M_z^2 - \left[\frac{fM_z}{2}(1+\Delta)\right]\left[\frac{fM_z}{2}(1-\Delta)\right]} = \frac{fM_z}{2}(\Delta^2 - 5).$$

Since the discriminant term is $\Delta = \sqrt{4(M_x^2 + M_y^2)/M_z^2 + 9}$, then the final expression for the scaled moment is

$$\mu(0,0,z) = \frac{f}{2}\sqrt{4(M_x^2 + M_y^2) + 9M_z^2 - 5M_z^2} = f\sqrt{M_x^2 + M_y^2 + M_z^2} = f|\mathbf{M}|. \tag{37}$$

This is an important result. It shows that the NSS on the vertical axis of the magnetised sphere is independent of the magnetisation direction (as is true at every point around the sphere) and, for a particular observation height $|z|$ above the centre, its magnitude is determined by the radius of the sphere and the intensity of magnetisation only.

The angle φ is defined as the angle between the line joining the centre of the dipole or magnetic sphere to the observation point $P(\mathbf{r}_s)$ and the magnetic moment vector $\mathbf{m}$ (Clark 2012). However, when the observation point is located on the vertical axis of the magnetised sphere, the ratio $\cos\varphi = \lambda_2/\mu$ yields an expression for the inclination I_M of magnetisation, namely,

$$\cos\varphi = \frac{\lambda_2}{\mu} = \frac{-fM_z}{f|\mathbf{M}|} = \frac{-M_z}{\sqrt{M_h^2 + M_z^2}} = \frac{-\text{sgn}M_z}{\sqrt{\cot^2 I_M + 1}} = -\sin I_M \quad \text{for } 0 \le \varphi \le \pi \text{ and } -\frac{\pi}{2} \le I_M \le \frac{\pi}{2}. \tag{38}$$

Therefore, for any axial observation point above a uniformly magnetised sphere, it may be deduced that $I_M = \varphi - \pi/2$.

An expression for the declination of magnetisation D_M may be derived from the each of the three eigenvectors $\hat{\mathbf{e}}_1, \hat{\mathbf{e}}_2, \hat{\mathbf{e}}_3$ of the magnetic gradient tensor $\mathbf{B}$

for an observation station $P(0,0,z)$ located at a height $|z|$ directly above an origin at the centre of a magnetised sphere. The declination angle D_M as defined here follows the palaeomagnetic convention, namely, it is defined as the azimuthal angle measured in degrees positive clockwise from true north to the horizontal direction of magnetisation ($0° \le D_M \le 360°$). The three eigenvectors $\hat{\mathbf{e}}_1, \hat{\mathbf{e}}_2, \hat{\mathbf{e}}_3$ of the magnetic gradient tensor are found by solving the linear equation $\mathbf{B}\hat{\mathbf{e}}_j = \lambda_j \hat{\mathbf{e}}_j$ for each of the three eigenvalues $\lambda_1, \lambda_2, \lambda_3$, respectively. A full derivation is given in Appendix A5.

The first eigenvector $\hat{\mathbf{e}}_1$ at an observation point $P(0,0,z)$ directly above the centre of a magnetic sphere or dipole source in which $M_z > 0$ and $\lambda_1 = \frac{fM_z}{2}(1+\Delta)$ is

$$\hat{\mathbf{e}}_1 = (e_{1x}, e_{1y}, e_{1z})^{\mathrm{T}} = \frac{\left(M_x, M_y, \frac{2M_h^2}{M_z(3-\Delta)}\right)^{\mathrm{T}}}{\sqrt{M_x^2 + M_y^2 + \frac{4M_h^4}{M_z^2(3-\Delta)^2}}}. \tag{39}$$

The second eigenvector $\hat{\mathbf{e}}_2$ at an observation point $P(0,0,z)$ directly above the centre of a magnetic sphere or dipole source in which $M_z > 0$ and $\lambda_2 = -fM_z$ is

$$\hat{\mathbf{e}}_2 = (e_{2x}, e_{2y}, e_{2z})^{\mathrm{T}} = \frac{(-M_y, M_x, 0)^{\mathrm{T}}}{\sqrt{M_x^2 + M_y{}^2}}$$
$$= \left(-\frac{M_y}{M_h}, \frac{M_x}{M_h}, 0\right)^{\mathrm{T}} = (-\sin D_M, \cos D_M, 0)^{\mathrm{T}}. \tag{40}$$

The third eigenvector $\hat{\mathbf{e}}_3$ at an observation point $P(0,0,z)$ directly above the centre of a magnetic sphere or dipole source in which $M_z > 0$ and $\lambda_3 = \frac{fM_z}{2}(1-\Delta)$ is

$$\hat{\mathbf{e}}_3 = (e_{3x}, e_{3y}, e_{3z})^{\mathrm{T}} = \frac{\left(M_x, M_y, \frac{2M_h^2}{M_z(3+\Delta)}\right)^{\mathrm{T}}}{\sqrt{M_x^2 + M_y^2 + \frac{4M_h^4}{M_z^2(3+\Delta)^2}}}. \tag{41}$$

By inspection of Equations (39) and (41), it is immediately evident that the declinations of the first D_{ev1} and third D_{ev3} eigenvectors at a point $P(0,0,z)$ are identical to the declination of magnetisation for the magnetised sphere, namely,

$$D_{ev1} = \arctan\left(\frac{e_{1y}}{e_{1x}}\right) = \arctan\left(\frac{M_y}{M_x}\right) = D_M$$
$$(0^\circ \le D_{ev1} \le 360^\circ), \tag{42.1}$$
$$D_{ev3} = \arctan\left(\frac{e_{3y}}{e_{3x}}\right) = \arctan\left(\frac{M_y}{M_x}\right) = D_M$$
$$(0^\circ \le D_{ev1} \le 360^\circ). \tag{42.2}$$

The inclinations of the first I_{ev1} and third I_{ev3} eigenvectors at a point $P(0,0,z)$ are

$$I_{ev1} = \arctan\left[\frac{e_{1z}}{\sqrt{e_{1x}^2 + e_{1y}^2}}\right] = \arctan\left[\frac{2M_h}{M_z(3-\Delta)}\right]$$
$$= \arctan\left[\frac{2\cot I_M}{(3-\Delta)}\right] \quad I_M > 0, \tag{43.1}$$
$$I_{ev3} = \arctan\left[\frac{e_{3z}}{\sqrt{e_{3x}^2 + e_{3y}^2}}\right] = \arctan\left[\frac{2M_h}{M_z(3+\Delta)}\right]$$
$$= \arctan\left[\frac{2\cot I_M}{(3+\Delta)}\right] \quad I_M > 0. \tag{43.2}$$

From Equations (36), (43.1) and (43.2), it can be shown that the inclinations of the first and third eigenvectors differ by 90°.

By inspection of Equation (40), the inclination of the second eigenvector at $P(0,0,z)$ is zero and its declination D_{ex2} is related to the declination of magnetisation D_M as follows:

$$D_M = \arctan\left(\frac{-e_{2x}}{e_{2y}}\right) = D_{ex2} \pm \frac{\pi}{2}. \tag{44}$$

Finally, I also note that estimates of the declination of magnetisation D_M may also be obtained from the magnetic gradient tensor directly. For example, by inspection of Equation (33), it is evident that the B_{xz} and B_{zx} tensor elements are given by $-M_x$ while the B_{yz} and B_{zy} tensor elements are given by $-M_y$. Hence an expression for the declination of magnetisation is

$$D_M = \arctan\left(\frac{M_y}{M_x}\right) = \arctan\left(\frac{-B_{yz}}{-B_{xz}}\right)$$
$$0^\circ \le D_M \le 360^\circ. \tag{45}$$

The use and effectiveness of these new methodologies to reliably determine both the inclination and declination of magnetisation for a series of ellipsoidal bodies will be investigated in the next section. Table 3 shows the symmetries and anti-symmetries in the eigenvalues and the direction of magnetisation parameters, namely, φ, I_M, D_M for a specific inclination of magnetisation in both the northern and southern magnetic hemispheres. The declinations and inclinations of the first and third eigenvectors, i.e. $D_{ev1}, I_{ev1}, D_{ev3}, I_{ev3}$ allow for the correct determination of the declination of magnetisation D_M in each magnetic hemisphere. In addition, the declination of magnetisation obtained from Equation (45) may be used to ensure that the declination estimates obtained from the eigenvector directions in Equations (42.1) and (42.2) have been correctly determined.

Table 3. Direction of magnetisation parameters in both the north and south magnetic hemispheres as estimated from the eigenvector-eigenvalue decomposition of the magnetic gradient tensor at observation points directly above the centre of a magnetic sphere with magnetisation **M**.

Parameter name	Northern magnetic hemisphere $I_M \geq 0$ and $M_z \geq 0$	Southern magnetic hemisphere $I_M < 0$ and $M_z < 0$
λ_1	$\lambda_{1N} = \frac{fM_z}{2}(1+\Delta) = -\lambda_{3S}$	$\lambda_{1S} = \frac{fM_z}{2}(1-\Delta) = -\lambda_{3N}$
λ_2	$\lambda_{2N} = -fM_z(\lambda_{2N} < 0) = -\lambda_{2S}$	$\lambda_{2S} = -fM_z(\lambda_{2s} > 0) = -\lambda_{2N}$
λ_3	$\lambda_{3N} = \frac{fM_z}{2}(1-\Delta) = -\lambda_{1S}$	$\lambda_{3S} = \frac{fM_z}{2}(1+\Delta) = -\lambda_{1N}$
φ	$\varphi = \arccos\left(\frac{\lambda_2}{\mu}\right); \frac{\pi}{2} \leq \varphi \leq \pi$	$\varphi = \arccos\left(\frac{\lambda_2}{\mu}\right); 0 \leq \varphi \leq \frac{\pi}{2}$
I_M	$I_M = \arccos\left(\frac{\lambda_2}{\mu}\right) - \frac{\pi}{2} = \varphi - \frac{\pi}{2}$	$I_M = \arccos\left(\frac{\lambda_2}{\mu}\right) - \frac{\pi}{2} = \varphi - \frac{\pi}{2}$
I_M	$I_M = \arctan\left(\frac{M_z}{M_h}\right) = \arctan\left(\frac{(B_{zz}/2)}{\sqrt{B_{xz}^2 + B_{yz}^2}}\right)$	$I_M = \arctan\left(\frac{M_z}{M_h}\right) = \arctan\left(\frac{(B_{zz}/2)}{\sqrt{B_{xz}^2 + B_{yz}^2}}\right)$
D_M	$D_M = \arctan\left(\frac{M_y}{M_x}\right) = \arctan\left(\frac{-B_{yz}}{-B_{xz}}\right)$	$D_M = \arctan\left(\frac{M_y}{M_x}\right) = \arctan\left(\frac{-B_{yz}}{-B_{xz}}\right)$
D_M	$D_M = \arctan\left(\frac{e_{jy}}{e_{jx}}\right) = D_{evj}; j = 1,3$	$D_M = \arctan\left(\frac{e_{jy}}{e_{jx}}\right) = D_{evj}; j = 1,3$
D_M	$D_M = \arctan\left(\frac{-e_{2x}}{e_{2y}}\right) = D_{ev2} \pm \frac{\pi}{2}$	$D_M = \arctan\left(\frac{-e_{2x}}{e_{2y}}\right) = D_{ev2} \pm \frac{\pi}{2}$
I_{ev1}	$I_{ev1N} = \arctan\left[\frac{2\cot I_M}{(3-\Delta)}\right] I_{ev1N} < 0$	$I_{ev1S} = \arctan\left[\frac{2\cot I_M}{(3+\Delta)}\right] = -I_{ev3N}$
I_{ev3}	$I_{ev3N} = \arctan\left[\frac{2\cot I_M}{(3+\Delta)}\right] I_{ev3N} > 0$	$I_{ev3S} = \arctan\left[\frac{2\cot I_M}{(3-\Delta)}\right] = -I_{ev1N}$

Parameters influencing the determination of magnetisation direction – a synthetic example using Magmod IV

In this section, I present an investigation into the influence of body shape, observation height and inclination of magnetisation on the determination of magnetisation direction using the eigenvector theory presented above. For this research, I have calculated the magnetic gradient tensor elements over a horizontal grid of magnetic stations at heights of 50, 75, 100 and 200 m above the centre of a series of magnetic spheres, spheroids and triaxial ellipsoids with the same intensity of magnetisation and magnetic moment but with different shape anisotropy, i.e. where the ellipticity $e = a_1/a_3$ in plan view was allowed to range from 1 to 20. My investigations will look at the influence of shape anisotropy on the accuracy of the magnetisation determinations at different observation heights. In addition, I present my findings from an initial investigation into the effect of changing magnetisation direction on the accuracy of the magnetisation determinations. This study will compare the relative accuracy of the magnetisation determinations for points directly over the centre of magnetisation with magnetisations determined at points where the NSS μ is at a maximum, the latter being the most obvious starting point for these determinations when the centre of magnetisation is unknown.

The model chosen for this investigation is the magnetic sphere model (Magmod IV) in Emerson, Clark, and Saul (1985). This model incorporates isotropic magnetic volume susceptibility and remanent magnetisation. Self-demagnetisation effects have been neglected for this study. The body properties of the magnetic sphere and ellipsoids are summarised in Table 4. The major and minor axes in each of the ellipsoidal bodies are horizontal with the major axis aligned north–south and the minor axis east–west. The intrinsic or bulk susceptibility k_b in each of these models was 0.125664 SI units (0.01 cgs units) while the remanent magnetisation $\mathbf{M}_{\mathbf{nrm}}$ in each of these models was intensity $|\mathbf{M}_{\mathbf{nrm}}| = 95.0094$ A/m with declination $D_{\mathrm{nrm}} = 328.64°$ and inclination $I_{\mathrm{nrm}} = -43.56°$. The intensity of total resultant magnetisation $M_{\mathbf{tot}}$ in each of these models was 100 A/m with declination $D_{\mathrm{tot}} = 330.00°$ and inclination $I_{\mathrm{tot}} = -45.00°$.

The position of global maxima in the NSS μ relative to the horizontal centre of magnetisation (hcm) of the ellipsoidal bodies depends on the observation height above the centre of the ellipsoid, the ellipticity e of the ellipsoidal sources and the direction of magnetisation in these sources. The effect of observation height and shape factor e on the location of global maxima $\mu_{\max}$ in the NSS is illustrated in Figure 4(a–c) for a resultant magnetisation model in the fourth quadrant ($D_M = 330°$) of the southern magnetic hemisphere ($I_M = -45°$), i.e. model Q4SH, as shown in Table 4. The model nomenclature used here is Q4 for declinations in the fourth quadrant (270°$\leq D_M <$360°) and SH for inclinations in the southern magnetic hemisphere (−90°$< I_M <$0°). Figure 4(a) shows the distance from the hcm to the position of the global maximum of NSS μ for observation heights of 50, 75, 100 and 200 m as the ellipticity is increased from 1 to 20. Figure 4(b) shows

Table 4. Body properties for the Magmod IV sphere and equivalent triaxial ellipsoids.

$e = a_1/a_3$	a_1 (m)	a_3 (m)	a_2 (m)	$\lvert z_{ts}\rvert$ for $\lvert z_c\rvert = 50$ m	$\lvert z_{ts}\rvert$ for $\lvert z_c\rvert = 75$ m	$\lvert z_{ts}\rvert$ for $\lvert z_c\rvert = 100$ m
1.000	13.3650	13.3650	13.3650	36.6350	61.6350	86.6350
1.100	14.0800	12.8000	13.2464	36.7536	61.7536	86.7536
1.250	15.0000	12.0000	13.2629	36.7371	61.7371	86.7371
1.500	16.2000	10.8000	13.6450	36.3550	61.3550	86.3550
1.750	17.5000	10.0000	13.6419	36.3581	61.3581	86.3581
2.000	18.0000	9.0000	14.7366	35.2634	60.2634	85.2634
2.500	20.0000	8.0000	14.9208	35.0792	60.0792	85.0792
3.000	21.0000	7.0000	16.2403	33.7597	58.7597	83.7597
4.000	24.0000	6.0000	16.5786	33.4214	58.4214	83.4214
5.000	26.0000	5.2000	17.6577	32.3423	57.3423	82.3423
6.000	28.2000	4.7000	18.0121	31.9879	56.9879	81.9879
7.000	29.4000	4.2000	19.3337	30.6663	55.6663	80.6663
8.000	31.4000	3.9250	19.3706	30.6294	55.6294	80.6294
10.000	35.0000	3.5000	19.4884	30.5116	55.5116	80.5116
12.000	37.8000	3.1500	20.0498	29.9502	54.9502	79.9502
15.000	42.0000	2.8000	20.3004	29.6996	54.6996	79.6996
20.000	48.0000	2.4000	20.7233	29.2767	54.2767	79.2767

Notes: The lengths of the a_2 semiaxis where $a_2 = 3v/(4\pi a_1 a_3)$ are shown to only 4 decimal spaces. The depths to the top surface z_{ts} in each of the ellipsoids are tabulated for the 50, 75 and 100 m depths to the centre $|z_c|$ of each ellipsoid model. The semiaxial lengths a_1, a_2, a_3 for the ellipsoids. Volume $v = \frac{4\pi}{3} a_1 a_2 a_3 = 10000.0\,\mathrm{m}^3$.
The ellipsoidal angles (α, δ, γ) forming a right-hand clockwise coordinate system
α (azimuth of the downward pointing a_1 semiaxis) $= 0.00°$
δ (plunge of the downward pointing a_1 semiaxis) $= 0.00°$
γ (rotation of the downward a_3 semiaxis from the $= -90.00°$ vertical plane containing the a_1 semiaxis)
Declination and inclination of the x_1, x_2, x_3 (or a_1, a_2, a_3) body axes:
Declination $\hat{\mathbf{u}}_1 = 0.00°$, Inclination $\hat{\mathbf{u}}_1 = 0.00°$
Declination $\hat{\mathbf{u}}_2 = 0.00°$, Inclination $\hat{\mathbf{u}}_2 = -90.00°$
Declination $\hat{\mathbf{u}}_3 = 90.00°$, Inclination $\hat{\mathbf{u}}_3 = 0.00°$
The local geomagnetic field vector $\mathbf{b_0}$ (nT):
$|\mathbf{b_0}| = 58000$ nT, Declination $\mathbf{b_0} = 11.00°$, Inclination $\mathbf{b_0} = -64.50°$
The bulk or intrinsic magnetic susceptibility k_b:
$k_b = 0.125663706$ SI units ($4\pi \times 10^{-2}$ SI units)
The intrinsic induced $\mathbf{M_{ind}}$ and intrinsic remanent magnetisation $\mathbf{M_{nrm}}$ vectors:
$|\mathbf{M_{ind}}| = 5.8000$ A/m, Declination $D_{\mathrm{ind}} = 11.00°$, Inclination $I_{\mathrm{ind}} = -64.50°$
$|\mathbf{M_{nrm}}| = 95.0094$ A/m, Declination $D_{\mathbf{nrm}} = 328.64°$, Inclination $I_{\mathrm{nrm}} = -43.56°$
Koenigsberger ratio $Q = |\mathbf{M_{nrm}}|/|\mathbf{M_{ind}}| = 16.38$
The intrinsic total resultant magnetisation vector $\mathbf{M_{res}} = \mathbf{M_{ind}} + \mathbf{M_{nrm}}$:
$|\mathbf{M_{res}}| = 100$ A/m, Declination $D_{\mathrm{res}} = 330.00°$, Inclination $I_{\mathrm{res}} = -45.00°$
Total magnetic moment $|\mathbf{m}| = \mathbf{M_{res}}|v = 10^6$ Am^2.

the azimuthal angle from the hcm to the position of the global maximum of NSS μ for observation heights of 50, 75, 100 and 200 m as the ellipticity is increased from 1 to 20. Figure 4(a) also shows the position of $\mu_{\max}$ relative to the centre of magnetisation for a magnetisation Q4NH (i.e. declination $D_M = 330°$ in the fourth quadrant Q4 and inclination $I_M = 45°$ in the northern – NH) at an observation height of 100 m. The positions of $\mu_{\max}$ are always offset from the hcm for ellipticies $e \geq 1.75$ and for observation heights $z \leq 100$m. This increases to an ellipticity $e \geq 3$ for an observation height of 200 m. For magnetisations in the southern magnetic hemisphere, the global maxima in $\mu_{\max}$ migrate very slightly in an E or NE direction from the centre of magnetisation of the ellipsoid as the ellipticities increase above 3.0. For a low observation height of 50 m, the maxima in $\mu_{\max}$ for model Q4SH are positioned directly north of the hcm along the major axis of the ellipsoidal bodies for ellipticities above 5. Moreover, for an equivalent magnetisation in the northern hemisphere (model Q4NH), the global maxima $\mu_{\max}$ in the NSS are positioned southwards from the hcm. This trend is less pronounced as the observation height increases (see Figure 4(b)). The difference in azimuth between model Q4NH and Q4SH at an observation height of 100 m is 180 degrees (see Figure 4(c)). The behaviour exhibited here is governed by the shape factor of the ellipsoids and the observation height above their centres. For low observation heights, the shape factor strongly influences the location of global maxima $\mu_{\max}$ in the NSS with the positions migrating towards points on the major axis of the ellipsoid as the degree of ellipticity increases. This migration is towards opposite ends of the ellipsoid for magnetisations in the north and south hemispheres. Furthermore as the observation height $|z|$ increases, the displacement in the position of $\mu_{\max}$ from the hcm is considerably reduced as is the degree of rotation towards the major axis. This is consistent with the dipole-like behaviour of ellipsoids as the observation height becomes large (Clark, Saul, and Emerson 1986; Foss 2017).

Figure 5(a,b) shows plots of the estimated inclination of magnetisation calculated from $I_M = \varphi - \pi/2$. at four different observation heights (i.e. 50, 75, 100 and 200 m) as the ellipticity $e = a_1/a_3$ of the ellipsoidal sources is increased from 1 to 20. Figure 5(a) shows the results for observation points directly above the centre of magnetisation (hcm) while Figure 5(b) shows results for observation points at the global maximum $\mu_{\max}$ in the NSS. Figure 5(c) displays the departures of

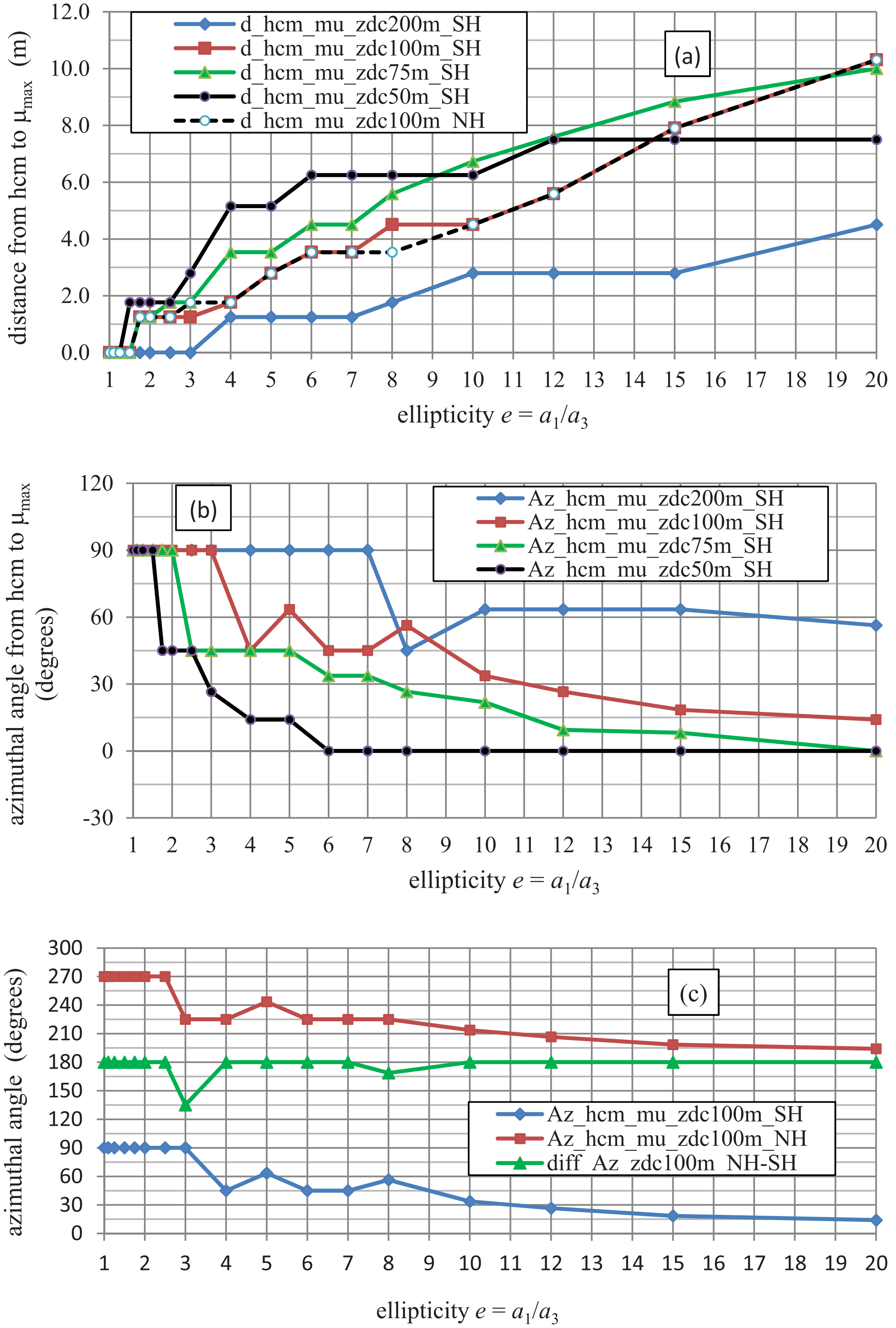

Figure 4. The location of global maxima in NSS μ_{max} relative to the hcm for a series of triaxial ellipsoids with ellipticities e ranging from 1–20 and observation heights 50, 75, 100 and 200 m above the centre of magnetisation . Figure 4(a) shows the distance from the hcm to the location of μ_{max} while Figure 4(b) shows the azimuth in degrees from true north. Figure 4(c) shows that the difference between the azimuthal angles from the hcm to the location of μ_{max} in the northern and southern magnetic hemispheres is 180°.

the estimated inclination of magnetisation $I_{M(est)}$ for the same series of ellipsoids, one with an inclination of magnetisation I_M of 45° in the northern hemisphere and the other with an inclination of magnetisation I_M of −45° in the southern magnetic hemisphere. The observation height is 100 m in both cases. The plots of estimated

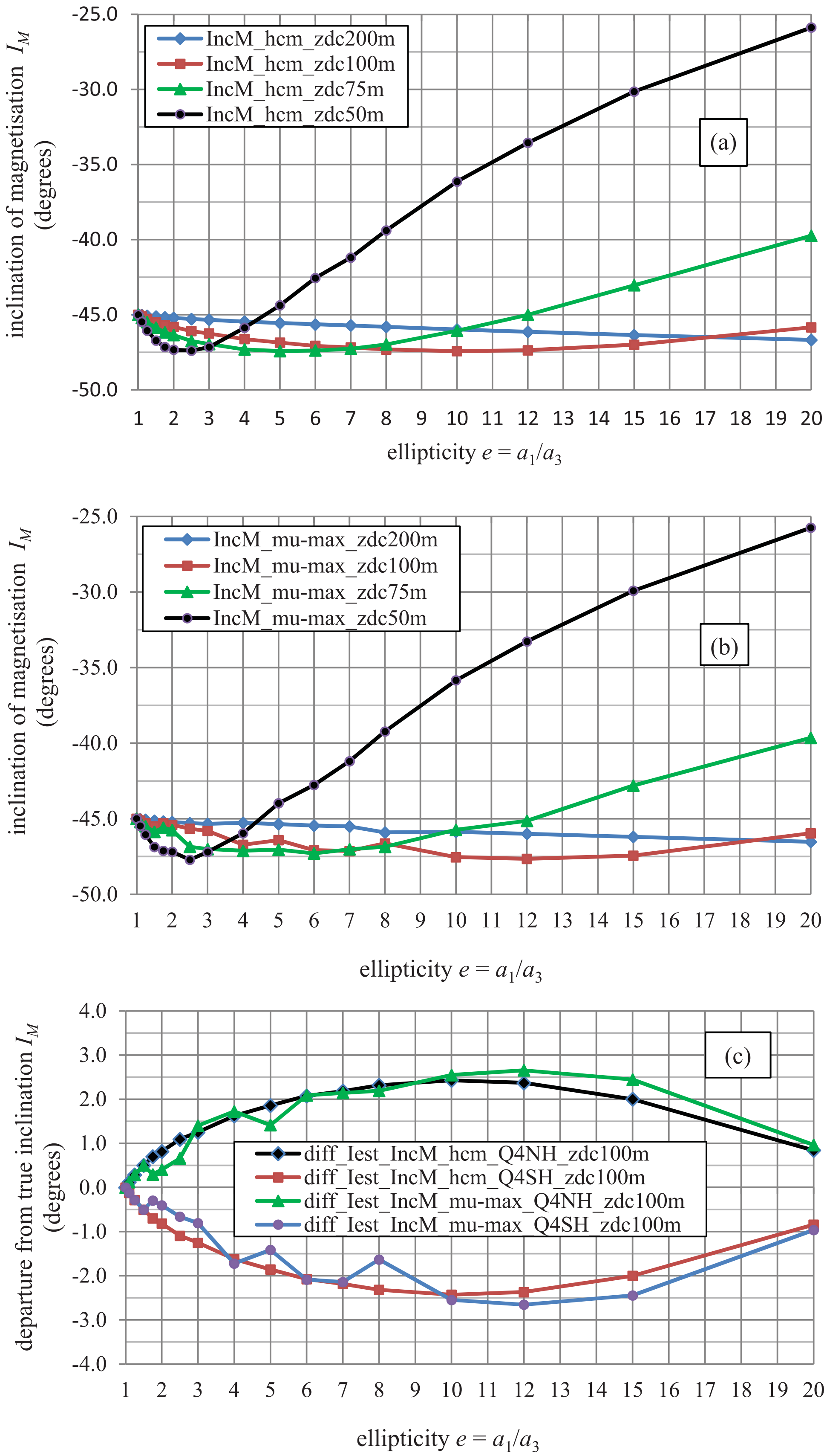

Figure 5. The estimated inclination of magnetisation $I_{M(est)}$ for a series of triaxial ellipsoids with ellipticities e ranging from 1 to 20 and observation heights at 50, 75, 100 and 200 m above the ellipsoid centre. Figure 5(a) shows the estimated inclination of magnetisation $I_{M(est)}$ at points above the centre of magnetisation while Figure 5(b) shows the estimated inclination of magnetisation at observation points where the NSS μ is a maximum. Figure 5(c) shows the departures of the estimated inclination from the true inclination of magnetisation I_M for the same series of triaxial ellipsoids at an observation height of 100 m in the northern and southern hemisphere.

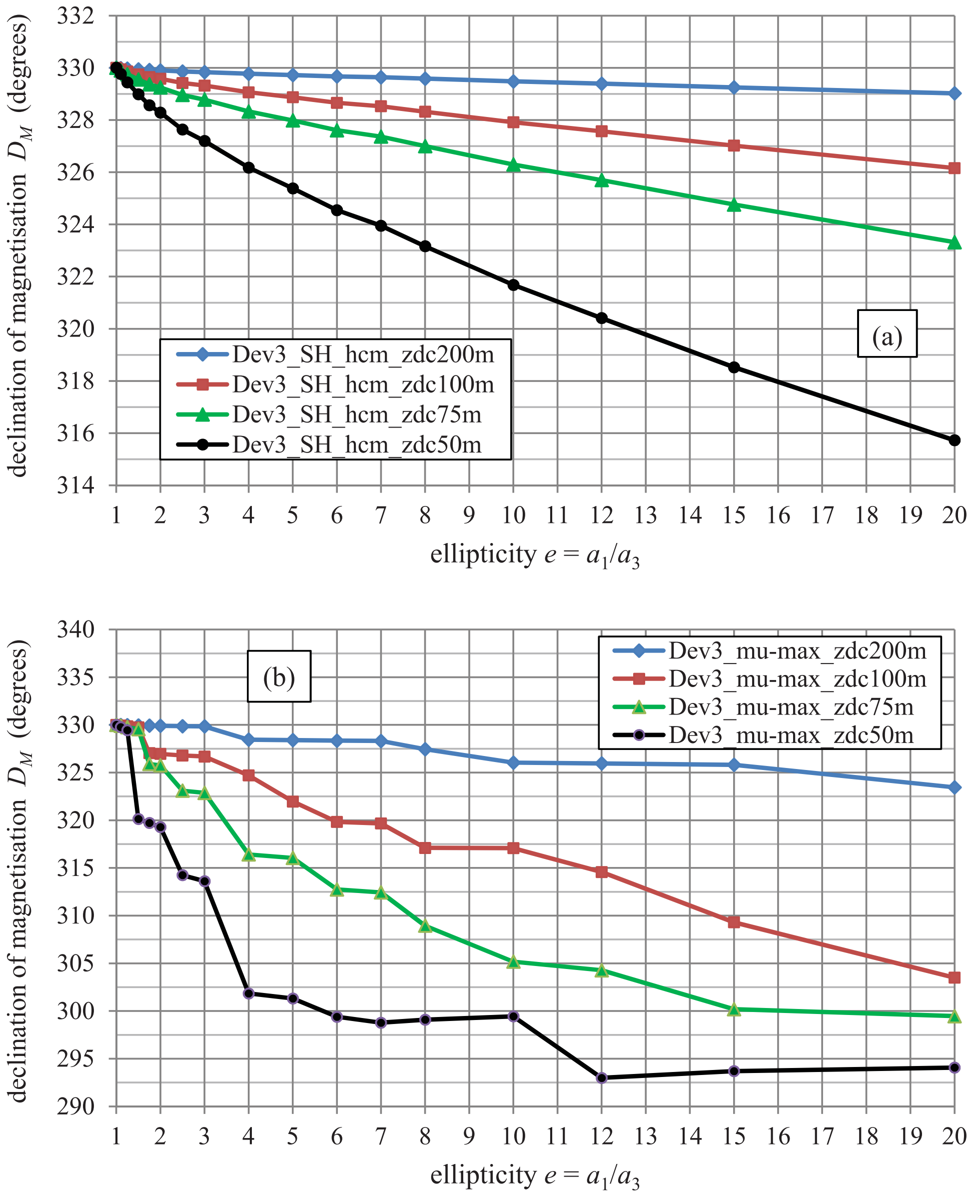

Figure 6. The declination of magnetisation D_M estimated from the principal eigenvector $\hat{\mathbf{e}}_3$ for a series of triaxial ellipsoids with ellipticities e ranging from 1 to 20 and at observation heights of 50, 75, 100 and 200 m above the ellipsoid centre. Figure 6(a) shows the estimated declination of magnetisation at points above the centre of magnetisation while Figure 6(b) shows the estimated declination of magnetisation at observation points where the NSS μ is a maximum.

inclination of magnetisation at the hcm in Figure 5(a) are smoothly varying while those in Figure 5(b) for the estimated inclination of magnetisation show discontinuous steps consistent with positional shifts in the global peaks in $\mu_{\max}$ as the ellipticity $e = a_1/a_3$ is increased from 1.75 to 20.

Most significantly, the estimated inclinations of magnetisation are not significantly affected by the degree of ellipticity of the ellipsoidal source at least for observation heights 100 m above the centre of the ellipsoid or $\sim$79.3–86.8 m above the top surface of the ellipsoidal sources. For example, the maximum deviation from the true inclination is less than $\sim$1.5° and $\sim$2.5° at observation heights of 200 and 100 m, respectively. Even for an observation height of 50 m above the centre or 29.3−36.8 m above the top surface the deviation from the true inclination of magnetisation is less than 10° for an ellipticity of 10 in Figure 5(a,b). This observation height is akin to a surface gradiometer survey with sources $\sim$30–40 m below ground. The accuracy of the inclination estimates increases as the observation height increases. Importantly the estimates of inclination of magnetisation are similar for observation points above the centre of magnetisation or where the NSS is at a global maximum for a particular observation height. For example, the mean absolute error between the estimates of inclination of magnetisation at the two measurement points is 0.090° at an observation height of 200 m, 0.258° at 100 m, 0.177° at 75 m and 0.152° at 50 m.

Figure 6(a,b) shows plots of the declination angles estimated from the declination D_{ev3} of the principal eigenvector $\hat{\mathbf{e}}_3$ (see Table 3) at four different observation heights as the ellipticity $e = a_1/a_3$ of the ellipsoidal

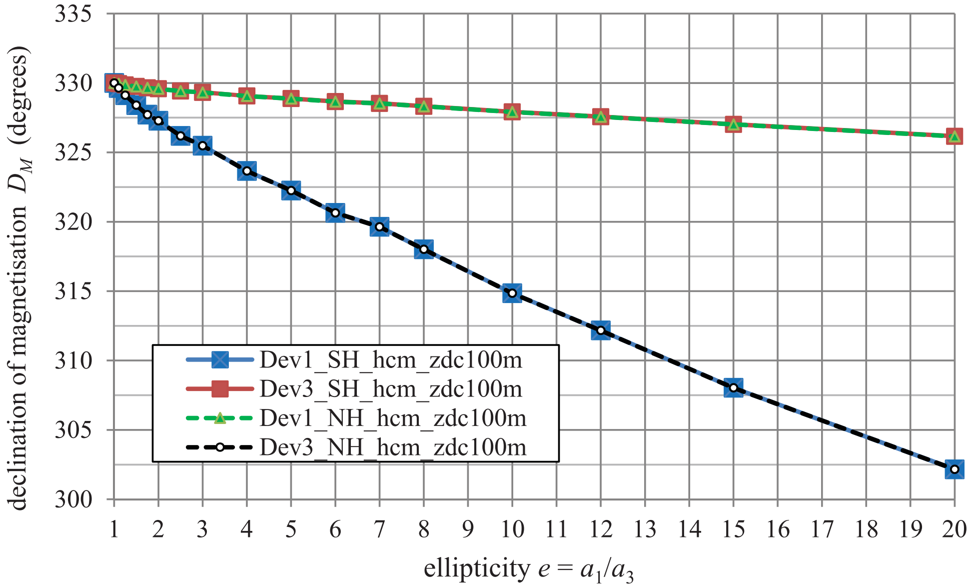

Figure 7. The declination of magnetisation D_M estimated from eigenvectors $\hat{\mathbf{e}}_1$ and $\hat{\mathbf{e}}_3$ for a series of triaxial ellipsoids with ellipticities e ranging from 1 to 20 in both the southern hemisphere (Model Q4SH) and northern hemisphere (Model Q4NH). In the former, the principal eigenvector is $\hat{\mathbf{e}}_3$ while in the latter it is $\hat{\mathbf{e}}_1$. The plots of declination of magnetisation for $\hat{\mathbf{e}}_1$ in the northern hemisphere exactly over-plot those for $\hat{\mathbf{e}}_3$ in the southern hemisphere and vice versa. The observation height is 100 m above the ellipsoid centre in both models.

sources is increased from 1 to 20. The accuracy of the declination estimates improves as the observation height increases. This is consistent with the diminishing influence of shape anisotropy as the observation height increases with magnetic ellipsoids behaving as quasi-dipoles. The estimates of declination at the global maxima in NSS in Figure 6(b) have higher absolute errors than those over the centre of magnetisation in Figure 6(a). Also the deviation from the true declination angle is approximately quasi-linear especially for ellipticities $e \geq 4$. Furthermore, for magnetisations in the southern magnetic hemisphere (Q4SH), the third eigenvector $\hat{\mathbf{e}}_3$ yields the smallest deviations from the true declination while the first eigenvector $\hat{\mathbf{e}}_1$ yields the largest. This is reversed for magnetisations in the northern magnetic hemisphere (Q4NH) where the first eigenvector $\hat{\mathbf{e}}_1$ yields the smallest deviations from the true declination while the third eigenvector $\hat{\mathbf{e}}_3$ yields the largest. In both instances the eigenvector yielding the smallest deviation from the true declination of magnetisation is associated with the principal or largest eigenvalue which is λ_3 in the southern magnetic hemisphere and λ_1 in the northern magnetic hemisphere. This is illustrated in Figure 7 where the estimated declination of magnetisation curves for $\hat{\mathbf{e}}_1$ in model Q4SH are identical to those from for $\hat{\mathbf{e}}_3$ in model Q4SH. It is noted that plots of the declination of magnetisation are smoothly varying for observation points above the centre of magnetisation while those at the global maxima of the NSS have discontinuities consistent with slight shifts in the position of $\mu_{\max}$. Figure 8(a,b) shows the departures of the estimated magnetisation direction from the true magnetisation direction for a series of triaxial ellipsoids with ellipticities e, ranging from 1 to 20 and at observation heights of 50, 75, 100 and 200 m above the ellipsoid centre. Estimates of the departure from the true magnetisation direction for points above the centre of magnetisation in Figure 8(a) are extremely accurate, i.e. $\leq 3°$ for ellipticities $e \leq 12$ and observation heights $z \geq 75$m.

The effect of shape anisotropy on the eigenvalues of the gradient tensor in model Q4SH is shown in Figure 9. The relative change in the normalised principal eigenvalues for model Q4SH is shown for observation heights of 50, 75, 100 and 200 m. There is little change in the relative amplitude of the normalised eigenvalues with increasing ellipticity for observation heights of 100 and 200 m, respectively. For example, at an ellipticity of 15, the amplitudes of the normalised eigenvalues at observation heights of 100 and 200 m, respectively, are still 92.6% and 97.4% of the amplitudes for the equivalent perfect sphere with ellipticity of 1. Figure 10 shows plots of the ratio of observation height above the top surface of the ellipsoid to its maximum dimension, i.e. $z_{tc}/2a_1$. This ratio is equivalent to the distance of closest approach at which the magnetic field or gradient tensor is measured to the maximum elongation of a magnetic source. For magnetic field measurements, Foss (2017) states that bodies with ratios above 2 display behaviour consistent with a dipole magnetisation. For magnetic gradient tensor measurements above or in close proximity to the centre of magnetisation of a triaxial ellipsoid source, reliable magnetisation directions may be obtained when the ratio $z_{tc}/2a_1$ is close to 1.0. The influence of magnetisation direction will be investigated in the next section.

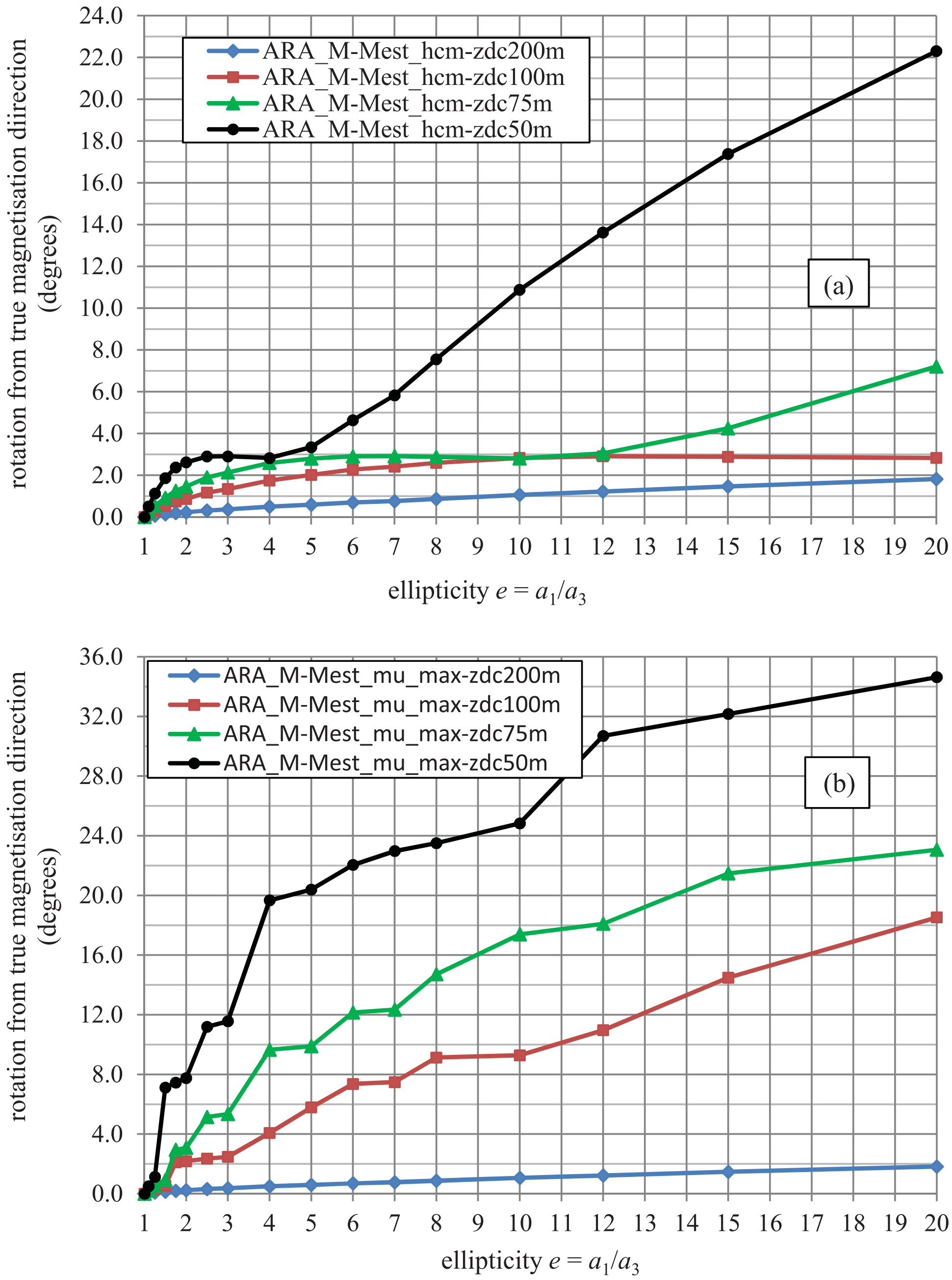

Figure 8. Rotation of the estimated magnetisation direction from the true magnetisation direction for a series of triaxial ellipsoids with ellipticities e ranging from 1 to 20 and at observation heights of 50, 75, 100 and 200 m above the ellipsoid centre. Figure 8(a) shows the ARA for the estimated magnetisation direction at points above the centre of magnetisation while Figure 8(b) shows the ARA for the estimated magnetisation direction at observation points where the NSS μ is a maximum.

The effect of magnetisation direction

Figure 11(a,b) and Figure 12(a,b) show plots of the estimated inclination $I_{M(\mathrm{est})}$ and declination $D_{M(\mathrm{est})}$ of magnetisation respectively for a series of ellipsoids with ellipticities of 2, 5, and 10 as the true inclination of magnetisation I_M is varied from $-90°$ to 0°. Figure 12(c) shows the departure or apparent rotation angle (ARA) of the estimated magnetisation direction from the true magnetisation direction for the same series of ellipsoids at observation points where the NSS μ is a maximum. The results shown here have been calculated at an observation height of 100 m above the centre of each ellipsoid. This yields shape factors $z_{ts}/2a_1$ of 2.36, 1.73 and 1.15, respectively, for the ellipsoids in Figure 11(a) and Figure 12(a). The step size between I_M estimates varies from $\sim 7°$ near the pole to $\sim 8.5°$ near the equator. The estimates of inclination of magnetisation in Figure 11(a,b) have been determined at both the hcm and at the position of each global maximum $\mu_{\max}$ in the NSS. The estimated inclinations are almost identical in both cases with the best results being achieved at low magnetic inclinations. However, the reliability of this method to estimate the inclination of magnetisation is shown to deteriorate at high inclinations of magnetisation particularly for ellipsoids where the shape anisotropy is high ($e > 5$) and where

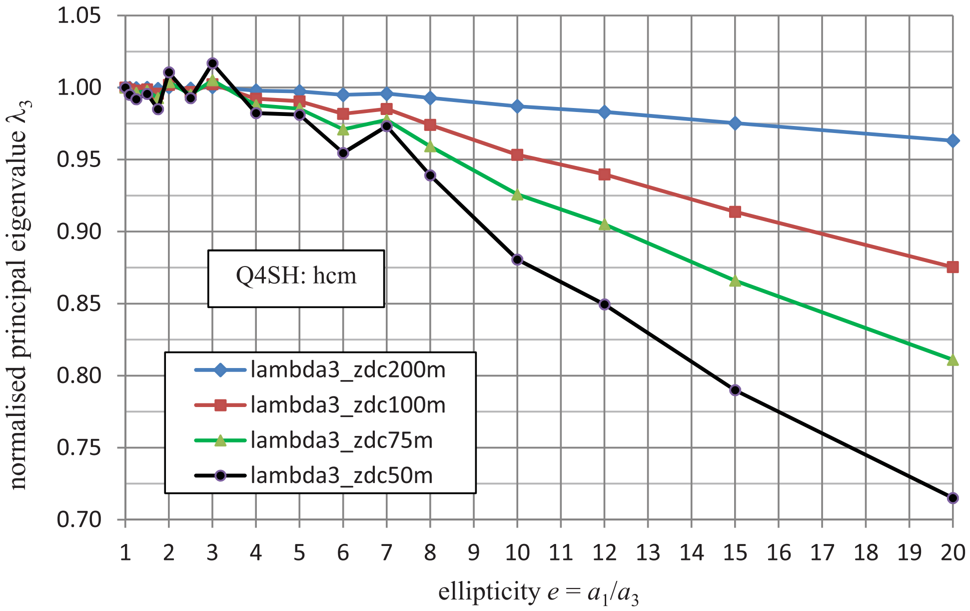

Figure 9. The normalised principal eigenvalues λ_3 for a series of triaxial ellipsoids with ellipticities e ranging from 1 to 20 and at observation heights of 50, 75, 100 and 200 m above the ellipsoid centre in model Q4SH.

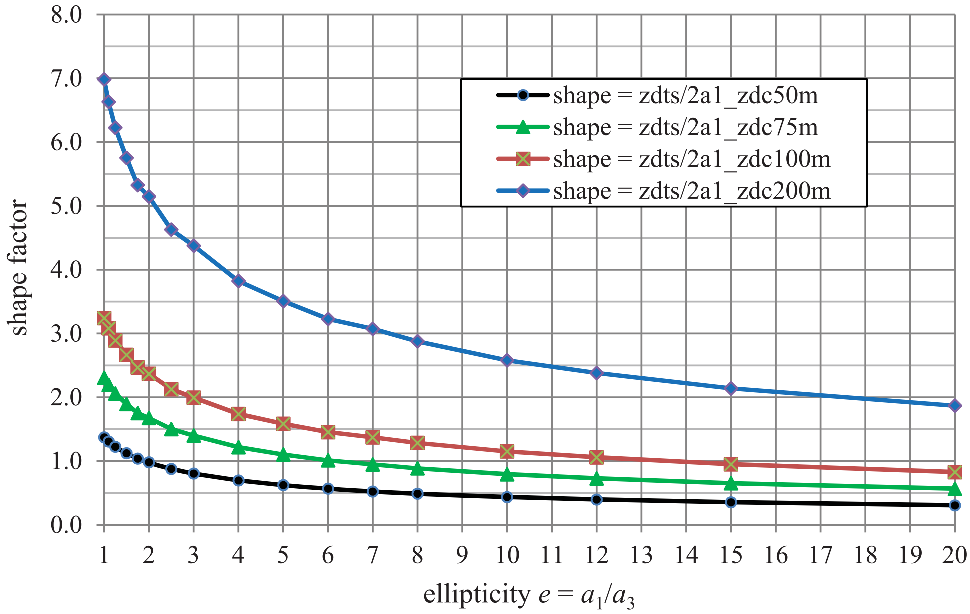

Figure 10. The shape factor $z_{tc}/2a_1$ for a series of triaxial ellipsoids with ellipticities e ranging from 1 to 20 and at observation heights of 50, 75, 100 and 200 m above the ellipsoid centre. Shape factors $z_{tc}/2a_1 > 1$ yield reliable estimates of magnetisation direction for each of the observation heights shown.

$z_{tc}/2a_1 < 1.5$. For example, at an observation height of 100 m, the estimated inclination of magnetisation for ellipsoids with ellipticities of 5 and 10 are unable to accurately resolve (i.e. to within 5°) inclinations of magnetisation $|I_M|$ above 70° and 65° respectively. This improves to $|I_M| < 81°$ at an observation height of 200 m and for ellipticities $e \leq 10$. The declination estimates in Figure 11(a,b) have been determined at both the hcm and at the position of each global maximum μ_{max} in the NSS. The plots in Figure 12(a) show that very accurate determinations of the declination of magnetisation may be obtained from the principal eigenvector of the gradient tensor (i.e. $\hat{\mathbf{e}}_3$ in the southern magnetic hemisphere) even at high inclinations of magnetisation near the south pole. These determinations are best made at the hcm where the effect of the true inclination of magnetisation is not significant. The plots in Figure 12(b) show that satisfactory determinations of the declination of magnetisation at points where the NSS μ is a maximum may be obtained from the principal eigenvector of the gradient tensor for magnetisations in the low to mid-latitudes, i.e. for $|I_M| < 50°$ at an observation height of 100 m above the centre of the ellipsoid bodies. This improves to $|I_M| < 65°$ for observation heights of 200 m and ellipticities $e \leq 10$. It is noted that the interpretation of differences between the true and estimated declinations can be misleading or even irrelevant especially at very steep inclinations. Under these circumstances, it is better to use the apparent rotation or departure angles (ARA's) as shown in Figure 12(c).

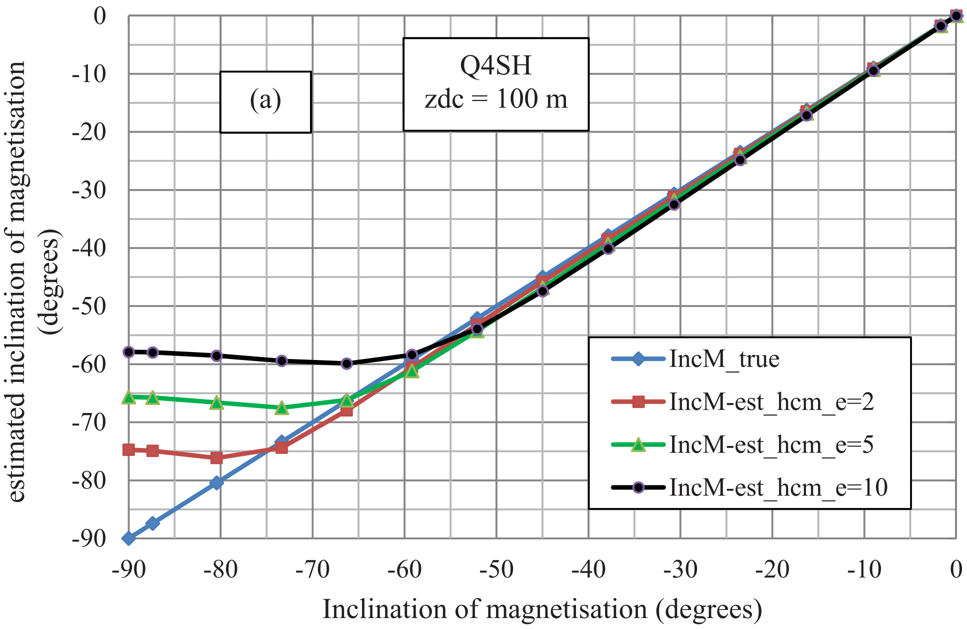

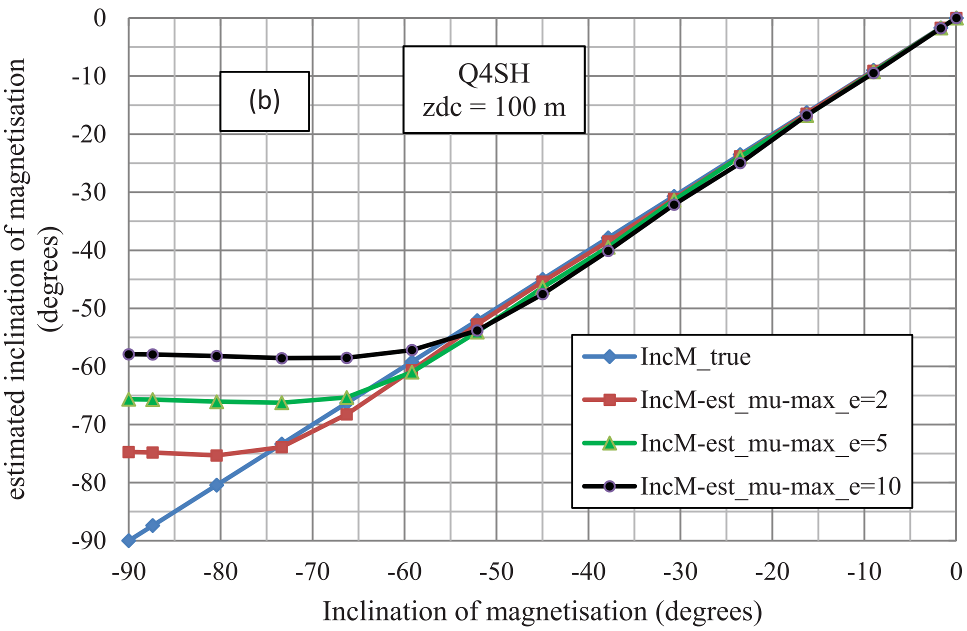

Figure 11. The inclination of magnetisation $I_{M(\mathrm{est})}$ estimated for a series of triaxial ellipsoids with ellipticities $e = 2, 5, 10$ in which the true inclination of magnetisation I_M is varied from $-90°$ to $0°$. Figure 11(a) shows the estimated inclination of magnetisation at points above the centre of magnetisation while Figure 11(b) shows the estimated inclination of magnetisation at observation points where the NSS μ is a maximum. The observation height above the centre of magnetisation is 100 m in each model.

The departure angles shown in Figure 12(c) indicate that quite accurate determinations of the magnetisation direction (within $\sim 15°$) may be obtained from the principal eigenvector at points where the NSS μ is a maximum for ellipsoids possessing steep magnetisations $|I_M| < 70°$ and moderate ellipticities $e \leq 5$.

Figure 13(a,b) shows the position of global maxima in the NSS μ relative to the hcm for a series of ellipsoids with ellipticities of 2, 5, and 10 in which the inclination of magnetisation in these sources is varied from $I_M = -90°$ to $0°$. Figure 13(a) shows the distance from the hcm to the position of the global maximum of NSS μ while Figure 13(b) shows the azimuthal angle from the hcm to the position of the global maximum of NSS μ. The observation height is 100 m in each of these plots. The positions of $\mu_{\max}$ become offset from the hcm as the inclination of magnetisation changes from low magnetic latitudes towards the magnetic pole. This offset of $\mu_{\max}$ from the hcm occurs at progressively lower inclinations of magnetisation as the shape anisotropy or ellipticity e increases. For example, Figure 13(a) shows that the offset in $\mu_{\max}$ occurs at inclination angles I_M in the range $(-37.9°, -45.0°)$ for an ellipticity $e = 2$, and in the range $(-16.3°, -23.5°)$ for $e = 5$, and in the range $(-9.0°, -16.3°)$ for $e = 10$.

For magnetisations in the southern magnetic hemisphere, the global maxima in μ migrate in an E or NE direction from the centre of magnetisation of the

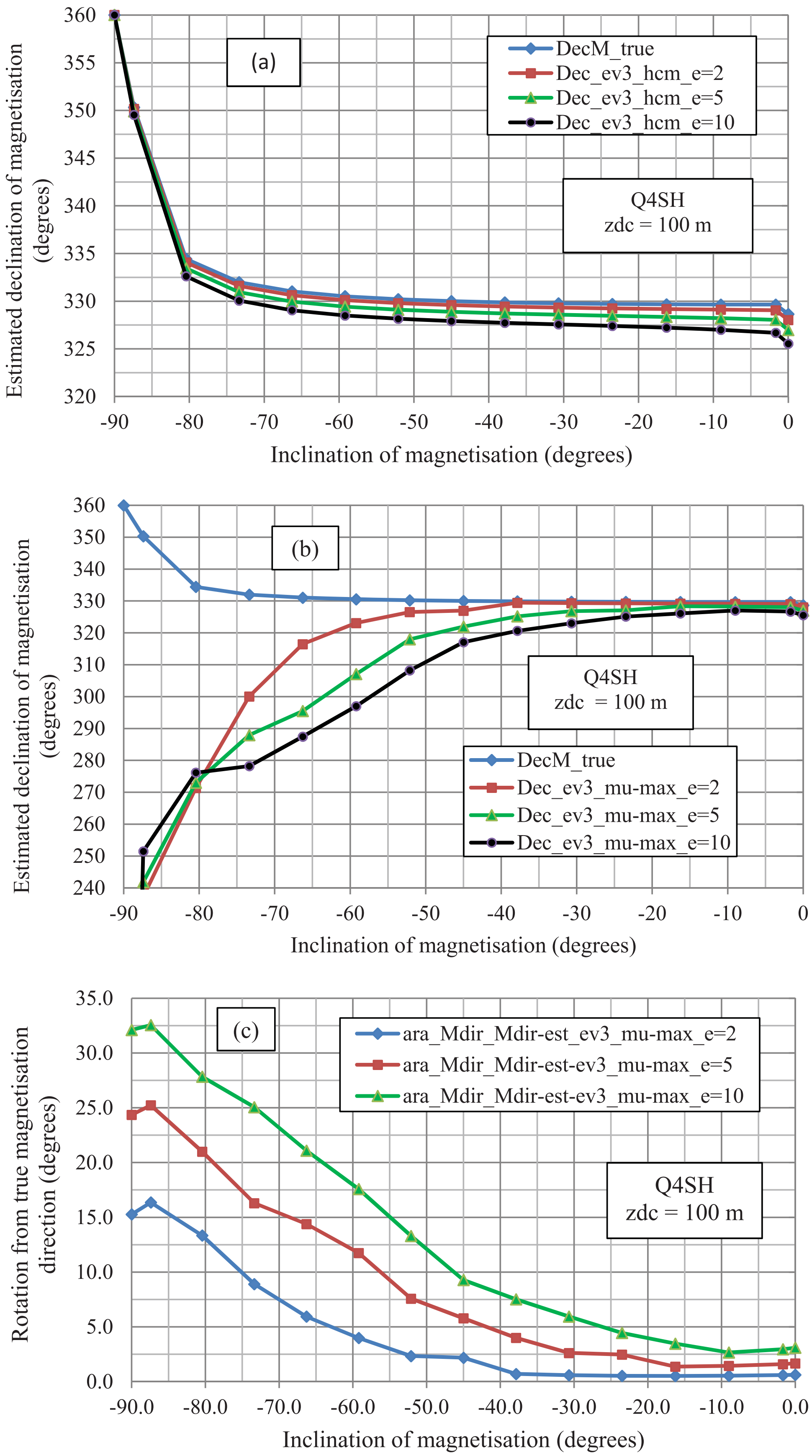

Figure 12. The declination of magnetisation D_M estimated from the principal eigenvector $\hat{\mathbf{e}}_3$ for a series of triaxial ellipsoids with ellipticities $e = 2, 5, 10$ in which the true inclination of magnetisation I_M is varied from $-90°$ to $0°$. Figure 12(a) shows the estimated declination of magnetisation at points above the centre of magnetisation (hcm) while Figure 12(b) shows the estimated declination of magnetisation at observation points where the NSS μ is a maximum. Figure 12(c) shows the departure or ARA of the estimated magnetisation direction from the true magnetisation direction at observation points where the NSS μ is a maximum. The observation height above the centre of magnetisation is 100 m in each model.

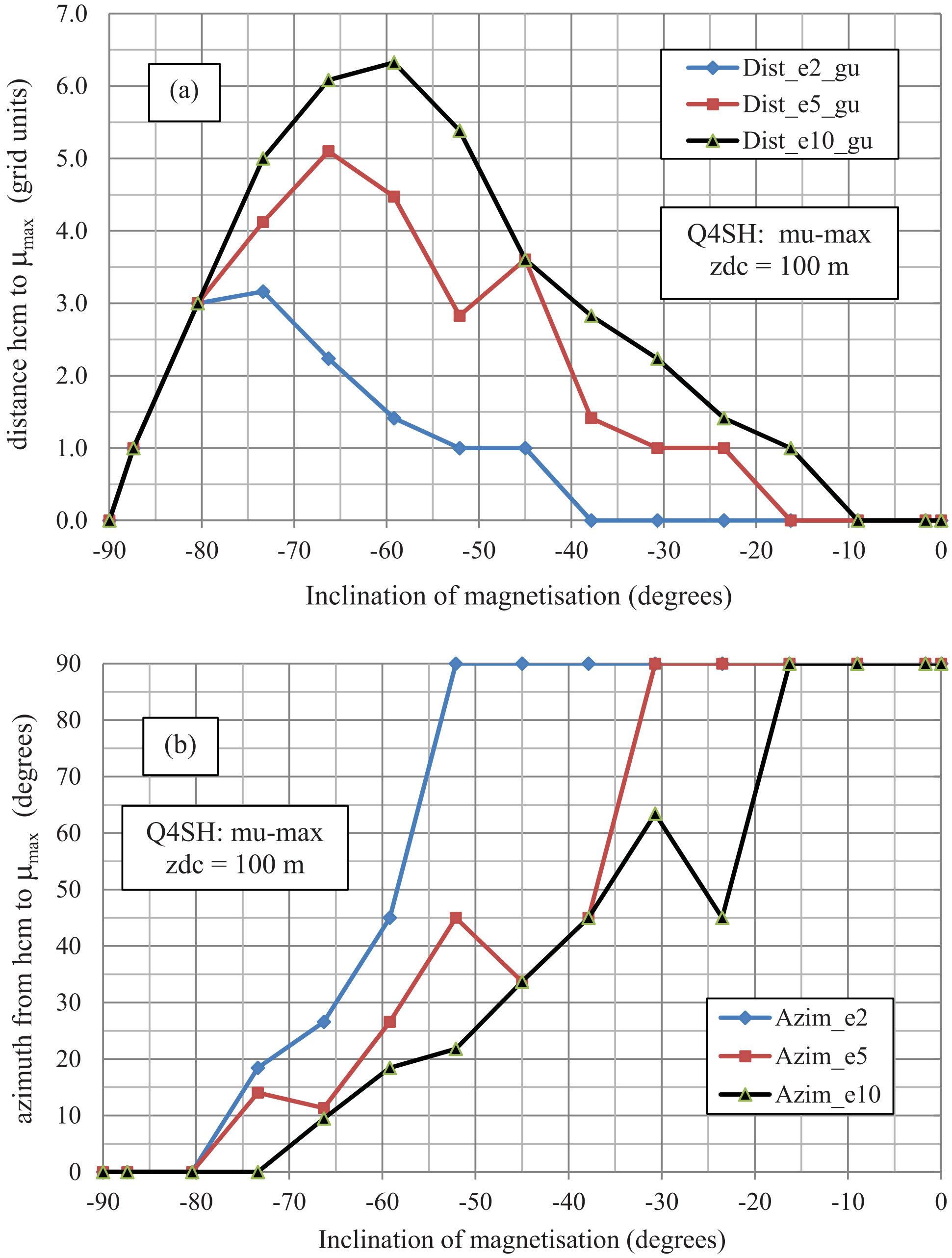

Figure 13. The location of global maxima in NSS μ_{max} relative to the hcm for a series of triaxial ellipsoids with ellipticities $e = 2, 5, 10$ in which the true inclination of magnetisation I_M is varied from $-90°$ to 0°. Figure 13(a) shows the distance in grid-spacing units (1 gu = 1.25 m) from the hcm to the location of μ_{max} while Figure 13(b) shows the azimuth in degrees from true north.

ellipsoid towards a point on the major axis of the ellipsoid as the inclination of magnetisation approaches the south magnetic pole. The offset distances reach a maximum at high inclinations of magnetisation ranging from $-60°$ to $-75°$ before declining substantially towards the centre of magnetisation for magnetisations near the magnetic pole. It is also confirmed that the position of μ_{max} is coincident with the hcm for an inclination of magnetisation at the magnetic pole, i.e. for $I_M = \pm 90°$ (see Figure 13(a)). The maximum offset distance increases with the degree of shape anisotropy (see Figure 13(a)). At very high inclinations of magnetisation and irrespective of the ellipticity or shape anisotropy, the global maxima in μ_{max} all lie on the major axis of the ellipsoid at a distance of only one grid spacing away from the hcm (see Figure 13(b)). This migration of μ_{max} back towards the hcm may explain the stability of declination of magnetisation estimates from $\hat{\mathbf{e}}_3$ at high inclinations of magnetisation as shown in Figure 12(a). I also note that the declination of the $\hat{\mathbf{e}}_1$ and $\hat{\mathbf{e}}_3$ eigenvectors is 0° or 360° for a magnetic sphere in which the inclination of magnetisation is $\pm 90°$ as shown in Figure 12(a) (see Equation (A57) in Appendix A5).

In summary

The effect of body shape or shape anisotropy (in this instance as defined by the ellipticity of an ellipsoid) diminishes with increasing observation height or distance at which the magnetic field is measured. Even for extremely elongated ellipsoidal bodies, its gradient tensor becomes more "dipole-like" as the observation distance becomes quite large. Provided that the gradient tensors are sufficiently well defined at these distances, this allows for reliable estimates of magnetisation direction.

A preliminary study into the effect of true magnetisation direction and particularly the inclination of magnetisation I_M has shown that magnetisations with lower inclination yield the most accurate determinations of magnetisation direction based on the eigenvector decomposition of the magnetic gradient tensor. The accuracy of this method improves as the observation height increases, i.e. where $z_{tc}/2a_1 > 1$, and as the degree of anisotropy of the ellipsoid decreases. However, the effect of the latter is much less pronounced particularly for observation heights where $z_{tc}/2a_1 > 2$ (see Figure 10). This is consistent with the dipole-like behaviour of uniformly magnetised magnetic ellipsoids as the observation height becomes large relative to the largest dimension of the body, i.e. the source magnetisation dominates the influence of body shape. Importantly, reliable estimates of the inclination of magnetisation I_M may be obtained at both the hcm and also at the global maxima $\mu_{\max}$ in the NSS. Estimates of the declination of magnetisation I_M are best obtained from the principal eigenvector of the gradient tensor, i.e. eigenvector $\hat{\mathbf{e}}_1$ in the northern magnetic hemisphere and $\hat{\mathbf{e}}_3$ in the southern magnetic hemisphere. However, these determinations are best made above the centre of magnetisation where the effect of the true inclination of magnetisation is not significant. Estimates of the declination of magnetisation at positions where μ is at a global maxima are less accurate particularly for observation heights where $z_{tc}/2a_1 < 1.5$ and for ellipticities $e > 10$.

The positioning of global maxima $\mu_{\max}$ in the NSS relative to the hcm is influenced by observation height, shape anisotropy and the inclination of magnetisation. For the ellipsoids studied here, the global maxima $\mu_{\max}$ in NSS migrate towards the major axis of the ellipsoid

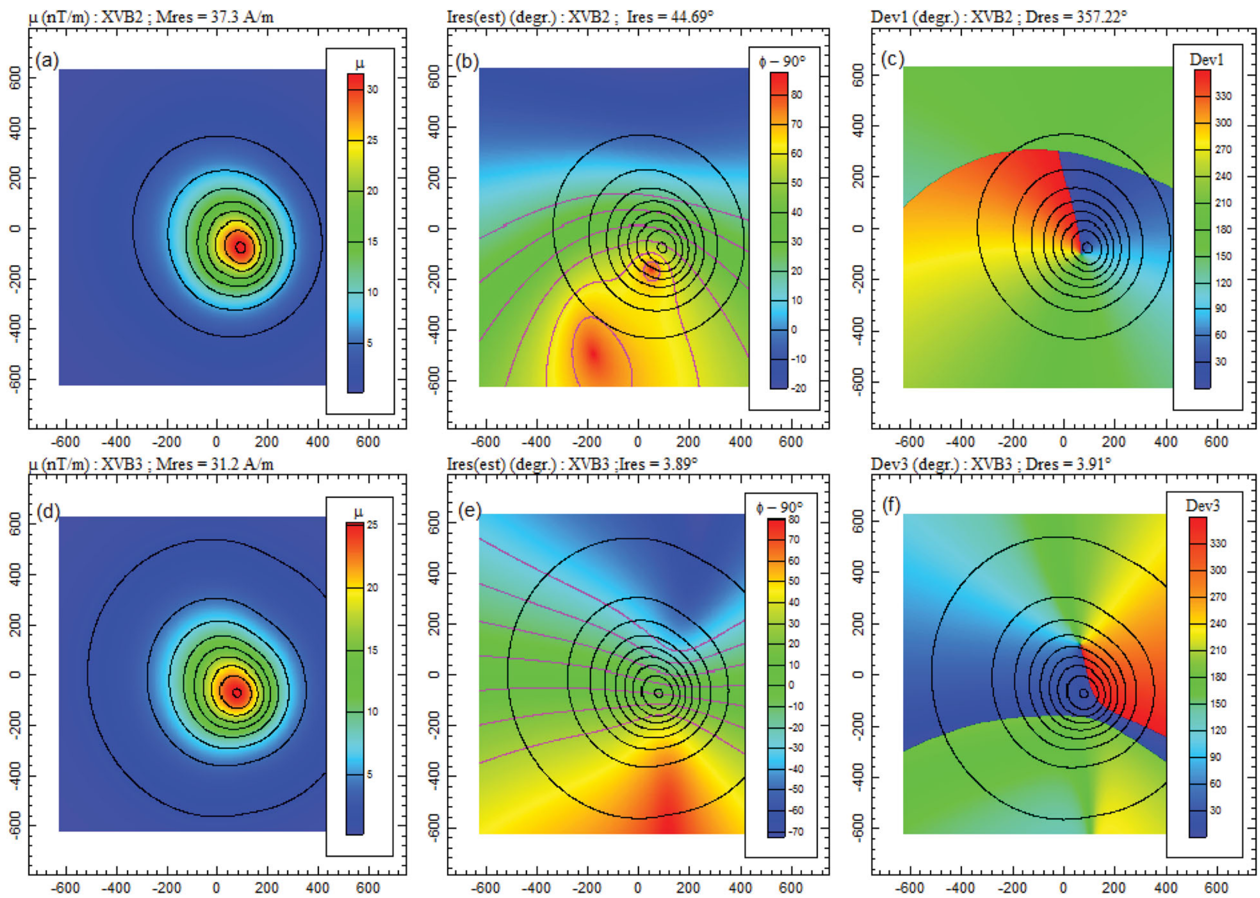

Figure 14. Figure 14(a–c) (top row: left to right) shows images of (a) the NSS μ, (b) the estimated inclination of magnetisation $I_{\varphi-\pi/2}$ based on $(\varphi - \pi/2)$, and and (c) the estimated declination of magnetisation D_{ev1} based on the principal $\hat{\mathbf{e}}_1$ eigenvector for ellipsoid Magmod XVB2 which has a bulk susceptibility of 1.90 SI, a resultant magnetisation intensity $|\mathbf{M_{res}}| = 37.3$ A/m, declination $D_{Mres} = 357.2°$ and inclination $I_{Mres} = 44.7°$. Figure 14(d–f) (bottom row: left to right) shows images of (d) the NSS μ, (e) the estimated inclination of magnetisation $I_{\varphi-\pi/2}$ based on $(\varphi - \pi/2)$, and (f) the estimated declination of magnetisation D_{ev3} based on the $\hat{\mathbf{e}}_3$ eigenvector for ellipsoid Magmod XVB3 which has a bulk susceptibility of 2.77 SI, a resultant magnetisation intensity $|\mathbf{M_{res}}| = 31.2$ A/m, declination $D_{Mres} = 3.91°$ and inclination $I_{Mres} = 3.89°$. The contours of estimated inclination of magnetisation $I_{M(est)}$ or $(\varphi - \pi/2)$ (shown in pink) range from 20° to 70° in Figure 14(b) and from −30° to 30° in Figure 14(e). The contour interval is 10° in both figures.

as the degree of shape anisotropy increases and also as the inclination of magnetisation increases towards high magnetic latitudes, i.e. $|I_M|$ from 60° to 75°. Also, the total offset distance from the hcm is less in more compact bodies and increases with increasing shape anisotropy and decreasing observation height. However, at low magnetic inclinations and also at the magnetic pole the positions of the global maximum $\mu_{\max}$ and the hcm are coincident for quasi-horizontal ellipsoids.

The reliability of the eigenvalue-eigenvector decomposition of the magnetic gradient tensor to estimate the inclination of magnetisation is shown to deteriorate for high inclination magnetisations particularly for ellipsoids where the shape anisotropy is high ($e > 5$) and where $z_{tc}/2a_1 < 1.5$.

Magnetisation estimates for a dipping triaxial ellipsoid: does it work?

In an earlier example, I presented images of the magnetic gradient tensor due to a plunging triaxial ellipsoid model, namely, Magmod XVB2. The spatial and magnetic properties of this model are listed in Tables 1 and 2 and the images of the six tensor elements are shown in Figure 3(a–f). As yet I have not shown how well the eigenvector decomposition is able to reveal the magnetisation direction for a plunging ellipsoid model which has significant shape anisotropy ($e = 2.5$), for example, in models Magmod XVB2 and XVB3 which plunge to the north-west and have quite different inclinations of magnetisation, i.e. 44.70° and 3.89° respectively. Figure 14 shows images of the (1) NSS μ, (2) estimates of the inclination $I_{M(\mathrm{est})}$ of magnetisation based on $(\varphi - \pi/2)$, and (3) estimates of the declination of magnetisation $D_{M(\mathrm{est})}$ based on the declinations D_{ev1} and D_{ev3} of the $\hat{\mathbf{e}}_1$ and $\hat{\mathbf{e}}_3$ eigenvectors for ellipsoidal models Magmod XVB2 and XVB3 respectively in Table 2. The contours of the NSS μ in Figure 14(a,d) are superimposed upon the images of the estimated inclination and declination in Figure 14(b,c,e,f). The direction of displacement of the location of $\mu_{\max}$ from the point above the centre of magnetisation for both these models is at −75.0 N, 67.5 E which is consistent with the azimuth of the upward directed major axis of these ellipsoids, i.e. at 140°. The estimates $I_{M(\mathrm{est})}$ of the inclination of magnetisation $I_{M\mathrm{res}}$ for Magmod XVB2 range from 41° above the centre of the ellipsoid to 49° at the location of $\mu_{\max}$ and for Magmod XVB3, the estimates of $I_{M\mathrm{res}}$ range from −3° above the centre of the ellipsoid to 10° at the location of $\mu_{\max}$. These estimates $I_{M(\mathrm{est})}$ of the inclination of magnetisation in both models are in close agreement with the true inclinations of magnetisation $I_{M\mathrm{res}}$ of 44.7° and 3.9°, respectively (see Figure 14). Importantly there is a region to the immediate north and west of the location of $\mu_{\max}$ where $I_{M(\mathrm{est})}$ is within ±15° of the true inclination of magnetisation with the lower inclination model MMXVB3 yielding the most consistent estimates over a broader region. The estimates of the declination of magnetisation D_{ev1} from the principal eigenvector $\hat{\mathbf{e}}_1$ for Magmod XVB2 range from 350° to 10° along a S–N trending line which extends from slightly west of the location of $\mu_{\max}$ to a point at about 250 N, −5 E. The strike of this line closely matches the declination of magnetisation in Magmod XVB2 which is 357.2°. The estimates D_{ev1} of the declination of magnetisation $D_{M\mathrm{res}}$ derived from the principal eigenvector $\hat{\mathbf{e}}_1$ in Magmod XVB3 range from 3.5° above the centre of the ellipsoid to 14° at the location of $\mu_{\max}$. The corresponding estimates for the declination of magnetisation from eigenvector $\hat{\mathbf{e}}_3$ are 29° above the centre to 359° at the location of $\mu_{\max}$.

To investigate further, Figure 15 shows images of (1) the difference between the estimated inclination of magnetisation and the true inclination of magnetisation, (2) the difference between the estimated declination of magnetisation $(D_{ev1} - D_{M\mathrm{res}})$ and $(D_{ev3} - D_{M\mathrm{res}})$ (based on the $\hat{\mathbf{e}}_1$ and $\hat{\mathbf{e}}_3$ eigenvectors) and the true declination of magnetisation, and (3) the departure or ARA between the estimated magnetisation direction and the true magnetisation direction for the pair of ellipsoidal models Magmod XVB2 and Magmod XVB3 in Table 2. The ARAs $\theta_{M-M\mathrm{est}}$ in Figure 15(c) are calculated as

$$\theta_{M-M\mathrm{est}} = \arccos\left(\hat{\mathbf{u}}_{\mathbf{M}}^{\mathbf{T}} \cdot \hat{\mathbf{u}}_{\mathbf{Mest}}\right),$$

where

$$\hat{\mathbf{u}}_{\mathbf{Mest}} = (\cos D_{ev1} \cos I_{Mest}, \sin D_{ev1} \cos I_{Mest}, \sin I_{Mest})^{\mathrm{T}}.$$

In addition to the overlain contours of NSS μ, Figure 15(a,b) also displays contours of $(I_{\varphi-\pi/2} - I_{M\mathrm{res}})$, while Figure 15(c,d) also displays contours of $(D_{ev1} - D_{M\mathrm{res}})$ and $(D_{ev3} - D_{M\mathrm{res}})$, respectively. These difference contours are shown in pink at an interval of 10° over a range from −30° to 30°. Figure 15(c,f) displays contours of the ARA (shown in pink at an interval of 10° over a range from 0° to 40°) superimposed upon the ARA images for ellipsoidal models Magmod XVB2 and Magmod XVB3 respectively.

For Magmod XVB2, Figure 15(b) reveals a fan-shaped region of low deviation from the true declination of magnetisation which extends northwards from the position of $\mu_{\max}$, while for Magmod XVB3, Figure 15(e) shows a band of low departures from the true declination extending west and east from the global maximum in NSS. Figure 15(d) reveals results which are even more consistent for the estimated inclination of magnetisation in Magmod XVB3. Here the departures from the true inclination of magnetisation extend in an east–west band across the region of maximum NSS. The average or mean inclination of magnetisation for Magmod XVB2 estimated within a rectangular region bounded by 125 S to 75 N and 300 W to 300 E (19,521 points) is 41.51°, i.e. a departure of −3.18° from the true inclination I_{res} of 44.69°. For Magmod XVB3 over the

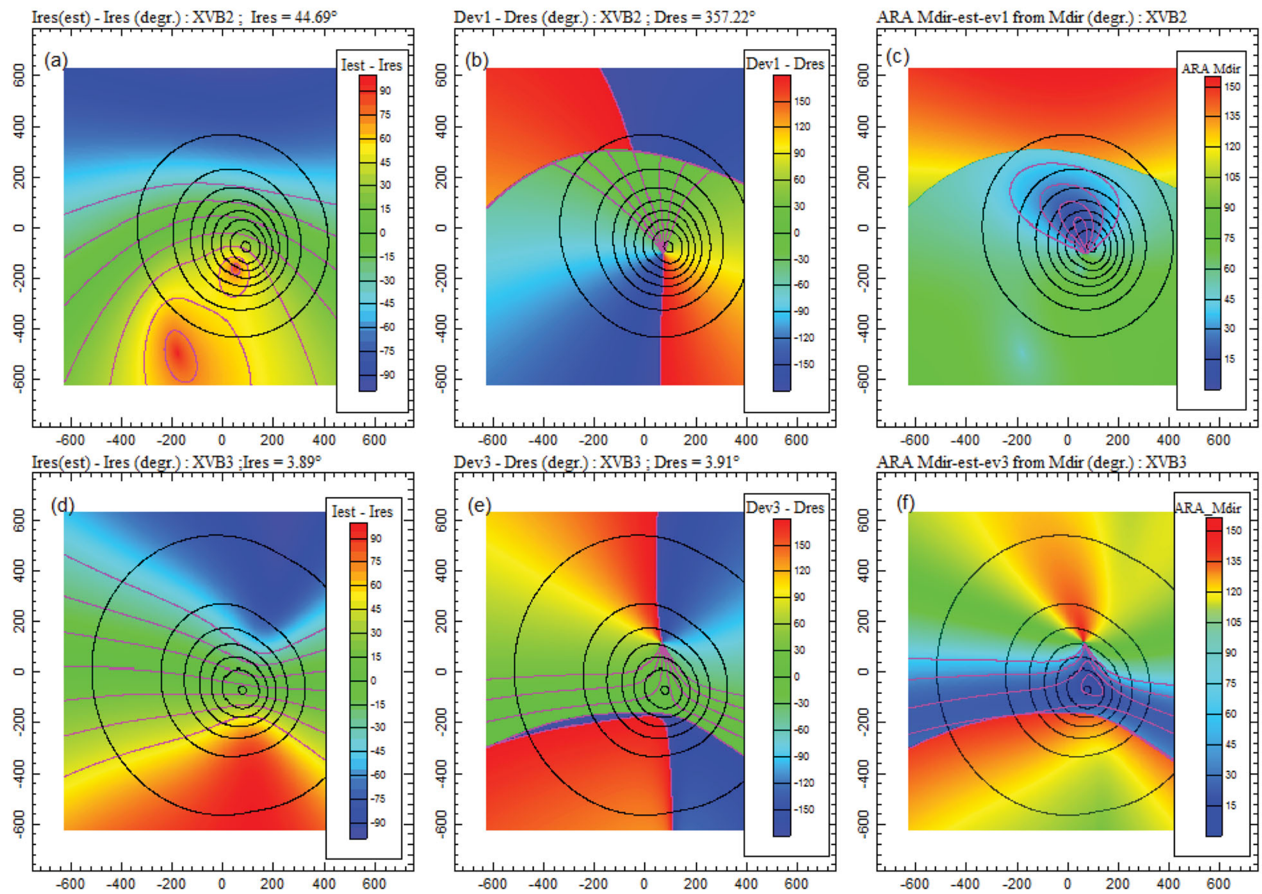

Figure 15. Figure 15 (a–c) (top row: left to right) shows images of (a) the difference ($I_{\varphi-\pi/2} - I_{Mres}$) between the estimated inclination of magnetisation $I_{\varphi-\pi/2}$ based on ($\varphi - \pi/2$) and the true inclination of magnetisation I_{Mres}, (b) the difference ($D_{ev1} - D_{Mres}$) between the estimated declination of magnetisation D_{ev1} based on the $\hat{\mathbf{e}}_1$ eigenvector and the true declination of magnetisation D_{Mres}, and (c) the apparent rotation (ARA) of the estimated magnetisation direction from the true magnetisation direction for Magmod XVB2 which has a resultant magnetisation intensity $|\mathbf{M_{res}}| = 37.3$ A/m, declination $D_{Mres} = 357.2°$ and inclination $I_{Mres} = 44.7°$. Figure 15(d–f) (bottom row: left to right) shows images of (d) the difference ($I_{\varphi-\pi/2} - I_{Mres}$) between the estimated inclination of magnetisation $I_{\varphi-\pi/2}$ and the true inclination of magnetisation I_{Mres}, (e) the difference ($D_{ev3} - D_{Mres}$) between the estimated declination of magnetisation D_{ev3} based on the $\hat{\mathbf{e}}_3$ eigenvector and the true declination of magnetisation D_{Mres}, and (f) the apparent rotation (ARA) of the estimated magnetisation direction from the true magnetisation direction for Magmod XVB3 which has a resultant magnetisation intensity $|\mathbf{M_{res}}| = 31.2$ A/m, declination $D_{Mres} = 3.91°$ and inclination $I_{Mres} = 3.89°$. Figure 15(a–f) displays contours of NSS μ, which are shown in black. Figure 15(a,b) displays contours of ($I_{\varphi-\pi/2} - I_{Mres}$) and ($D_{ev1} - D_{Mres}$) while Figure 15(d,e) shows contours of ($I_{\varphi-\pi/2} - I_{Mres}$) and ($D_{ev3} - D_{Mres}$). These contours are displayed in pink at an interval of 10° over a range from −30° to 30°. The images in Figure 15(c,f) also display contours of the departure angles ARA_M_M$_{est-ev1}$ and ARA_M_M$_{est-ev3}$, respectively. These are shown in pink at an interval of 10° over a range from 0° to 40°.

same region, the average inclination of magnetisation is 1.37°, i.e. a departure of −2.51° from the true inclination of 3.89°, while the average declination of magnetisation estimated from D_{ev3} within a rectangular region bounded by 125 S to 25 N and 300 W to 300 E (14,701 points) is 7.28° which is a departure of 3.37° from the true declination D_{Mres} of 3.91°. The mean declination of magnetisation estimated for Magmod XVB2 from D_{ev3} over the fan-shaped region in Figure 15(b) extending from 50 S to 150 N and from 0 E to 100E at 50 S to 300 W to 300 E at 150 N (∼16,461 points) is 355.13°. This estimate is a departure of only −2.09° from the true declination D_{Mres} of 357.22°. For Magmod XVB2, the average departure angle from the true direction of magnetisation using the average estimated declination and inclination angles of $D_{Mest} = 355.13°$ and $I_{Mest} = 41.51°$ respectively is $\theta_{M-Mest} = 3.52°$. For Magmod XVB3, the average departure angle from the true direction of magnetisation using the average estimated declination and inclination angles of $D_{Mest} = 7.28°$ and $I_{Mest} = 1.37°$ respectively is $\theta_{M-Mest} = 4.20°$. These results are superior to those obtained by taking an average of the ARAs over the same regions in Figure 15(c,f). For example, when averaging was performed over two smaller regions enclosed by the 30° ARA contour, the average departures from the true magnetisation directions were 19.46° for Magmod XVB and 12.56° for Magmod XVC. These results for Magmod XVB2 and XVC3 are deemed satisfactory.

This example shows that it is possible to accurately estimate the magnetisation direction of a dipping triaxial ellipsoid using gridded parameters derived from the eigenvector-eigenvector decomposition of its magnetic gradient tensor.

Conclusion

The formulation presented here allows for the rapid computation of the magnetic gradient tensor due to a uniformly magnetised triaxial ellipsoid in which the sources of the magnetisation are considered to be completely general and may include isotropic or anisotropic magnetic susceptibility, remanence and self-demagnetisation. The expressions are quite generic and allow for the computation of the potential fields, gradient tensors, gradient tensor invariants and canonical invariants of the gradient tensor including the eigenvalues and eigenvectors for all classes of ellipsoidal bodies. It has been demonstrated that maxima in the NSS or scaled moment $\mu_{\max}$ provide a means for the determining the magnetisation of ellipsoidal bodies even when the position of $\mu_{\max}$ is displaced from the true horizontal true centre of magnetisation of an ellipsoid. This allows for the determination of magnetisation direction in highly magnetised sheet-like bodies or extremely elongated bodies which may be remanently magnetised or possess significant shape anisotropy due to self-demagnetisation.

Acknowledgements

First I would like to acknowledge my supervisor Mark Lackie. I should like to thank David Clark, David Pratt and Clive Foss for encouraging me to write this paper. I also acknowledge the efforts of David Pratt, Clive Foss and David Clark for having the foresight to support the development of theory and software for calculating the magnetic tensors well before these became of general interest in potential field geophysics.

Disclosure statement

No potential conflict of interest was reported by the author.

References

Abramowitz, M., and I.A. Stegun. 1964. *Handbook of mathematical functions, Applied mathematical series*. Vol. 58, National bureau of standards, reprinted 1968. New York: Dover.

Austin, J., S. Geuna, D. Clark, and D. Hillan. 2014. Remanence, self-demagnetisation and their ramifications for magnetic modelling of iron oxide copper-gold deposits: An example from Candelaria, Chile. *Journal of Applied Geophysics* 109: 242–55. doi:10.1016/j.jappgeo.2014..08.002.

Beiki, M., D.A. Clark, J.R. Austin, and C.A. Foss. 2012. Estimating source location using normalised magnetic source strength calculated from gradient tensor data. *Geophysics* 77: J23–J37. doi:10.1190/geo2011-0437.1.

Blakely, R.J. 1995. *Potential theory in gravity and magnetic applications*. Cambridge: Cambridge University Press.

Clark, D.A. 2000. Self-demagnetisation in practice: The Osborne Cu-Au deposit. *Preview* 85: 31–36.

Clark, D.A. 2012. New methods for interpretation of magnetic vector and gradient tensor data I: Eigenvector analysis and the normalised source strength. *Exploration Geophysics* 43: 267–82. doi:10.1071/EG12020.

Clark, D.A. 2014. Methods for determining remanent and total magnetisations of magnetic sources – A review. *Exploration Geophysics* 45: 271–304. doi:10.1071/EG14013.

Clark, D.A., and C. Tonkin. 1987. Magnetic properties of ironstones and host rocks from the Tennant Creek area: CSIRO division of mineral physics and mineralogy restricted investigation report 1691R, 124p. doi:10.13140/RG.2.2.17660.49283.

Clark, D.A., and D.W. Emerson. 1999. Self-demagnetisation. *Preview*, Magazine of the Australian Society of Exploration Geophysicists, 22–5.

Clark, D.A., S.J. Saul, and D.W. Emerson. 1986. Magnetic and gravity anomalies of a triaxial ellipsoid. *Exploration Geophysics* 17: 189–200.

Emerson, D.W., D.A. Clark, and S.J. Saul. 1985. Magnetic exploration models incorporating remanence, demagnetisation and anisotropy: HP41C handheld computer algorithms. *Exploration Geophysics* 16: 1–122.

Farrar, L.J.D. 1979. Some comments on detailed magnetic investigations of ellipsoidal bodies at Tennant Creek. *Bulletin of the Australian Society of Exploration Geophysicists* 10: 26–33. doi:10.1071/EG979026.

Foss, C.A. 2006. The improvements in source resolution that can be expected from inversion of magnetic field tensor data. *The Leading Edge* 25: 81–4. doi:10.1190/1.2164761.

Foss, C.A. 2017. Resultant-magnetisation based magnetic Field interpretation. In *Proceedings of exploration 17: Sixth decennial international conference on mineral exploration*, ed. V. Tschirhart and M.D. Thomas, 637–48.

Grant, F.S., and G.F. West. 1965. *Interpretation theory in applied geophysics*. New York: McGraw-Hill.

Hoschke, T. 1991. Geophysical discovery and evaluation of the West Peko copper-gold deposit, Tennant Creek. *Exploration Geophysics* 22: 485–95. doi:10.1071/EG991485.

Kellogg, O.D. 1929. *Foundations of potential theory*. Reprinted 1953. New York: Dover.

Pedersen, L.B., and T.M. Rasmussen. 1990. The gradient tensor of potential field anomalies: some implications on data collection and data processing of maps. *Geophysics* 55: 1558–66. doi:10.1190/1.1442807.

Phillips, J.D., M.N. Nabighan, D.V. Smith, and Y. Li. 2007. Estimating locations and total magnetisation vectors of compact magnetic sources from scalar, vector, or tensor magnetic measurements through combined Helbig and Euler analysis. Paper presented at the SEG Antonio 2007 Meeting, 770–4.

Press, W.H., S.A. Teukolsky, W.T. Vetterling, and B.P. Flannery. 1992. *Numerical recipes in Fortran the art of scientific computing*. 2nd ed. Cambridge: Cambridge University Press.

Reid, A.B., and J.B. Thurston. 2014. The structural index in magnetic and gravity interpretation: Errors, uses, and abuses. *Geophysics* 79: 161–6. doi:10.1190/geo2013-0235.1.

Schmidt, P.W., and D.A. Clark. 2006. The magnetic gradient tensor: its properties and uses in source characterisation. *The Leading Edge* 25: 75–8. doi:10.1190/1.2164759.

Stoner, E.C. 1945. The demagnetizing factors for ellipsoids. *Philosophical Magazine* 36: 803–21.

Stratton, J.A. 1941. *Electromagnetic theory*. New York: McGraw-Hill.

Takahashi, D., and V.C. Oliviera. 2017. Ellipsoids (v1.0): 3-D magnetic modelling of ellipsoid bodies. *Geoscientific Model Development* 10: 3591–608. doi:10.5194/gmd-10-3591-2017.

Wilson, H. 1985. Analysis of the magnetic gradient tensors. Defence Research Establishment Pacific, Canada, Technical Memorandum, 85-13, 47.

Wynn, W.M. 1999. Detection, localization, and characterization of static magnetic-dipole sources. In *Detection and identification of visually obscured targets*, ed. C. E. Baum, 337–74. Boca Raton: Taylor and Francis.

Appendices

Appendix A1. The Green's functions $A_1(\lambda), A_2(\lambda), A_3(\lambda)$ for the general triaxial ellipsoid

Expressions for the Green's Functions which arise in expressions for the gravity and magnetic potential at an external point due to a general triaxial ellipsoid are derived by solving the following definite integral,

$$A_i(\lambda) = \int_\lambda^\infty \frac{1}{(a_i^2+u)\sqrt{(a_1^2+u)(a_2^2+u)(a_3^2+u)}}\mathrm{d}u \quad \text{for } i = 1,2,3, \tag{A1}$$

where λ is the principal ellipsoidal coordinate of the observation point $P(x_1, x_2, x_3)$ with respect to the centre of the ellipsoid (see Clark, Saul, and Emerson 1986, Equations (2–9)). It is noted that λ is unique for any observation point. Furthermore λ is positive ($\lambda > 0$) for all external points, negative ($\lambda < 0$) for all internal points and zero ($\lambda = 0$) for points on the surface of the ellipsoid. The integral in Equation (A1) has been evaluated by Kellogg (1929),

$$A_1(\lambda) = \frac{2}{(a_1^2-a_2^2)\sqrt{(a_1^2-a_3^2)}}[F(k,\beta)-E(k,\beta)], \tag{A2}$$

$$A_2(\lambda) = \frac{2\sqrt{(a_1^2-a_3^2)}}{(a_1^2-a_2^2)(a_2^2-a_3^2)} \times \left[E(k,\beta) - \frac{(a_2^2-a_3^2)}{(a_1^2-a_3^2)}F(k,\beta) - \frac{k^2\sin\beta\cos\beta}{\sqrt{1-k^2\sin\beta}}\right], \tag{A3}$$

$$A_3(\lambda) = \frac{2}{(a_2^2-a_3^2)\sqrt{(a_1^2-a_3^2)}}\left[\frac{\sin\beta\sqrt{1-k^2\sin\beta}}{\cos\beta} - E(k,\beta)\right], \tag{A4}$$

where $F(k,\beta)$ and $E(k,\beta)$ are the incomplete elliptic integrals of the first and second kind respectively with modulus k and angular amplitude β, namely,

$$F(k,\beta) = \int_0^\beta \frac{1}{\sqrt{1-k^2\sin\theta}}\,\mathrm{d}\theta, \tag{A5}$$

and

$$E(k,\beta) = \int_0^\beta \sqrt{1-k^2\sin\theta}\,\mathrm{d}\theta, \tag{A6}$$

where

$$k^2 = \sin\alpha = \frac{(a_1^2-a_2^2)}{(a_1^2-a_3^2)} \quad 0 \le \alpha \le \frac{\pi}{2}$$
$$\text{and } \sin\beta = \frac{(a_1^2-a_3^2)}{(a_1^2+\lambda)} \quad 0 \le \beta \le \frac{\pi}{2}. \tag{A7}$$

Appendix A2. Derivation of expressions for the external gravitational field due to a uniform general triaxial ellipsoid

The gravitational potential $U_{\text{ext}}(\mathbf{r}_\text{b})$ at an external observation point $P(\mathbf{r}_\text{b})$ in the body axis coordinate system of the ellipsoid, i.e. $\mathbf{r}_\text{b} = (x_1, x_2, x_3)^T$, is

$$U_{\text{ext}}(\mathbf{r}_\text{b}) = \pi G\rho a_1a_2a_3\left[D(\lambda) - \sum_{i=1}^3 A_i(\lambda)x_i^2\right], \tag{A8}$$

where

$$D(\lambda) = \int_\lambda^\infty \frac{1}{R(u)}\mathrm{d}u,$$
$$A_i(\lambda) = \int_\lambda^\infty \frac{1}{(a_i^2+u)R(u)}\mathrm{d}u \quad \text{for } i = 1,2,3,$$

and

$$R(u) = \sqrt{(a_1^2+u)(a_2^2+u)(a_3^2+u)}.$$

Expressions for the body axis components of the external gravitational field due to a triaxial ellipsoid are derived by taking the gradient of its potential $U_{\text{ext}}(\mathbf{r}_\text{b})$:

$$g_i(\mathbf{r}_\text{b}) = \frac{\partial U_{\text{ext}}}{\partial x_i} = \pi G\rho a_1a_2a_3\frac{\partial}{\partial x_i}\left[D(\lambda) - \sum_{i=1}^3 A_i(\lambda)x_i^2\right] \quad \text{for } i = 1,2,3, \tag{A9}$$

$$\frac{\partial D(\lambda)}{\partial x_i} = \frac{\partial D(\lambda)}{\partial\lambda}\frac{\partial\lambda}{\partial x_i} = \left(\frac{\partial\lambda}{\partial x_i}\right)\left(\frac{\partial}{\partial u}\int_\lambda^\infty \frac{1}{R(u)}\right)\mathrm{d}u = \left(\frac{\partial\lambda}{\partial x_i}\right)\left(\frac{1}{R(u)}\right)_\lambda^\infty = -\frac{1}{R(\lambda)}\left(\frac{\partial\lambda}{\partial x_i}\right), \tag{A10}$$

$$\begin{aligned}
&\frac{\partial}{\partial x_i}\sum_{i=1}^3 A_i(\lambda)x_i^2 \\
&= \left(\sum_{j=1}^3 x_j^2\frac{\partial}{\partial\lambda}A_j(\lambda)\right)\left(\frac{\partial\lambda}{\partial x_i}\right) + \sum_{j=1}^3 A_j(\lambda)\frac{\partial x_j^2}{\partial x_i}\delta_{ij} \quad \text{for } i = 1,2,3 \\
&= \left(\frac{\partial\lambda}{\partial x_i}\right)\left[\sum_{j=1}^3 x_j^2\frac{\partial}{\partial\lambda}\left(\int_\lambda^\infty \frac{1}{(a_j^2+u)R(u)}\mathrm{d}u\right)\right] + 2x_iA_i(\lambda) \\
&= \left(\frac{\partial\lambda}{\partial x_i}\right)\left[\sum_{j=1}^3 x_j^2\left(\frac{1}{(a_j^2+u)R(u)}\right)_\lambda^\infty\right] + 2x_iA_i(\lambda) \\
&= -\left(\frac{1}{R(\lambda)}\right)\left(\frac{\partial\lambda}{\partial x_i}\right)\left[\sum_{j=1}^3\left(\frac{x_j^2}{(a_j^2+\lambda)}\right)\right] + 2x_iA_i(\lambda) \quad \text{for } i = 1,2,3.
\end{aligned} \tag{A11}$$

However from Equation (2), $\sum_{j=1}^3 \frac{x_j^2}{(a_j^2+\lambda)} = 1$, so that Equation (A11) becomes

$$\frac{\partial}{\partial x_i}\sum_{i=1}^3 A_i(\lambda)x_i^2 = -\left(\frac{1}{R(\lambda)}\right)\left(\frac{\partial\lambda}{\partial x_i}\right) + 2x_iA_i(\lambda) \text{ for } i = 1,2,3. \tag{A12}$$

Thus on substitution of the expressions for the x_i partial derivatives in Equations (A10) and (A12) into Equation (A9)

$$\begin{aligned}
g_i(\mathbf{r}_\text{b}) &= \pi G\rho a_1a_2a_3\frac{\partial}{\partial x_i}\left[D(\lambda) - \sum_{i=1}^3 A_i(\lambda)x_i^2\right] \quad \text{for } i = 1,2,3 \\
&= \pi G\rho a_1a_2a_3x_i\left\{-\left(\frac{1}{R(\lambda)}\right)\left(\frac{\partial\lambda}{\partial x_i}\right) - \left[-\left(\frac{1}{R(\lambda)}\right)\left(\frac{\partial\lambda}{\partial x_i}\right) + 2x_iA_i(\lambda)\right]\right\} \quad \text{for } i = 1,2,3.
\end{aligned}$$

By inspection the terms involving $\frac{\partial \lambda}{\partial x_i}$ have opposite signs and therefore cancel, hence

$$g_i(\mathbf{r}_b) = -2\pi G\rho a_1 a_2 a_3 x_i A_i(\lambda) \quad \text{for } i = 1,2,3. \qquad \text{(A13)}$$

Appendix A3. Expressions for the transformation matrix U from the IGRF coordinate system to the body axis coordinate system of a general triaxial ellipsoid

The survey axis coordinate system $\mathbf{r}_s = (x,y,z)^T$ used here is identical to the convention for the IGRF, i.e. x is North, y is East and z is vertically down. The body axis coordinate system x_1, x_2, x_3 parallel to the a_1, a_2, a_3semiaxes respectively of a general triaxial ellipsoid $a_1 > a_2 > a_3$ is defined by three direction cosine vectors $\hat{\mathbf{u}}_1, \hat{\mathbf{u}}_2, \hat{\mathbf{u}}_3$ whose orientation is specified via three ellipsoidal angles α, δ, γ (see Figure 1), namely,

α is the horizontal azimuth of the downward pointing major or a_1 semiaxis measured positive clockwise from reference north $0° \leq \alpha < 360°$

δ is the downward plunge of the a_1 semiaxis measured positive clockwise from the horizontal azimuthal direction $0° \leq \delta \leq 90°$

γ is angle measured positive anticlockwise through which the ellipsoid must be rotated about its downward pointing major a_1 semiaxis until the intermediate semiaxis a_2 is horizontal and the minor semiaxis a_3 points downward in the principal vertical plane containing the a_1 semiaxis $-90° \leq \gamma \leq 90°$.

The unit direction cosine vectors $\hat{\mathbf{u}}_1, \hat{\mathbf{u}}_2, \hat{\mathbf{u}}_3$ along the x_1, x_2, x_3 body axes of the ellipsoid are defined as follows:

$$\hat{\mathbf{u}}_1^T = (\cos\alpha\cos\delta, \sin\alpha\cos\delta, \sin\delta), \qquad \text{(A14)}$$

$$\hat{\mathbf{u}}_2^T = [-(\sin\alpha\cos\gamma + \cos\alpha\sin\delta\sin\gamma), (\cos\alpha\cos\gamma - \sin\alpha\sin\delta\sin\gamma), \cos\delta\sin\gamma], \qquad \text{(A15)}$$

$$\hat{\mathbf{u}}_3^T = [(\sin\alpha\sin\delta + \cos\alpha\sin\delta\cos\gamma), -(\cos\alpha\sin\gamma + \sin\alpha\sin\delta\cos\gamma), \cos\delta\cos\gamma]. \qquad \text{(A16)}$$

Hence the transformation matrix $\mathbf{U}$ from the survey coordinate system to the body axis coordinate system of a general triaxial ellipsoid is

$$\mathbf{U} = \begin{pmatrix} \hat{\mathbf{u}}_1^T \\ \hat{\mathbf{u}}_2^T \\ \hat{\mathbf{u}}_3^T \end{pmatrix} = \begin{bmatrix} u_{1x} & u_{1y} & u_{1z} \\ u_{2x} & u_{2y} & u_{2z} \\ u_{3x} & u_{3y} & u_{3z} \end{bmatrix}. \qquad \text{(A17)}$$

Both the survey axis coordinates and the body axis coordinates defined here form right-hand clockwise coordinate systems. When the three ellipsoidal axes α, δ, γ are zero then the body axis coordinates are identical to the survey axis coordinates, i.e. $\hat{\mathbf{u}}_1$ is North, $\hat{\mathbf{u}}_2$ is East and $\hat{\mathbf{u}}_3$ is vertically down.

As already stated, all computations of the magnetic and gravity field components and their respective gradient tensors are made in the body axis coordinate system of the triaxial ellipsoid. In order to do this, all survey coordinates $P(\mathbf{r}_s)$ and magnetisations including $\mathbf{M}_{\mathbf{ind}}$ and $\mathbf{M}_{\mathbf{nrm}}$ must first be transformed from the survey axis coordinate system $\mathbf{r}_s = (x,y,z)^T$ to the body axis coordinate system $\mathbf{r}_b = (x_1,x_2,x_3)^T$. For example if $\mathbf{U}$ is the transformation matrix, then

$$\mathbf{r}_b = \mathbf{U}\mathbf{r}_s; \mathbf{M}_{\mathbf{ind}}(\mathbf{r}_b) = \mathbf{U}\mathbf{M}_{\mathbf{ind}}(\mathbf{r}_s); \mathbf{M}_{\mathbf{rem}}(\mathbf{r}_b) = \mathbf{U}\mathbf{M}_{\mathbf{rem}}(\mathbf{r}_s), \qquad \text{(A18)}$$

and

$$x_i = \hat{\mathbf{u}}_i^T \cdot \mathbf{r}_s \text{ or } x_i = u_{ix}x + u_{iy}y + u_{iz}z,$$

$$M_{i(\text{ind})} = \hat{\mathbf{u}}_i^T \cdot \mathbf{M}_{\mathbf{ind}}(\mathbf{r}_s) \text{ and } M_{i(\text{nrm})} = \hat{\mathbf{u}}_i^T \cdot \mathbf{M}_{\text{nrm}}(\mathbf{r}_s),$$

and where $\hat{\mathbf{u}}_i^T = (u_{ix}, u_{iy}, u_{iz})$ is the ith row vector of the transformation matrix $\mathbf{U}$ and $\mathbf{r}_s$ is the column vector $(x,y,z)^T$.

Once the magnetisation $\mathbf{M}$, field components $\mathbf{b}(\mathbf{r}_b)$ and gradient tensors $\mathbf{B}(\mathbf{r}_b)$ of the triaxial ellipsoid have been calculated, then these quantities need to be transformed back to the survey axis coordinate system. To transform the body axis components of the magnetic field vector $\mathbf{b}$ and the effective or resultant magnetisation vector $\mathbf{M}$ to survey axis coordinates, the following orthogonal transformation is required

$$\mathbf{b}(\mathbf{r}_s) = (b_x, b_y, b_y)^T = \mathbf{U}^T\mathbf{b}(\mathbf{r}_b),$$

$$\mathbf{M}(\mathbf{r}_s) = (M_x, M_y, M_y)^T = \mathbf{U}^T\mathbf{M}(\mathbf{r}_b), \qquad \text{(A19)}$$

where $\mathbf{U}^T$ the transpose of $\mathbf{U}$, is the inverse of the orthogonal transformation matrix $\mathbf{U}$, i.e. $\mathbf{U}^{-1} = \mathbf{U}^T$ and $\mathbf{U}^T\mathbf{U} = \mathbf{I}$. Therefore expanding Equation (A19)

$$b_x = u_{1x}b_1 + u_{2x}b_2 + u_{3x}b_3; b_y = u_{1y}b_1 + u_{2y}b_2 + u_{3y}b_3; b_z = u_{1z}b_1 + u_{2z}b_2 + u_{3z}b_3$$

$$M_x = u_{1x}M_1 + u_{2x}M_2 + u_{3x}M_3; M_y = u_{1y}M_1 + u_{2y}M_2 + u_{3y}M_3; M_z = u_{1z}M_1 + u_{2z}M_2 + u_{3z}M_3. \qquad \text{(A20)}$$

To transform the magnetic gradient tensor $\mathbf{B}(\mathbf{r}_b) = \nabla\mathbf{b}(\mathbf{r}_b)$ from the body axis coordinate system of the ellipsoid to the survey axis coordinate system the following transformation is applied:

$$\mathbf{B}(\mathbf{r}_s) = B_{ij}(\mathbf{r}_s) = \mathbf{U}^T\mathbf{B}(\mathbf{r}_b)\mathbf{U}; \quad i,j = 1,2,3 \text{ for } x,y,z, \text{ respectively.} \qquad \text{(A21)}$$

The transformations from body axis coordinates to survey coordinates in Equations (A20) and (A21) also apply to the gravity gradient tensor $\Gamma(\mathbf{r}_b)$ and the gravitational field vector $\mathbf{g}(\mathbf{r}_b)$ respectively.

Appendix A4. The demagnetisation factors for the general triaxial ellipsoid

The three demagnetising factors $N_i, i = 1,2,3$ of a general triaxial ellipsoid with uniform magnetisation $\mathbf{M}$ are related to its internal magnetic field components $H_{i(\text{int})}$ by the following relation:

$$H_{i(\text{int})} = -N_i M_i = -\left(\frac{1}{4\pi}\right)\frac{\partial V_{\text{int}}}{\partial x_i} = -\left(\frac{1}{4\pi}\right)2\pi a_1 a_2 a_3 A_i(0) M_i \quad \text{for } i = 1,2,3, \qquad \text{(A22)}$$

where

$$A_i(0) = \int_0^\infty \frac{1}{(a_i^2+u)\sqrt{(a_1^2+u)(a_2^2+u)(a_3^2+u)}}du \quad \text{for } \lambda = 0 \text{ and } i = 1,2,3. \qquad \text{(A23)}$$

Hence by inspection of Equation (A22), the demagnetising factors N_i are directly proportional to the Green's functions $A_i(0)$, namely,

$$N_i = \left(\frac{1}{4\pi M_i}\right)2\pi a_1 a_2 a_3 A_i(0) M_i = \frac{1}{2}a_1 a_2 a_3 A_i(0) \quad \text{for } i = 1,2,3. \qquad \text{(A24)}$$

The integrals in Equation (A23) have been evaluated by Stoner (1945). Closed form expressions for $A_1(0), A_2(0)$ and

$A_3(0)$ functions are given in Clark, Saul, and Emerson (1986) and also in Takahashi and Oliviera (2017). Hence the expressions for the demagnetisation factors of the general triaxial ellipsoid in SI units are:

$$N_1 = \frac{1}{2}a_1a_2a_3A_1(0) = \frac{a_1a_2a_3}{(a_1^2-a_2^2)\sqrt{(a_1^2-a_3^2)}}[F(k,\beta)-E(k,\beta)], \tag{A25.1}$$

$$\begin{aligned} N_2 &= \frac{1}{2}a_1a_2a_3A_2(0) \\ &= \frac{a_1a_2a_3\sqrt{(a_1^2-a_3^2)}}{(a_1^2-a_2^2)(a_2^2-a_3^2)}\left[E(k,\beta)-\frac{(a_2^2-a_3^2)}{(a_1^2-a_3^2)}F(k,\beta)\right. \\ &\left.\quad -\frac{a_3(a_1^2-a_2^2)}{a_1a_2\sqrt{(a_1^2-a_3^2)}}\right], \end{aligned} \tag{A25.2}$$

$$\begin{aligned} N_3 &= \frac{1}{2}a_1a_2a_3A_3(0) \\ &= \frac{a_1a_2a_3}{(a_2^2-a_3^2)\sqrt{(a_1^2-a_3^2)}}\left[\frac{a_2\sqrt{(a_1^2-a_3^2)}}{a_1a_3}-E(k,\beta)\right], \end{aligned} \tag{A25.3}$$

where $F(k,\beta)$and $E(k,\beta)$ are the incomplete elliptic integrals of the first and second kind respectively as given in Equations (A5) and (A6) with modulus k and angular amplitude β

$$k^2 = \sin^2\alpha = \frac{(a_1^2-a_2^2)}{(a_1^2-a_3^2)} \quad 0 \le \alpha \le \frac{\pi}{2} \text{ and}$$

$$\sin^2\beta = \frac{(a_1^2-a_3^2)}{a_1^2} \text{ or } \cos\beta = \frac{a_3}{a_1} 0 \le \beta \le \frac{\pi}{2}.$$

Importantly, it may be shown that the sum of all three Green's functions $A_i(\lambda)$, $i = 1,2,3$ given in Equations (A2)–(A4) of Appendix A1 is exactly $2/R(\lambda)$ with the sum of terms involving both $F(k,\beta)$ and$E(k,\beta)$ being identically zero. Since the expression for $R(\lambda)$ is $R(\lambda) = \sqrt{(a_1^2+\lambda)(a_2^2+\lambda)(a_3^2+\lambda)}$ then for the special case of $\lambda = 0$ in Equation (A24) above,

$$\sum_{i=1}^{3} A_i(0) = A_1(0)+A_2(0)+A_3(0) = \frac{2}{R(0)} = \frac{2}{a_1a_2a_3}. \tag{A26}$$

Therefore the sum of the three demagnetisation factors N_i is identically 1,

$$\sum_{i=1}^{3} N_i = \frac{1}{2}a_1a_2a_3\sum_{i=1}^{3}A_i(0) = \left[\frac{1}{2}a_1a_2a_3\right]\left[\frac{2}{a_1a_2a_3}\right] = 1. \tag{A27}$$

Appendix A5. Expressions for the magnetic gradient tensor, its eigenvalues and eigenvectors at a measurement point directly above a magnetic dipole or uniformly magnetised sphere of radius *a* and magnetisation M

The expression for the magnetic gradient tensor due at a measurement point $P(\mathbf{r})$ due to a magnetic dipole with magnetic moment $\mathbf{m}$ centred at the origin is given by Wilson (1985), namely,

$$B_{ij}(\mathbf{r}) = u_{ri}\mu_j + u_{rj}\mu_i + (\boldsymbol{\mu}\cdot\hat{\mathbf{u}}_r)\delta_{ij} - 5(\boldsymbol{\mu}\cdot\hat{\mathbf{u}}_r)u_{ri}u_{rj} \quad \text{for } i,j = 1,2,3 \text{ or } x,y,z, \tag{A28}$$

where $\boldsymbol{\mu} = (\mu_x,\mu_y,\mu_z)$ is the scaled magnetic moment and $\hat{\mathbf{u}}_r = \frac{\mathbf{r}}{|\mathbf{r}|} = (u_{rx},u_{ry},u_{rz})^T$ is a unit vector in the direction of the line joining the dipole to the measurement point $P(\mathbf{r})$ and δ_{ij} is Kronecker delta. For a uniformly magnetised sphere of radius a, volume v and magnetisation $\mathbf{M}$, the scaled magnetic moment $\boldsymbol{\mu}(\mathbf{r})$ is

$$\boldsymbol{\mu}(\mathbf{r}) = \frac{3C_m\mathbf{m}}{r^4} = \frac{3C_m\mathbf{M}v}{r^4} = \frac{4\pi C_m a^3\mathbf{M}}{r^4}, \tag{A29}$$

where C_m is a constant which depends on the system of electromagnetic units used (see Blakely 1995, 67–68). In the SI system of units used here, C_m has a value of 100 nH/m or 100 nTm/A for magnetic fields expressed in nanotesla (nT) and magnetisations expressed in ampere per metre (A/m). The expressions in Equations (A28) and (A29) for the gradient tensor due to a uniformly magnetised sphere are completely general and apply to any external observation point. However for an observation station $P(0,0,z)$ located at a height $|z| > a$ directly above an origin at the centre of a magnetised sphere, the expressions for its gradient tensor become greatly simplified since $\hat{\mathbf{u}}_r = (u_{rx},u_{ry},u_{rz})^T = (0,0,-1)^T$. Hence all terms in Equation (A28) not involving u_{rz} are identically zero. Therefore, at any observation station $\mathbf{r} = (0,0,z)^T$ where $z < -a$, the elements of the gradient tensor $B_{ij}(\mathbf{r})$ are

$$\begin{aligned} B_{xx} &= B_{11} = (\boldsymbol{\mu}\cdot\hat{\mathbf{u}}_r)\delta_{11} = -\mu_z \\ &= -\frac{4\pi C_m a^3}{r^4}M_z \quad \text{for } i=1, j=1, \end{aligned} \tag{A30.1}$$

$$B_{xy} = B_{12} = 0 \quad \text{for } i=2, j=1, \tag{A30.2}$$

$$B_{xz} = B_{13} = u_{r3}\mu_1 = -\mu_x = -\frac{4\pi C_m a^3}{r^4}M_x \quad \text{for } i=1, j=3, \tag{A30.3}$$

$$B_{yx} = B_{21} = 0 = B_{xy} \quad \text{for } i=2, j=1, \tag{A30.4}$$

$$\begin{aligned} B_{yy} &= B_{22} = (\boldsymbol{\mu}\cdot\hat{\mathbf{u}}_r)\delta_{22} \\ &= -\mu_y = -\frac{4\pi C_m a^3}{r^4}M_y \quad \text{for } i=2, j=2, \end{aligned} \tag{A30.5}$$

$$B_{yz} = B_{23} = u_{r3}\mu_2 = -\mu_y = -\frac{4\pi C_m a^3}{r^4}M_y \quad \text{for } i=2, j=3, \tag{A30.6}$$

$$\begin{aligned} B_{zx} &= B_{31} = u_{r3}\mu_1 = -\mu_x = -\frac{4\pi C_m a^3}{r^4}M_x \\ &= B_{xz} \quad \text{for } i=3, j=1, \end{aligned} \tag{A30.7}$$

$$\begin{aligned} B_{zy} &= B_{32} = u_{r3}\mu_2 = -\mu_y = -\frac{4\pi C_m a^3}{r^4}M_y \\ &= B_{yz} \quad \text{for } i=3, j=2, \end{aligned} \tag{A30.8}$$

$$\begin{aligned} B_{zz} &= B_{33} = 2u_{r3}\mu_3 + (\boldsymbol{\mu}\cdot\hat{\mathbf{u}}_r)\delta_{33} - 5(\boldsymbol{\mu}\cdot\hat{\mathbf{u}}_r)u_{r3}^2 \\ &= -2\mu_3 + (-\mu_3)\delta_{33} - 5(-\mu_3)u_{r3}^2 \\ &= -3\mu_3 + 5\mu_3 = 2\mu_3 = 2\mu_z \\ &= \frac{8\pi C_m a^3}{r^4}M_z \quad \text{for } i=3, j=3. \end{aligned} \tag{A30.9}$$

Hence the magnetic gradient tensor $B_{ij}(0,0,z)$ for $|z| > a$ is

$$\begin{aligned} \mathbf{B}(0,0,z) &= \frac{4\pi C_m a^3}{r^4}\begin{bmatrix} -M_z & 0 & -M_x \\ 0 & -M_z & -M_y \\ -M_x & -M_y & 2M_z \end{bmatrix} \\ &= f\begin{bmatrix} -M_z & 0 & -M_x \\ 0 & -M_z & -M_y \\ -M_x & -M_y & 2M_z \end{bmatrix}. \end{aligned} \tag{A31}$$

The three eigenvalues $\lambda_1, \lambda_2, \lambda_3$ are found by solving for the roots the of the characteristic equation $\det(\mathbf{B} - \lambda\mathbf{I}) = 0$. On expanding Equation (A31), I obtain the following depressed cubic equation whereby it is immediately evident that $\lambda = -fM_z$ is an eigenvalue of the gradient tensor $\mathbf{B}(0,0,z)$:

$$\begin{aligned}&(-fM_z - \lambda)^2(2fM_z - \lambda)\\&\quad - f^2M_y^2(-fM_z - \lambda) - f^2M_x^2(-fM_z - \lambda) = 0. \qquad \text{(A32)}\end{aligned}$$

The two remaining eigenvalues are found by solving the following quadratic equation:

$$\lambda^2 - fM_z\lambda - f^2(M_x^2 + M_y^2 + 2M_z^2) = 0. \qquad \text{(A33)}$$

And hence

$$\begin{aligned}\lambda &= \frac{f}{2}\left[M_z \pm \sqrt{4(M_x^2 + M_y^2) + 9M_z^2}\right] \text{ or } \lambda\\&= \frac{fM_z}{2}\left[1 \pm \sqrt{4\cot^2 I_M + 9}\right], \qquad \text{(A34)}\end{aligned}$$

where I_M is the inclination of the magnetisation vector $\mathbf{M}$,

$$I_M = \arctan\left[\frac{M_z}{\sqrt{(M_x^2 + M_y^2)}}\right] \text{ or } I_M = \arctan\left(\frac{M_z}{M_h}\right). \qquad \text{(A35)}$$

The ordering of the three eigenvalues is determined by the sign of the vertical component of magnetisation M_z. For $M_z > 0$, the eigenvalues for an axial station in descending order $\lambda_1 > \lambda_2 > \lambda_3$ are

$$\begin{aligned}\lambda_1 &= \frac{f}{2}\left[M_z + \sqrt{4(M_x^2 + M_y^2) + 9M_z^2}\right]\\&= \frac{fM_z}{2}\left[1 + \sqrt{4\cot^2 I_M + 9}\right] = \frac{fM_z}{2}(1 + \Delta), \qquad \text{(A36.1)}\\\lambda_2 &= -fM_z, \qquad \text{(A36.2)}\\\lambda_3 &= \frac{f}{2}\left[M_z - \sqrt{4(M_x^2 + M_y^2) + 9M_z^2}\right]\\&= \frac{fM_z}{2}\left[1 - \sqrt{4\cot^2 I_M + 9}\right] = \frac{fM_z}{2}(1 - \Delta). \qquad \text{(A36.3)}\end{aligned}$$

Importantly for magnetisations where M_z is positive (such as induced magnetisations in the northern magnetic hemisphere), the second eigenvalue λ_2 is always negative whereas for magnetisations in the southern magnetic hemisphere where M_z is negative, the second eigenvalue λ_2 is always positive and the λ_1 and λ_3 eigenvalues are interchanged. The NSS $\mu(0,0,z)$ along the vertical axis of the magnetic sphere may now be derived from Equation (31) and Equations (A36.1)–(A36.3), namely,

$$\begin{aligned}\mu(0,0,z) &= \sqrt{-\lambda_2^2 - \lambda_1\lambda_3}\\&= \sqrt{-f^2M_z^2 - \left[\frac{fM_z}{2}(1+\Delta)\right]\left[\frac{fM_z}{2}(1-\Delta)\right]}\\&= \frac{fM_z}{2}(\Delta^2 - 5),\end{aligned}$$

where

$$\begin{aligned}\Delta &= \sqrt{4(M_x^2 + M_y^2)/M_z^2 + 9} = \sqrt{4(M_h^2/M_z^2) + 9}\\&= \sqrt{4\cot^2 I_M + 9}.\end{aligned}$$

Since the discriminant term is $\Delta = \sqrt{4(M_x^2 + M_y^2)/M_z^2 + 9}$, then the final expression for the scaled moment is

$$\begin{aligned}\mu(0,0,z) &= \frac{f}{2}\sqrt{4(M_x^2 + M_y^2) + 9M_z^2 - 5M_z^2}\\&= f\sqrt{M_x^2 + M_y^2 + M_z^2} = f|\mathbf{M}|. \qquad \text{(A37)}\end{aligned}$$

This is an important result. It shows that the NSS on the vertical axis of a uniformly magnetised sphere is independent of the magnetisation direction and, for a particular observation height, its magnitude is determined by the radius of the sphere and intensity of magnetisation only. From Equation (32.2), it may be deduced that for any horizontal observation plane, the NSS μ peaks directly above the centre of the magnetised sphere.

The angle φ is defined as the angle between the line joining the centre of the dipole or magnetic sphere to the observation point $P(\mathbf{r}_s)$ and the magnetic moment vector $\mathbf{m}$ (Clark 2012). However when the observation point is located on the vertical axis of the magnetised sphere, the ratio $\cos\varphi = \lambda_2/\mu$ yields expressions for the inclination I_M and coinclination I'_M directions of magnetisation. For example, the inclination angle I_M is related to the angle φ as follows:

$$\begin{aligned}\cos\varphi &= \frac{\lambda_2}{\mu} = \frac{-fM_z}{f|\mathbf{M}|} = \frac{-M_z}{\sqrt{M_h^2 + M_z^2}} = \frac{-\mathrm{sgn}M_z}{\sqrt{\cot^2 I_M + 1}}\\&= -\sin I_M \quad \text{for } 0 \le \varphi \le \pi \text{ and } -\frac{\pi}{2} \le I_M \le \frac{\pi}{2}. \qquad \text{(A38)}\end{aligned}$$

Therefore, for any axial observation point above a magnetic sphere, it may be deduced that $I_M = \varphi - \pi/2$.

An expression for the declination of magnetisation D_M may be derived from the second eigenvector $\hat{\mathbf{e}}_2 = (e_{2x}, e_{2y}, e_{2z})^{\mathrm{T}}$ of the magnetic gradient tensor $\mathbf{B}$ for an observation station $P(0,0,z)$ located at a height $|z| > a$ directly above an origin at the centre of a magnetised sphere. The second eigenvector $\hat{\mathbf{e}}_2 = (e_{2x}, e_{2y}, e_{2z})^{\mathrm{T}}$ of the magnetic gradient tensor is found by solving the linear equation $\mathbf{B}\hat{\mathbf{e}}_2 = \lambda_2\hat{\mathbf{e}}_2$ where λ_2 is the second eigenvalue. Hence for $\lambda_2 = -fM_z$:

$$f\begin{bmatrix}-M_z & 0 & -M_x\\0 & -M_z & -M_y\\-M_x & -M_y & 2M_z\end{bmatrix}\begin{pmatrix}e_{2x}\\e_{2y}\\e_{2z}\end{pmatrix} = fM_z\begin{pmatrix}e_{2x}\\e_{2y}\\e_{2z}\end{pmatrix}.$$

By expanding either row 1 or row 2 of the matrix equation, it becomes immediately apparent that $e_{2z} = 0$, for example,

$$-fM_ze_{2x} - fM_xe_{2z} = -fM_ze_{2x} \text{ so that } e_{2z} = 0.$$

Furthermore since $e_{2z} = 0$ and from the expansion of row 3, it is now possible to express component e_{2y} in terms of e_{2x} and vice versa.

$$\begin{aligned}&-fM_xe_{2x} - fM_ye_{2y} + 2fM_ze_{2z} = -fM_ze_{2z} \text{ so that } e_{2y}\\&= -\frac{M_x}{M_y}e_{2x} \text{ or } e_{2x} = -\frac{M_y}{M_x}e_{2y}.\end{aligned}$$

Hence the second eigenvector is given by $\mathbf{e}_2 = \left(-\frac{M_y}{M_x}e_{2y}, e_{2y}, 0\right)^{\mathrm{T}}$. This vector requires normalisation to unit amplitude. Therefore the normalised second eigenvector $\hat{\mathbf{e}}_2$

is

$$\hat{\mathbf{e}}_2 = \frac{\mathbf{e}_2}{|\mathbf{e}_2|} = \frac{\left(-\frac{M_y}{M_x}e_{2y}, e_{2y}, 0\right)^{\mathrm{T}}}{e_{2y}\sqrt{1+\left(\frac{M_y}{M_x}\right)^2}} = \frac{(-M_y, M_x, 0)^{\mathrm{T}}}{\sqrt{{M_x}^2+{M_y}^2}}$$

$$= \left(-\frac{M_y}{M_h}, \frac{M_x}{M_h}, 0\right)^{\mathrm{T}},$$

$$\text{or } \hat{\mathbf{e}}_2 = (e_{2x}, e_{2y}, e_{2z})^{\mathrm{T}} = (-\sin D_M, \cos D_M, 0)^{\mathrm{T}}. \quad \text{(A39)}$$

The declination of magnetisation D_M may now be estimated from the second eigenvector as follows:

$$\tan D_M = \frac{-e_{2x}}{e_{2y}} \text{ or } D_M = \arctan\left(\frac{-e_{2x}}{e_{2y}}\right). \quad \text{(A40)}$$

Similarly the first $\hat{\mathbf{e}}_1 = (e_{1x}, e_{1y}, e_{1z})^{\mathrm{T}}$ and third eigenvectors $\hat{\mathbf{e}}_3 = (e_{3x}, e_{3y}, e_{3z})^{\mathrm{T}}$ of the magnetic gradient tensor are found by solving the pair of linear equations $\mathbf{B}\hat{\mathbf{e}}_1 = \lambda_1\hat{\mathbf{e}}_1$ and $\mathbf{B}\hat{\mathbf{e}}_3 = \lambda_3\hat{\mathbf{e}}_3$ respectively where $\lambda_1 = fM_z(1+\Delta)/2$ and $\lambda_3 = fM_z(1-\Delta)/2$ are the first and third eigenvalues respectively for magnetisations in the northern magnetic hemisphere, i.e. for $M_z > 0$. The first eigenvector $\hat{\mathbf{e}}_1 = (e_{1x}, e_{1y}, e_{1z})^{\mathrm{T}}$ is found by solving the equation

$$f\begin{bmatrix} -M_z & 0 & -M_x \\ 0 & -M_z & -M_y \\ -M_x & -M_y & 2M_z \end{bmatrix}\begin{pmatrix} e_{1x} \\ e_{1y} \\ e_{1z} \end{pmatrix} = \frac{fM_z}{2}(1+\Delta)\begin{pmatrix} e_{1x} \\ e_{1y} \\ e_{1z} \end{pmatrix}. \quad \text{(A41)}$$

Expanding the three rows of Equation (A41), leads to the following expressions for e_{1x}, e_{1y} ande_{1z}

$$e_{1x} = -\frac{M_x}{M_z}\frac{2}{(\Delta+3)}e_{3z}; e_{1y} = -\frac{M_y}{M_z}\frac{2}{(\Delta+3)}e_{1z}; e_{1z}$$

$$= \frac{2M_h^2}{M_xM_z(3-\Delta)}e_{1x} \text{ and } e_{1y} = \frac{M_y}{M_x}e_{1x}, \quad \text{(A42)}$$

where $M_h = \sqrt{M_x^2+M_y^2}$ is the horizontal component of magnetisation. Hence from Equation (A42), the unnormalised eigenvector $\mathbf{e}_1 = (e_{1x}, e_{1y}, e_{1z})^{\mathrm{T}}$ is

$$\mathbf{e}_1 = (e_{1x}, e_{1y}, e_{1z})^{\mathrm{T}} = \left(e_{1x}, \frac{M_y}{M_x}e_{1x}, \frac{2M_h^2}{M_xM_y(3-\Delta)}e_{1x}\right)^{\mathrm{T}}.$$

This vector requires normalisation to unit amplitude. Therefore the normalised eigenvector $\hat{\mathbf{e}}_1$ at a point $P(0,0,z)$ directly above the centre of a magnetic sphere in which $M_z > 0$ is

$$\hat{\mathbf{e}}_1 = \frac{\mathbf{e}_1}{|\mathbf{e}_1|} = \frac{e_{1x}\left(1, \frac{M_y}{M_x}, \frac{2M_h^2}{M_xM_y(3-\Delta)}\right)^T}{e_{1x}\sqrt{1+\left(\frac{M_y}{M_x}\right)^2+\frac{4M_h^4}{M_x^2M_z^2(3-\Delta)^2}}}$$

$$= \frac{\left(M_x, M_y, \frac{2M_h^2}{M_z(3-\Delta)}\right)^T}{\sqrt{M_x^2+M_y^2+\frac{4M_h^4}{M_z^2(3-\Delta)^2}}}. \quad \text{(A43)}$$

By inspection of Equations (A42) and (A43), the declination D_{ev1} and inclination I_{ev1} of the first eigenvector $\hat{\mathbf{e}}_1$ at $P(0,0,z)$ are

$$D_{ev1} = \arctan\left(\frac{e_{1y}}{e_{1x}}\right) = \arctan\left(\frac{M_y}{M_x}\right)$$

$$= D_M \quad (0^\circ \le D_M \le 360^\circ), \quad \text{(A44.1)}$$

$$I_{ev1} = \arctan\left[\frac{e_{1z}}{\sqrt{e_{1x}^2+e_{1y}^2}}\right] = \arctan\left[\frac{2M_h}{M_z(3-\Delta)}\right]$$

$$= \arctan\left[\frac{2\cot I_M}{(3-\Delta)}\right] \quad I_M > 0. \quad \text{(A44.2)}$$

Similarly the third eigenvector $\hat{\mathbf{e}}_3 = (e_{3x}, e_{3y}, e_{3z})^{\mathrm{T}}$ is found by solving the matrix equation

$$f\begin{bmatrix} -M_z & 0 & -M_x \\ 0 & -M_z & -M_y \\ -M_x & -M_y & 2M_z \end{bmatrix}\begin{pmatrix} e_{3x} \\ e_{3y} \\ e_{3z} \end{pmatrix} = \frac{fM_z}{2}(1-\Delta)\begin{pmatrix} e_{3x} \\ e_{3y} \\ e_{3z} \end{pmatrix}. \quad \text{(A45)}$$

Expanding the three rows of Equation (A45), leads to the following expressions for e_{3x}, e_{3y} and e_{3z}

$$e_{3x} = \frac{M_x}{M_z}\frac{2}{(\Delta-3)}e_{3z}; e_{3y} = \frac{M_y}{M_z}\frac{2}{(\Delta-3)}e_{3z}; e_{3z}$$

$$= \frac{2M_h^2}{M_xM_z(3+\Delta)}e_{3x} \text{ and } e_{3y} = \frac{M_y}{M_x}e_{3x}. \quad \text{(A46)}$$

Therefore the normalised third eigenvector $\hat{\mathbf{e}}_3$ at an observation point $P(0,0,z)$ directly above the centre of a magnetic sphere in which $M_z > 0$ is

$$\hat{\mathbf{e}}_3 = \frac{\mathbf{e}_3}{|\mathbf{e}_3|} = \frac{e_{3x}\left(1, \frac{M_y}{M_x}, \frac{2M_h^2}{M_xM_z(3+\Delta)}\right)^{\mathrm{T}}}{e_{3x}\sqrt{1+\left(\frac{M_y}{M_x}\right)^2+\frac{4M_h^4}{M_x^2M_z^2(3+\Delta)^2}}}$$

$$= \frac{\left(M_x, M_y, \frac{2M_h^2}{M_z(3+\Delta)}\right)^{\mathrm{T}}}{\sqrt{M_x^2+M_y^2+\frac{4M_h^4}{M_z^2(3+\Delta)^2}}}. \quad \text{(A47)}$$

By inspection of Equations (A46) and (A47), the declination and inclination of the third eigenvector $\hat{\mathbf{e}}_3$ at $P(0,0,z)$ are

$$D_{ev3} = \arctan\left(\frac{e_{3y}}{e_{3x}}\right) = \arctan\left(\frac{M_y}{M_x}\right)$$

$$= D_M \quad (0^\circ \le D_M \le 360^\circ), \quad \text{(A48.1)}$$

$$I_{ev3} = \arctan\left[\frac{e_{3z}}{\sqrt{e_{3x}^2+e_{3y}^2}}\right] = \arctan\left[\frac{2M_h}{M_z(3+\Delta)}\right]$$

$$= \arctan\left[\frac{2\cot I_M}{(3+\Delta)}\right] \quad I_M > 0. \quad \text{(A48.2)}$$

Thus the first and third eigenvectors have the same declination, equal to the declination of the magnetisation D_M. Also Equations (A44.2) and (A48) imply that the inclinations of the first I_{ev1} and third I_{ev3} eigenvectors differ by 90°. This is confirmed using the formula for $\tan(I_{ev3} - I_{ev1})$ and the expression for the discriminant term $\Delta = \sqrt{4\cot^2 I_M + 9}$.

Some special cases:

(1) The gradient tensor at a station directly above the centre of a uniformly magnetised sphere in which the inclination of magnetisation is zero, i.e. when $I_M = 0$ and $M_z = 0$. Therefore from Equation (A31)

$$\mathbf{B}(0,0,z) = f\begin{bmatrix} 0 & 0 & -M_x \\ 0 & 0 & -M_y \\ -M_x & -M_y & 0 \end{bmatrix}$$

$$\text{where } f = \frac{4\pi C_m a^3}{z^4}. \quad \text{(A49)}$$

From Equations (A36.1)–(A36.3), the second eigenvalue $\lambda_2 = 0$, since $M_z = 0$, and therefore,

$$\lambda = \frac{f}{2}\left[\pm\sqrt{4(M_x^2 + M_y^2)}\right] = \pm fM_h \text{ and } \lambda_1 = fM_h, \lambda_2 = 0, \lambda_3 = -fM_h. \quad \text{(A50)}$$

The pair of eigenvectors $\hat{\mathbf{e}}_1$ and $\hat{\mathbf{e}}_3$ are

$$\hat{\mathbf{e}}_1 = (e_{1x}, e_{1y}, e_{1z})^{\mathrm{T}} = \left(\frac{M_x}{\sqrt{2}M_h}, \frac{M_y}{\sqrt{2}M_h}, -\frac{1}{\sqrt{2}}\right)^{\mathrm{T}} = \frac{1}{\sqrt{2}}(\cos D_M, \sin D_M, -1)^{\mathrm{T}}, \quad \text{(A51.1)}$$

$$\hat{\mathbf{e}}_3 = (e_{3x}, e_{3y}, e_{3z})^{\mathrm{T}} = \left(\frac{M_x}{\sqrt{2}M_h}, \frac{M_y}{\sqrt{2}M_h}, \frac{1}{\sqrt{2}}\right)^{\mathrm{T}} = \frac{1}{\sqrt{2}}(\cos D_M, \sin D_M, 1)^{\mathrm{T}}. \quad \text{(A51.2)}$$

By inspection the declination D_M of magnetisation is identical to the declinations of the first and third eigenvectors,

$$\tan D_{ev1} = \frac{e_{1y}}{e_{1x}} = \frac{M_y}{M_x} = \tan D_M \text{ and } \tan D_{ev3} = \frac{e_{3y}}{e_{3x}} = \frac{M_y}{M_x} = \tan D_M. \quad \text{(A52)}$$

Furthermore the inclinations of the first and third eigenvectors are $I_{ev1} = -45^\circ$ and $I_{ev3} = 45^\circ$, respectively, namely,

$$\tan I_{ev1} = \frac{e_{1z}}{e_{1h}} = \frac{-1}{\sqrt{\cos^2 D_M + \sin^2 D_M}} = -1 \text{ and } \tan I_{ev3} = \frac{e_{3z}}{e_{3h}} = \frac{1}{\sqrt{\cos^2 D_M + \sin^2 D_M}} = 1.$$

(2) The gradient tensor at station directly above the centre of a uniformly magnetised sphere in which the inclination of magnetisation is vertical, i.e. when $I_M = \pm 90^\circ$, is given by

$$\mathbf{B}(0,0,z) = f\begin{bmatrix} -M_z & 0 & 0 \\ 0 & -M_z & 0 \\ 0 & 0 & 2M_z \end{bmatrix} \text{ where } f = \frac{4\pi C_m a^3}{z^4}. \quad \text{(A53)}$$

For a magnetisation in the northern magnetic hemisphere where $I_M = 90^\circ$, and $M_z > 0$, the eigenvalues of the gradient tensor in descending order are

$$\lambda_1 = 2fM_z, \lambda_2 = -fM_z, \lambda_3 = -fM_z, \quad \text{(A54)}$$

so that λ_1 is the principal or largest eigenvector in magnitude, while the remaining pair of eigenvalues are equal in magnitude and negative. By inspection, the principal eigenvalue λ_1 is associated with the third column vector in Equation (A53), hence the three eigenvectors in this instance are

$$\hat{\mathbf{e}}_1 = \hat{\mathbf{u}}_z = (0,0,1)^{\mathrm{T}}, \hat{\mathbf{e}}_2 = \hat{\mathbf{u}}_y = (0,1,0)^{\mathrm{T}} \text{ and } \hat{\mathbf{e}}_3 = \hat{\mathbf{u}}_x = (1,0,0)^{\mathrm{T}} \quad \text{(A55)}$$

Thus for a magnetisation at the north magnetic pole where $I_M = 90^\circ$, the second and third eigenvectors are horizontal with declinations $D_{ev2} = 90°$ and $D_{ev3} = 0°$ respectively, while the inclination of the principal eigenvector $\hat{\mathbf{e}}_1$, is vertical and parallel to the inclination of magnetisation.

For a magnetisation in the southern magnetic hemisphere where $I_M = -90^\circ$ and $M_z < 0$, the eigenvalues of the gradient tensor in descending order are

$$\lambda_1 = -fM_z, \lambda_2 = -fM_z, \lambda_3 = 2fM_z, \quad \text{(A56)}$$

so that λ_3 is the largest eigenvector in magnitude while the remaining pair of eigenvalues are equal in magnitude and positive. By inspection the principal eigenvalue λ_3 is associated with the third column vector in Equation (A53), hence the three eigenvectors in this instance are

$$\hat{\mathbf{e}}_1 = \hat{\mathbf{u}}_x = (1,0,0)^{\mathrm{T}}, \hat{\mathbf{e}}_2 = \hat{\mathbf{u}}_y = (0,1,0)^{\mathrm{T}} \text{ and } \hat{\mathbf{e}}_3 = \hat{\mathbf{u}}_z = (0,0,1)^{\mathrm{T}}. \quad \text{(A57)}$$

Thus for a magnetisation at the south magnetic pole where $I_M = -90^\circ$, the first and second eigenvectors are horizontal with declinations $D_{ev1} = 0°$ and $D_{ev2} = 90°$, respectively, while the inclination of the principal eigenvector $\hat{\mathbf{e}}_3$, is vertical and antiparallel to the inclination of magnetisation.

Appendix A6. The effective magnetisation of a triaxial ellipsoid accounting for self-demagnetisation, remanence and anisotropy of magnetic susceptibility

Accounting for self-demagnetisation, the effective induced magnetisation $\mathbf{M'}_{\mathbf{ind}}$ of a triaxial ellipsoid with resultant magnetisation $\mathbf{M} = \mathbf{M}_{\mathbf{res}}$ in an external geomagnetic field $\mathbf{H}_0(\mathbf{r}_b)$ is defined as follows (Clark, Saul, and Emerson 1986)

$$\mathbf{M'}_{\mathbf{ind}} = \mathbf{K}[\mathbf{H}_0 + \mathbf{H}_{\mathbf{int}}] = \mathbf{K}[\mathbf{H}_0 - \mathbf{N}^{\mathrm{T}}\mathbf{M}] = \mathbf{K}[\mathbf{H}_0 - \mathbf{N}^{\mathrm{T}}(\mathbf{M'}_{\mathbf{ind}} + \mathbf{M}_{\mathbf{rem}})], \quad \text{(A58)}$$

where $\mathbf{K}$ is a symmetric matrix containing elements k_{ij} of the magnetic volume susceptibility tensor in the body axis coordinate system of the ellipsoid, $\mathbf{N} = (N_1, N_2, N_3)^{\mathrm{T}}$ are the demagnetisation factors along the a_1, a_2, a_3 axes of the ellipsoid and $\mathbf{M}_{\mathbf{rem}}$ is the remanent magnetisation vector. Hence on gathering terms in $\mathbf{M'}_{\mathbf{ind}}$

$$\mathbf{M'}_{\mathbf{ind}} + \mathbf{N}^{\mathrm{T}}\mathbf{M'}_{\mathbf{ind}} = \mathbf{M'}_{\mathbf{ind}}(\mathbf{I} + \mathbf{KN}) = \mathbf{KH}_0 - \mathbf{KNM}_{\mathbf{rem}}$$

$$\mathbf{M'}_{\mathbf{ind}} = (\mathbf{I} + \mathbf{KN})^{-1}(\mathbf{KH}_0 - \mathbf{KNM}_{\mathbf{rem}}). \quad \text{(A59)}$$

The effective or resultant magnetisation vector $\mathbf{M}_{\mathbf{res}}$ corrected for self-demagnetisation is the vector sum of the effective induced magnetisation and remanent magnetisation. Therefore if I make $[\mathbf{I} + \mathrm{K}\mathbf{N}]^{-1}$ a common factor in the expressions for $\mathbf{M'}_{\mathbf{ind}}$ and $\mathbf{M}_{\mathbf{rem}}$, it becomes evident that the pair of terms involving $\mathbf{KNM}_{\mathbf{rem}}$ cancel so that

$$\begin{aligned}\mathbf{M}_{\mathbf{res}} &= \mathbf{M'}_{\mathbf{ind}} + \mathbf{M}_{\mathbf{rem}} \\ &= [\mathbf{I} + \mathbf{KN}]^{-1}(\mathbf{KH}_0 - \mathbf{KNM}_{\mathbf{rem}} + [\mathbf{I} + \mathbf{KN}]\mathbf{M}_{\mathbf{rem}}) \\ &= [\mathbf{I} + \mathbf{KN}]^{-1}(\mathbf{KH}_0 + \mathbf{M}_{\mathbf{rem}}) \\ &= [\mathbf{I} + \mathbf{KN}]^{-1}(\mathbf{M}_{\mathbf{ind}} + \mathbf{M}_{\mathbf{rem}}) = [\mathbf{I} + \mathbf{KN}]^{-1}\mathbf{M}_{\mathbf{tot}}, \quad \text{(A60)}\end{aligned}$$

where $\mathbf{M}_{\mathbf{ind}} = \mathbf{KH}_0$ is the intrinsic induced magnetisation uncorrected for self-demagnetisation and $\mathbf{M}_{\mathbf{tot}}$ is the total resultant magnetisation uncorrected for self-demagnetisation. This expression for the effective or resultant magnetisation of an ellipsoid agrees with Equation (38) in Clark, Saul, and Emerson (1986). All vectors shown here are in the body axis coordinate system of the ellipsoid.